5-2015

Bio-Inspired Materials and Micro/Nanostructures Enabled by Peptides and Proteins

Swathi Swaminathan
Utah State University

Utah State University
MERRILL-CAZIER LIBRARY

BIO-INSPIRED MATERIALS AND MICRO/NANOSTRUCTURES ENABLED BY

PEPTIDES AND PROTEINS

by

Swathi Swaminathan

A dissertation submitted in partial fulfillment
of the requirements for the degree

of

DOCTOR OF PHILOSOPHY

in

Biological Engineering

Approved:

_____   _____
Dr. Yue Cui   Dr. Ronald Sims
Committee Chairman   Committee Member

_____   _____
Dr. Anhong Zhou   Dr. Ling Liu
Committee Member   Committee Member

_____   _____
Dr. Jixun Zhan   Dr. Mark McLellan
Committee Member   Vice President for Research and
                                                              Dean of the school of Graduate Studies

UTAH STATE UNIVERSITY
Logan, Utah

2015

ABSTRACT

Bio-inspired materials and micro/nanostructures enabled by peptides and proteins

by

Swathi Swaminathan, Doctor of Philosophy

Utah State University, 2015

Major Professor: Dr. Yue Cui

Department: Biological Engineering

The development of a general approach for non-destructive chemical and biological functionalization of materials could expand opportunities for both fundamental studies and creating various device platforms. Phage display has emerged as a powerful method for selecting peptides that possess enhanced selectivity and binding affinity toward a variety of targets. In this study, a powerful yet benign approach for identifying binding motifs to

materials like (Poly) dimethylsiloxane, epoxy, and (Poly) ethylenetetraphthalate and peptide nanotubes has been demonstrated via comprehensively screened phage-displayed peptides. Further, along with the development of microstructures, micropatterns and micro-molecular self-assembly, recognition with phage-displayed peptides can be specifically localized in these microstructures.

In addition, the development of a facile approach for fabricating a library of precisely positioned nanostructures and microfluidic systems based on mammalian hair offers exciting opportunities in fundamental research and practical applications. The current top-down and bottom-up nanofabrication methods have been restricted in accessibility in standard labs due to their high cost and complexity. Novel fabrication methods utilizing biomimetic materials and natural proteins for large-scale nanopatterning with hierarchical assembly of functional materials have been reported. It is anticipated that these results could open up exciting opportunities in the use of peptide-recognized materials in fundamental biochemical recognition studies, as well as in applications ranging from analytical storage devices, hybrid materials, sensors, surface and interface, to cell biology.

(175 pages)

PUBLIC ABSTRACT

Bio-Inspired materials and micro/nanostructures enabled by peptides and proteins

Bio-nanotechnology refers to the field of science that intersects nanotechnology with biology. The study involves in the creation of bio-mimetic devices that emulate elements and systems of nature finding use in various applications. Nanotechnology involves the characterization of nanomaterials along with the study of molecular self-assembly and nanoelectronics. Controlled binding and assembly of proteins onto nanomaterials is at the core of biological materials science and engineering with wide-ranging applications. This hybrid technology opens up several avenues in the field of sensors, pharmaceuticals, artificial implants and so on.

In this work, different biomaterials and polymers were characterized for phage displayed peptide recognition moieties, followed by designing bifunctional entities of these peptides to construct devices of biological or electrical importance. Further, the instability of these nanomaterials was exploited to create nano/micropatterns, which could also be transferred to other substrates or subjected to self-assembly, creating bottom-up or top

down fabrication systems. Finally, cumulating the techniques of microfluidics and immunoassay, a biosensor was designed to enable the detection of cardiac markers.

Swathi Swaminathan

ACKNOWLEDGEMENT

TABLE OF CONTENTS

LIST OF FIGURES

PART I

PHAGE DISPLAY TECHNOLOGY

I.1. Introduction [1]

Oligopeptides are robust biorecognition molecules, displaying broad chemical diversity (acidity, hydrophobicity, etc.), and can be chemically engineered to bind specific targets [2]. Further, peptides can form complex, self-assembled hybrid conjugates with a variety of materials or assemble specific materials on patterned or microstructured surfaces, with their ability to be linked into multifunctional networks [3].

Phage display has emerged as a powerful method for identifying peptide motifs with enhanced binding affinities toward specific targets. In phage display, a library of approximately a billion (109) peptide variants is displayed on the phage as a fusion with the surface coat protein of the bacteriophage, which allows for rapid, combinatorial screening of sequences displaying high affinities toward specific targets. Phage display has been investigated to identify specific binding peptides for a wide range of target analytes, including metals [4, 5], semiconductors [6-8], polymers [9, 10], small molecules [11], graphene [12] and small molecule ink [13].

I.2. Experimental [1]

An aliquot of the phage display library was incubated with an epoxy slab (non-oxidized)/PDMS slab (oxidized/ non-oxidised)/ PET film / Peptide Nanotubes grown on a glass slide in Tris buffered saline containing 0.1-0.5% Tween-20 (TBST) for 1 h at room temperature. The slab was then washed several times with TBST buffer. The phages were eluted from the epoxy by addition of glycine-HCl (pH 2.2) for 15 min, neutralized with Tris-HCl, pH 9.1, amplified, and subjected to additional pannings. Eluted phages were then amplified in *E. coli*, and the panning was repeated for up to three rounds. This was conducted under increasingly stringent conditions, to obtain phage clones expressing peptides with the highest binding affinities to the samples. After the final round of panning, DNA sequence analysis of the isolated phage clones yielded heptameric epoxy-binding peptides.
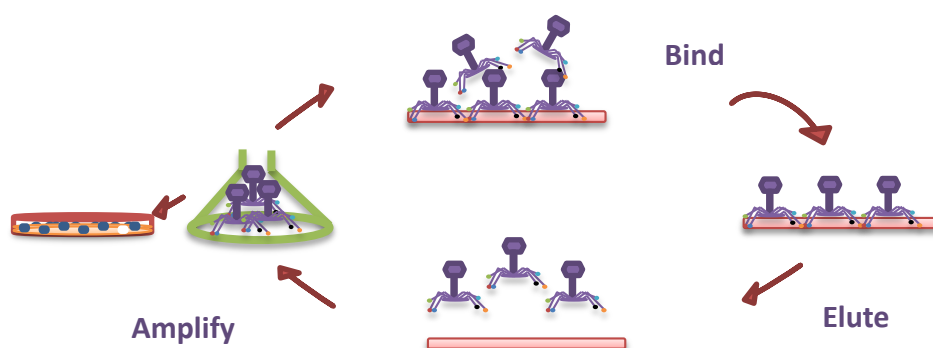
Fig.1. Schematic of the Phage display technique.

CHAPTER 1

RECOGNITION AND NON-LITHOGRAPHIC PATTERNING OF (POLY)

DIMETHYLSILOXANE USING PHAGE-DISPLAYED PEPTIDES [1, 14]

1.1.   Abstract

A powerful yet benign approach for identification of binding motifs to poly (dimethylsiloxane) (PDMS) *via* comprehensively screened phage displayed peptides is demonstrated for the first time. These results show that PDMS can be selectively recognized with peptide-displaying phages and bifunctional peptides. Further, along with the development of PDMS-based microstructures, recognition of PDMS with phage displayed peptides can be specifically localized in these microstructures. In addition, the development of controlled patterning of phage (viruses) could expand opportunities for both fundamental studies and creating various materials platforms. Inducing the elastomeric instability of PDMS film provides a non-lithographic, tunable, controlled method for generating micro/nanoscale wrinkle patterns. Phage display has emerged as a powerful method for selecting peptides that possess enhanced selectivity and binding affinity toward a variety of targets. The non-lithographic patterning of phage-displayed

peptides with wrinkled elastomers is also represented in this study. The results show that the phage-displayed peptides can be patterned on specific locations in controlled and tuneable ways, be transferred to other substrates and induce the self-assembly of hybrid materials. It is anticipated that these results could open up exciting opportunities in fundamental studies and in applications ranging from sensors, hybrid materials, self-assembly, surface and interface, to micro/nanoelectronics.

1.2. Introduction

Poly(dimethylsiloxane) (PDMS) is a silicon-based elastomer, which has been widely used for a variety of in vitro and in vivo applications, including microfluidic devices [1, 15], micro-nanostructures [16], surface and interface [17], construction of hybrid materials [18], and cell biology [19]. PDMS has shown excellent thermal stability, optical, electrical, mechanical, and biocompatible properties [19-21]. A variety of surface functionalization and recognition of PDMS has been studied for its biological [22], chemical [22], mechanical [23], and electrical applications [24].

To date, the developed surface modification methods are based on either physical non-covalent or chemical covalent modification with silanes or plasma treatment

[25]. Physical modifications mainly depend on the surface functionalization either via hydrophobic, hydrophilic or electrostatic interactions and polymer/copolymer coatings [26]. This has proven to facilitate a much simpler and efficient means of molecular separation studies to avoid nonspecific interactions in comparison to the covalent modifications. Also, no issues of solvent based swelling of PDMS encountered during silanization or other covalent methods, is observed with non-covalent functionalization [27]. A general method for chemical and biological functionalization of PDMS with specific binding motifs is thus highly desired [1].

The development of controlled patterning of phage (viruses) could expand opportunities for both fundamental studies and creating various materials platforms. Inducing the elastomeric instability of PDMS film provides a non-lithographic, tunable, controlled method for generating micro/nanoscale wrinkle patterns. The spatial control of phage-displayed peptides has attracted great interest, which can open up new opportunities in self-assembly, selective sensors, and nano- and microelectronic devices. Photolithography [28] and e-beam lithography [29] are widely used for generating microscale and nanoscale patterns. Having already aimed at patterning of phage-displayed peptides on specific locations with photolithography and soft lithography [30], it is thus desired to pattern these peptides on specific locations of a wrinkled elastomer [14].

Spontaneous formations of textured surface patterns [31-33] via inducing the surface instability of elastomer have attracted great attention and have been investigated under a variety of methodologies. Due to the elastomeric property, the geometry of wrinkle patterns can be changed with a stretching strain producing a resolution of 50nm up to several micrometers, which opens up opportunities for developing tunable hybrid materials. Recently, we have also demonstrated a flame oxidation method for the generation of tunable wrinkle patterns [34].

1.3.   Experimental

The PDMS prepolymer and its curing agent (Sylgard 184 silicone elastomer kit) were thoroughly mixed in a ratio of 10:1, followed by degassing in vacuum for 30 min. The mixture was then poured over a petri dish and microstructured masters, and cured at 80 °C for 2 h, followed by peeling off to obtain a flat PDMS surface, PDMS microdots and PDMS microchannels. The PDMS slabs were then used for incubation with phages or treated by plasma oxidation. The masters for PDMS microdots are TEM grids. The masters for PDMS microchannels were prepared according to a reported procedure [35], and briefly, the channel structures were printed on shrink-dink plastics by a laser printer, and after curing and drilling holes, the PDMS microchannels with an inlet and an outlet were

sealed to a glass slide as shown in Fig.1. The solutions were delivered into the microfluidic

channels with a syringe pump through Teflon tubing. Plasma oxidation (15 W, 30 s) was

performed with a plasma etcher for changing the PDMS surface from being hydrophobic

to hydrophilic, and for bonding the PDMS slab with microchannels to a glass substrate.

Generation of wrinkles: PDMS prepolymer and curing agent (Sylgard 184) were

thoroughly mixed at a weight ratio of 10:1, followed by degassing and curing at 80 °C for

2 h. A PDMS film (0.5 mm thick) was stretched by 25% with a uniaxial stretching strain,

followed by exposure to oxygen plasma at 80 w for 10-30 min to generate consistent one-
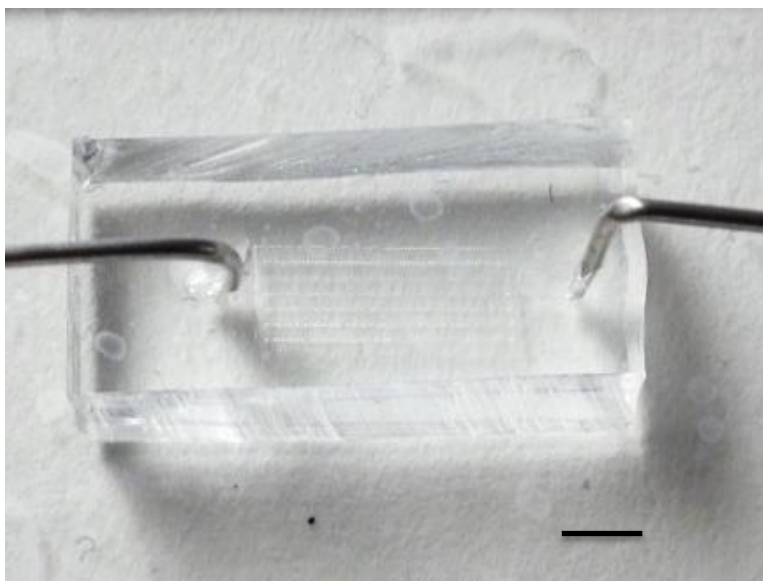
Fig. 2. Schematic of a microfluidic channel. Scale bar: 0.5cm [1]

directional wrinkles, proportional to the direction of the strain with different sizes based on the duration of etching as shown in Fig. 2. By using a 20% biaxial stretching strain with plasma oxidation at 80 w for 20 min, herringbone-structured PDMS wrinkles could be generated.

Printing of phage-displayed peptides: A wrinkled PDMS slab was brought into contact with the glass surface coated by PDMS-binding phage-displayed peptide. Then the phage-displayed peptides with PDMS binding motif were bound to the PDMS surface, followed by washing and characterization. Similarly, a PDMS stamp with SiO2-binding peptide (HKKPSKS) was brought into contact a SiO2 surface,as shown in Fig. 4., followed by washing and characterization.
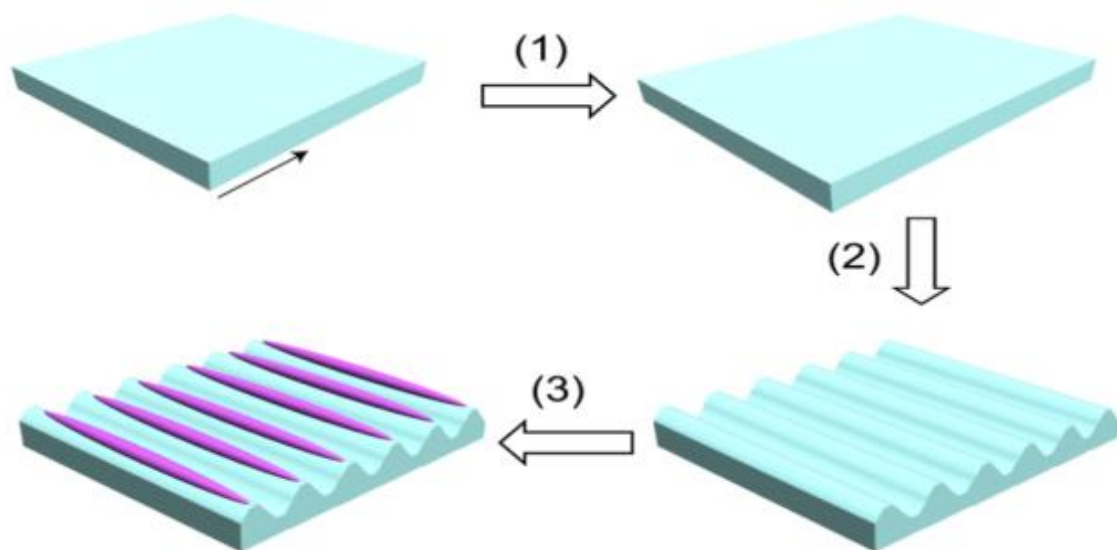
Fig. 3. Schematic of the production of wrinkled elastomer **[14]**

Fluorescent characterization: Fluorescent characterization of the binding of phage-displayed peptides was accomplished by incubating the substrates sequentially with (i) the phage-displayed peptides (5.6x10^10 phage molecules ml⁻1), (ii) blocking buffer 0.1 M NaHCO3, 1% BSA, (iii) biotin-conjugated antibody M13 anti-phage antibody (1 mg ml⁻1) and (iv) avidin-FITC (2 unit ml⁻1), with TBS buffer washing steps in between to remove non-specific binding. Fluorescent characterization for the binding of bifunctional peptides (Peptide 2.0 Inc., VA, USA) was accomplished by incubating the substrates sequentially in (i) the bifunctional peptide (0.5 mg ml⁻1 TBS), (ii) blocking buffer 0.1 M NaHCO3, 1% BSA and (iii) streptavidin-FITC (1 mg ml⁻1), with TBS buffer washing steps in between to remove non-specific binding. The color intensity of the surface was observed through an Olympus IX71 inverted fluorescence microscope equipped with an Olympus DP30BW CCD camera (emission and excitation wavelengths of FITC being 495 and 519 nm, respectively).
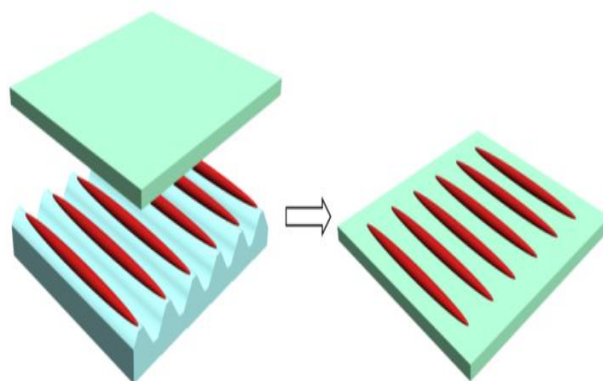
Fig. 4. Schematic of printing the phage displayed peptide on the surface of the wrinkles [14].

Peptide in-situ synthesis of nanoparticles: A bifunctional peptide was designed and synthesied with a binding motif for PDMS, a GGGG spacer, and a motif for synthesis of silver nanoparticles (NPSSLFRYLPSD). First, solutions of the bifunctional peptide (0.5 µg ml^{-1}) and silver nitrate solution (pH 7, 30 mM) were mixed and incubated with PDMS wrinkles and kept in the dark for three days [36], resulting in the growth of nanoparticles on the entire PDMS wrinkled surface. Second, the bifunctional peptides were printed on PDMS wrinkles, followed by incubating with silver nitrate solution to result in the growth of nanoparticles on the wrinkled PDMS surface as shown in the Fig. 5.
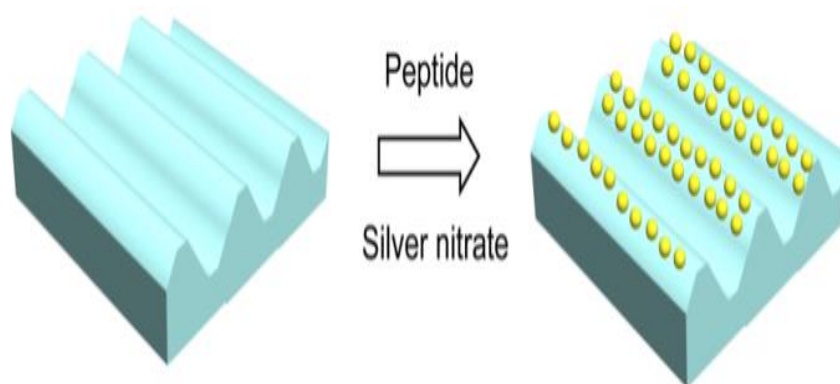
Fig. 5. Schematic of the synthesis of silver nanoparticles after incubation with bifuntional peptide in silver nitrate solution [14].

1.4.   Results and Discussion
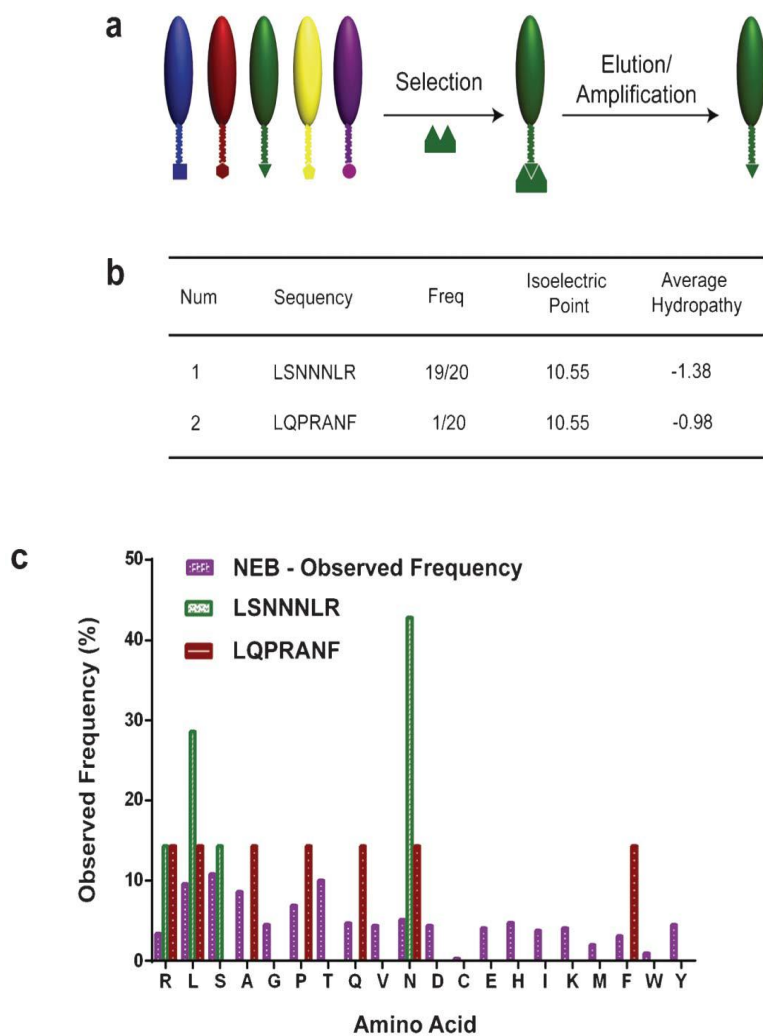
Fig. 6. (a) Schematic of the phage displayed peptide technique. (b) Table showing phage displayed peptides for PDMS, (c) Analysis of the amino acid frequencies in the phage displayed peptides in comparison to the NEB observed library frequency [1].

As shown in Fig. 6a, after performing biocombinatorial screening from a phage display library, specific peptides binding to PDMS can be identified. Fig. 6b shows the characteristics of the peptide sequences screened from three rounds of biopanning, and LSNNNLR appears to show the highest frequency from the biopanning process with a frequency of 19/20. A comparative analysis of the observed frequency of the amino acids binding to PDMS and the recorded frequency in the NEB library has also been recorded in Fig. 6c. A plot analysis of these peptide sequences shows that asparagine and leucine are frequently the binding amino acid residues. The dominant phage displayed peptide (LSNNNLR) was also isolated as a single colony and selected for further investigation.

First, the fluorescent characterization for the binding of LSNNNLR to a flat PDMS surface was investigated, as shown in Fig. 7a. This was accomplished by incubating the substrates sequentially with (1) the phage displayed peptides or M13 phages with the same concentrations, (2) blocking buffer 0.1 M NaHCO3, 1% BSA, (3) biotin conjugated anti-M13 antibody (1 mg ml$^-$1), and (4) avidin- FITC (1 mg ml$^-$1), with TBS buffer washing steps in between to remove non-specific binding. Significantly, the PDMS surface with peptide-displaying phages (LSNNNLR) shows much higher fluorescent intensity relative to the PDMS incubated with M13 phages (without phage displayed peptides on the coat; isolated from the phage display library).

The absence of phage displayed peptide on the coat of M13 phage can be correlated with the absence of fluorescence on the surface of PDMS. Thus, the phage displayed peptide is essential for binding to PDMS. In addition, by using a plasma-oxidized PDMS slab (15 w, 30 s) which shows hydrophilic surface behavior, the fluorescent characterization exhibits similar behavior as the non-oxidized hydrophobic PDMS. Similarly, the low frequency peptide (LQPRANF) can also bind to both non-oxidized and slightly oxidized PDMS slabs. The results suggest that the phage displayed peptides can bind to PDMS with different surface behaviors.

Recent studies showed that the PDMS surface did not suffer from considerable chemical modifications with a mild plasma oxidation, and the chemical groups on the PDMS surface remained largely unaltered [27–31]. Thus, the PDMS-binding phage displayed peptides can bind to both non-oxidized PDMS and slightly oxidized PDMS. While for PDMS that has suffered from a strong plasma oxidation, the chemical groups on the PDMS surface were changed significantly, and the fluorescent characterization showed that the phage displayed peptides did not bind to the strongly oxidized PDMS. The water contact angles of PDMS before and after incubation with peptide-displaying phages were also investigated using a goniometer (Sindatek Model 100 SB, Sindatek Instruments Co, Ltd, Taipei City, Taiwan). As shown in Fig. 7b, the water contact angle for a plain PDMS (without plasma oxidation) was found to be hydrophobic with a contact angle of 100°, while that of the PDMS with the peptide-displaying phages showed a hydrophilic contact angle

of 17. The results suggest that the change in the surface behavior of PDMS is due to the strong binding of phage displayed peptides to PDMS.
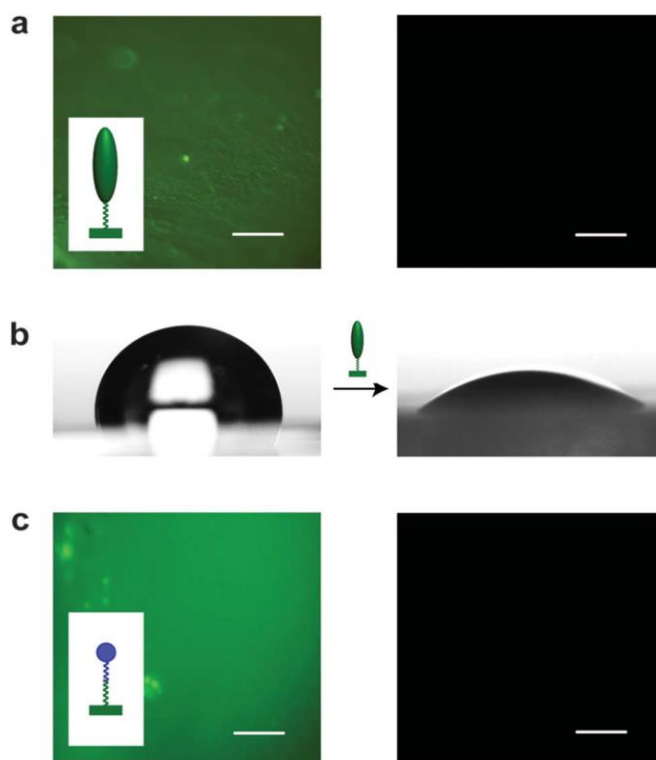
Fig. 7. (a) Fluorescence characterization of phage displayed peptide (LSNNNLR) on PDMS (L) and control (M13 phage with no displayed peptide (R)). (b) Goniometer study of the PDMS without (L) and with (R) phage displayed peptide (LSNNNLR). (c) Bifunctional peptide (LSNNNLRGGGGHPQ) analysis on PDMS (L) and control with no bifunctional peptide (R). Scale bar: 50 μm [1].

We explored a synthetic peptide for binding to the PDMS. A synthetic bifunctional peptide (LSNNNLRGGGGHPQ) (Peptide 2.0, Chantilly, VA) was designed and synthesized, with a PDMS binding motif LSNNNLR, a linker GGGG, and a streptavidin binding motif HPQ.32 Here, we use streptavidin-FITC as the analyte, which is expected to be bound to the PDMS surface via the HPQ binding motif. The fluorescent characterization of the binding of bifunctional peptides was accomplished by incubating the substrates sequentially with (1) the bifunctional peptide (50 mg ml$^-$1 TBS), (2) blocking buffer 0.1 M NaHCO3, 1% BSA, and (3) streptavidin-FITC (1 mg ml$^-$1), with TBS buffer washing steps in between to remove non-specific binding. The control experiment for the PDMS slab without the bifunctional peptide was accomplished by incubating the substrates sequentially to (1) blocking buffer 0.1 M NaHCO3, 1% BSA, and (2) streptavidin-FITC (1 mg ml$^-$1), with TBS buffer washing steps in between. The fluorescent intensity due to FITC, is a measure of the bifunctional peptide bound to PDMS. As shown in Fig. 7c left image, the PDMS slab incubated with the bifunctional peptides shows much higher fluorescent intensity compared to the PDMS slab without the bifunctional peptide (Fig. 7c right image), indicating the strong binding of the bifunctional peptide to both PDMS and streptavidin- FITC. In this work, we used HPQ to perform the initial study. Further, via design of bifunctional peptides for PDMS and other materials, a variety of materials can be explored for binding to the PDMS surface to form hybrid materials, such as Au nanoparticles on PDMS, carbon nanotubes on PDMS, etc. Further, we investigated the localized binding of phage displayed peptide (LSNNNLR) to microstructured PDMS, including that of peptide-displaying phages and bifunctional peptides to PDMS microfluidic channels and micropatterns, as shown in Fig. 8. Fig. 8a shows the binding of

the peptide-displaying phages and the bifunctional peptides to PDMS microfluidic channels.
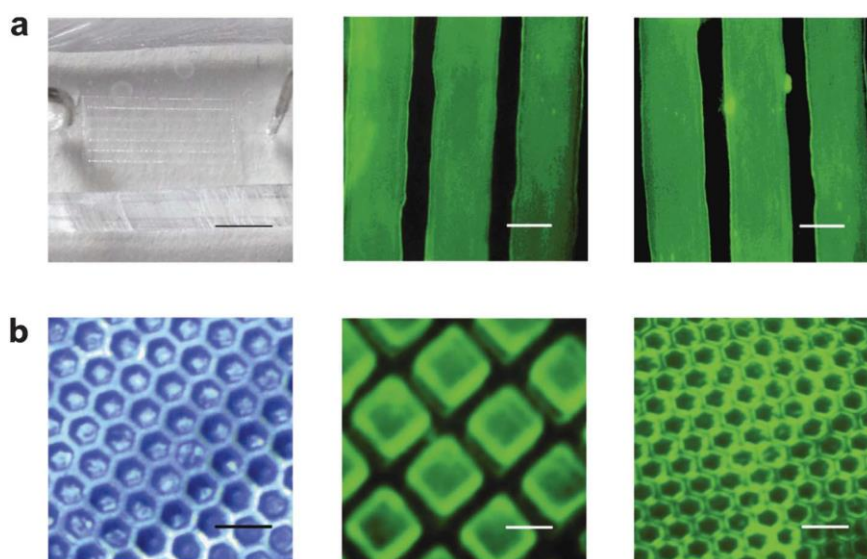
Fig. 8. (a) LSNNNLR phage displayed peptide binding to PDMS based microfluidic channels and microstructures (b). Scale bar: 50 µm [1].

The microfluidic channels exhibit strong fluorescent signals with the binding of both peptide-displaying phages (Fig. 8a middle) and bifunctional peptides (Fig. 8a right). Next, we investigated the binding of phage displayed peptides to PDMS micropatterned stamp, as shown in Fig. 8b. The fluorescent characterization shows that the peptide-displaying phages (Fig. 8b middle image) and bifunctional peptides (Fig. 8b right image) bind to the micropatterned PDMS effectively, and both of them show strong patterned fluorescent signals. Blank experiments with M13 phages binding to microfluidic channels

and micropatterns were investigated for fluorescent characterization, and no fluorescent signal was observed. This result clearly indicates that microstructures, including microfluidic channels and micropatterns, can map the binding of phage displayed peptides to PDMS.

The patterning of phage-displayed peptides with uniaxial wrinkle patterns was studied. As shown in Fig. 3a, a PDMS film was stretched with a uniaxial stretching strain and subjected to plasma oxidation to generate a hard silica layer on its surface (Fig. 3a, step 1), followed by releasing the strain form wrinkle patterns (Fig. 3a, step 2). Bringing the wrinkled PDMS surface into contact with a glass substrate coated with PDMS-binding phage-displayed peptides resulted in the patterning of phage-displayed peptides on the crests of the wrinkles (Fig. 3a, step 3). We investigated the fluorescent characterization of the binding of these PDMS-binding phage-displayed peptides to PDMS wrinkles. As shown in Fig. 9a, the crests of the wrinkle patterns showed much higher fluorescence intensity than the other part of the PDMS, owing to the binding of the phage displayed peptides or bifunctional peptide. The enhanced binding is attributed to the height of the wrinkles on the surface of the elastomer. This fluorescent differential was much larger than control experiments where we incubated PDMS-binding phage-displayed peptides on the entire surface of the PDMS wrinkles. In addition, a bifunctional peptide (LSNNNLRGGGGHPQ) with a PDMS-binding motif (LSNNNLR) and a streptavidin binding motif (HPQ) [16] was designed. Similarly, the bifunctional peptides were printed on the crests of the wrinkles. As shown in Fig. 9b, the bifunctional peptides bind to the

wrinkle crests effectively and generate clear fluorescent signals. The results suggest that phage-displayed peptides and the derived bifunctional peptides can be patterned non-lithographically via inducing elastomeric instability.
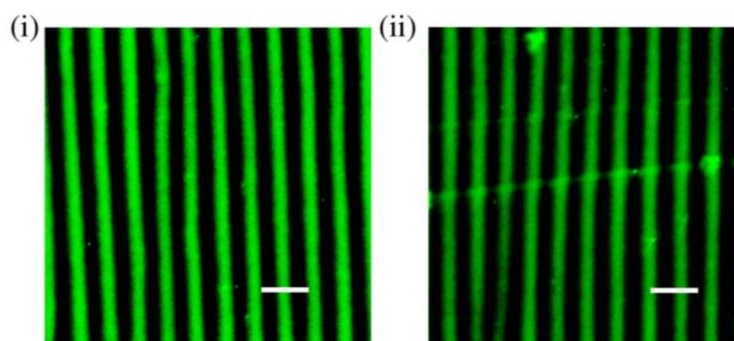
Fig. 9. Florescence characterization on wrinkled elastomer using (a) LSNNNLR and bifunctional peptide with HPQ (b). Scale bar: 10 μm [14].

Wrinkle patterns are generated by compressing the hard surface layer that is formed on the stretched PDMS film by plasma oxidation. By tuning the stretching strains imposed on PDMS wrinkles, the geometry of the patterned phage displayed peptides, which were bound to the crests of the wrinkles, can be tuned accordingly. We first studied the tuning of the patterned phage-displayed peptides on wrinkles with a 908 stretching strain to the direction of wrinkle lines. The amount and direction of the stretching strain are the same as those of the initial stretching strain. With the stretching strain, the PDMS wrinkles in sinusoidal wave disappeared and the surface became smooth, as shown in the optical image (Fig. 10a (i)). The phage displayed peptides were patterned on the wrinkle crests before

stretching. With the stretching strain, the phage-displayed peptides remained on the PDMS surface, confirmed by fluorescent characterization (Fig. 10a (ii)). The pitches of the fluorescent lines, which were bound with phage-displayed peptides, increased by approximately 25% compared with that of the initial wrinkles. Similarly, with a $0°$ stretching strain to the wrinkle lines, the width of the wrinkles and the pitch of the fluorescent lines decreased by approximately 18%, as shown in Fig. 10b.

Further, by using biaxial stretching strains on a stretched PDMS film, followed by plasma oxidation and releasing the strain, tuned wrinkles could be generated, and the phage-displayed peptide patterns could be tuned in accordance with the patterns of the wrinkles, as shown in Fig. 10c. These results indicate that tuning the geometry of the PDMS-wrinkled surface with external stretching strains could change the location of the phage-displayed peptides, and phage-displayed peptides can be patterned tunable on wrinkled elastomers.

Next, we studied the transfer-printing of phage-displayed peptides with wrinkled elastomers. The phage-displayed peptides for SiO_2 were identified, and phage-displayed peptide (HKKPSKS) was chosen for further study. The SiO_2-binding peptides did not bind to PDMS and can bind to SiO_2 specifically.
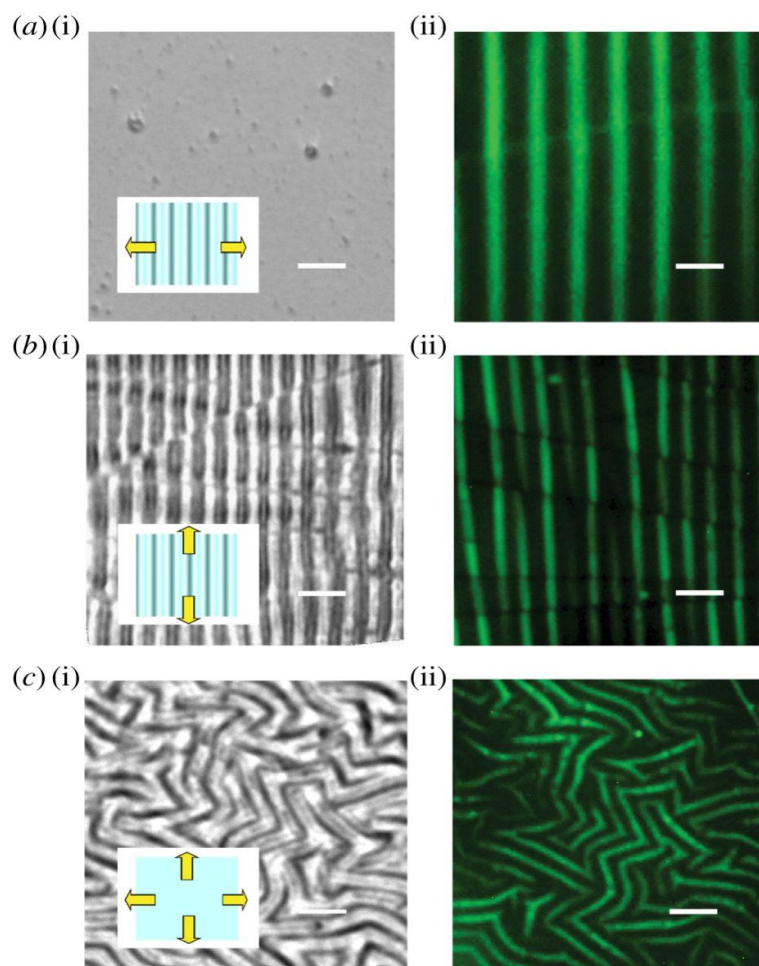
Fig. 10. Fluorescent characterization of phage displayed peptide on tunable wrinkled elastomer surfaces. Scale bar: 10 μm [14].

The SiO₂-binding peptides were brought into contact with PDMS wrinkles, and owing to the height difference of the wrinkles, the SiO₂-binding peptides stayed on the crests of the PDMS wrinkles. The peptide-immobilized PDMS wrinkles were further brought into contact with the SiO₂ surface, and the SiO₂-binding peptides on the crests of the PDMS wrinkles were in contact with and bound to the SiO₂ surface. Uniaxial PDMS and biaxial PDMS wrinkles were used as stamps for printing SiO₂-binding phage-displayed

peptides onto SiO$_2$. As shown in Fig. 11, the fluorescence characterization showed that the patterning of SiO$_2$-binding phage-displayed peptides on SiO$_2$ was in accordance with the structure of the PDMS wrinkles.
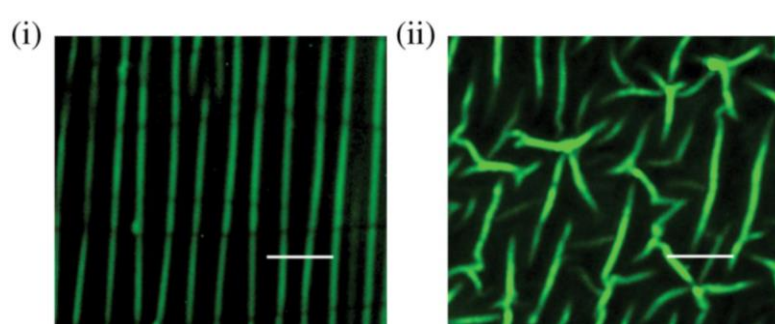
Fig. 11. Fluorescent characterization of phage displayed peptide printing (a) uniaxial and (b) biaxial on SiO$_2$ surface. Scale bar: 10 μm [14].

The results indicate that by using the elastomeric wrinkle patterns, phage-displayed peptides can be transferred from PDMS wrinkles to another substrate and the location of phage-displayed peptides are in accordance with the geometry of the PDMS wrinkle patterns.

Further, we studied the self-assembly of nanoparticles via specific peptides on spatially regulated wrinkled surfaces to develop multi-functional materials, as shown in Fig. 5. A bifunctional peptide, with a PDMS-binding motif (LSNNNLR) and a silver

synthesis motif (NPSSLFRYLPSD), was designed and synthesized. Incubating the PDMS-wrinkled surface with bifunctional peptide and silver nitrate resulted in the growth of silver nanoparticles on the entire PDMS-wrinkled surface in an uncontrolled way (Fig. 12 (i)), which showed an average diameter of 75.0+11.9 nm. Printing bifunctional peptides on the wrinkled surface with microcontact printing, followed by incubating with silver nitrate solution, enabled the formation of uniformly sized silver nanoparticles on the wrinkled surface (Fig. 12(ii)), which showed an average diameter of 64.8+11.8 nm.
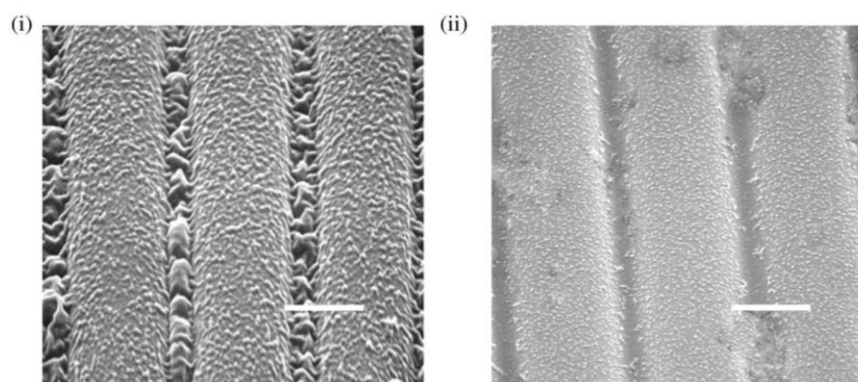
Fig. 12. SEM characterization of silver nanoparticles grown in-situ using bifunctional peptides (i) grown everywhere and (ii) by printing on the PDMS wrinkle surface. Scale bar:1 μm [14].

Contact angle analyses of PDMS surfaces were performed, as shown in Fig. 13. It can be seen that the bifunctional peptide-immobilized PDMS-wrinkled surface showed a hydrophilic water contact angle of 45°. After the self-assembly of nanoparticles, the PDMS

wrinkles containing both the bound bifunctional peptide and the synthesized nanoparticles show a hydrophobic water contact angle of 115°. This indicates that the presence of nanoparticles resulted in the change of hydrophobicity. The results suggest that phage-displayed peptides on elastomeric wrinkles can be used for the development of new hybrid materials.

(i)   (ii)
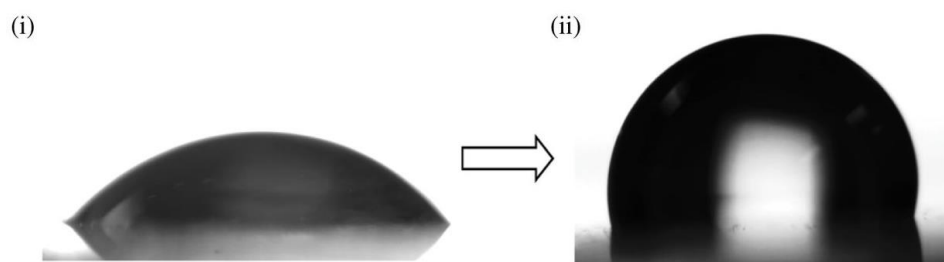
Fig. 13. Goniometer analysis of before (i) and (ii) after bifunctional silver peptide incubation on the wrinkled elastomer surface [14].

1.5.   Conclusion

In summary, we have demonstrated for the first time the recognition of PDMS with specific peptides identified from a combinatorial phage display library. We have also demonstrated non-lithographic patterning of phage-displayed peptides via inducing

elastomeric instability, which does not involve standard photolithography or e-beam lithography process. The method can result in controlled and tunable patterning of phage-displayed peptides on specific locations of wrinkled elastomer and other substrates (e.g. SiO2), and the development of hybrid materials via peptide enabled self-assembly nanomaterials on wrinkles. The approach we describe here may open new avenues for a variety of PDMS-based fundamental studies and practical applications, including biological analytical devices, self-assembly of PDMS-based hybrid materials, surface and interface, cell biology, etc. Although these results are promising, further studies are needed to help elucidate the mechanism of the peptides in recognizing PDMS, the properties of the peptide functionalized PDMS, effect of selectivity and strength of phage-displayed peptides on non-lithographic patterning and self-assembly.

CHAPTER 2

RECOGNITION OF EPOXY USING PHAGE DISPLAYED PEPTIDES [26]

2.1. Abstract

The development of a general approach for non-destructive chemical and biological functionalization of epoxy could expand opportunities for both fundamental studies and creating various device platforms. Epoxy shows unique electrical, mechanical, chemical and biological compatibility and has been widely used for fabricating a variety of devices. Phage display has emerged as a powerful method for selecting peptides that possess enhanced selectivity and binding affinity toward a variety of targets. In this letter, we demonstrate for the first time a powerful yet benign approach for identifying binding motifs to epoxy via comprehensively screened phage displayed peptides. Our results show that the epoxy can be selectively recognized with peptide-displaying phages. Further, along with the development of epoxy-based microstructures; recognition of the epoxy with phage displayed peptides can be specifically localized in these microstructures. We anticipate that

these results could open up exciting opportunities in the use of peptide-recognized epoxy in fundamental biochemical recognition studies, as well as in applications ranging from analytical devices, hybrid materials, surface and interface, to cell biology.

2.2. Introduction:

Epoxies are advanced thermosetting polymers, which exhibit excellent electrical [37], mechanical [38], and chemical [39] properties for a wide variety of applications as adhesives [40], protective coatings [41], electrical encapsulates [42] , pharmaceuticals [39, 43], etc. Recently, microstructured epoxies have attracted great interest in developing multi-analyte nanoarray sensors[44] and studying surface properties for designing biomimetic analogs [45]. To date, various surface functionalization methods for epoxy have been studied, such as silanization [46], and anchoring colloidal iron oxide nanocrystals [47]. This brings up the need for a benign approach for identifying binding motifs to epoxy via comprehensively screened phage displayed peptides along with the development of epoxy-based microstructures and recognition of the epoxy with phage displayed peptides can be specifically localized in these microstructures.

2.3. Experimental

Preparation of epoxy resin and epoxy based micropatterns: Epoxy (Epoxies, Cranston, RI) consisting of urethane isocyanate and urethane polyol, mixed with a weight ratio of 1:1.6 and cured at 120 °C for 30 min, was used for the biopanning process. Then the epoxy solution was diluted with acetone with a weight ratio of 1:5 and deposited on a glass slide (18 mm x 18 mm) with a spin coating at 7500 rpm for 2 min, followed by curing. The epoxy-coated glass was covered with stencil masks (TEM grids) and subjected to plasma etching at 100 W, 15 min to generate micropatterned epoxy [26].

Fluorescent characterization: Fluorescent characterization was accomplished by incubating the substrates sequentially with (1) the phage displayed peptides or M13 phages, (2) blocking buffer 0.1 M NaHCO3, 1% BSA, (3) anti-M13 phage coat protein monoclonal antibody, biotin conjugate E1 (for pIII coat protein of the M13 phage) (1 mg ml^{-}1), and (4) avidin–FITC (2 unit ml^{-}1), with TBS buffer washing steps in between to remove non-specific binding. The color intensity of the surface was observed through a fluorescence microscope.

Water contact angle measurement: An epoxy coated glass slide, and an epoxy coated glass slide bounded with phage displayed peptides, were each placed on the leveled

stage of the Goniometer to obtain the water contact angles. The contact angles were determined by fitting a Young–Laplace curve around the drop (Goniometer Sindatek Model 100 SB, Sindatek Instruments Co, Ltd, Taipei City, Taiwan).

2.4. Results and Discussion

After performing the combinatorial screening from a phage display library, specific peptides binding to epoxy were identified, as shown in Fig. 14a. Fig. 14b shows the peptide sequences screened from three rounds of biopanning. TLHPAAD appears as a dominant peptide from the biopanning process, with a frequency of 7/20. Interestingly, the results show that phage displayed peptide sequences exhibit high hydrophobicity, with low ratios of hydrophilic to total number of residues. A comparative analysis of the observed frequency of amino acids binding to epoxy and the frequency in NEB was also recorded in Fig.14c. In the phage display system, the peptides interact with the target surface either by hydrophobic or electrostatic interaction. Hydrophobic interactions occur at very high ionic concentrations while electrostatic interactions occur at low ionic strengths. Since our biopanning experiment was conducted at a moderate ionic strength (0.05 M Tris–HCl, pH 7.5, 0.15 M NaCl), a combined electrostatic and hydrophobic interactions contribute to the binding of phage displayed peptides to epoxy.

Num	Sequence	Freq	Hydrophilic Ratio
1	TLHPAAD	7/20	29
2	NERALTL	5/20	29
3	SHSGYFS	5/20	14
4	APTEHWA	2/20	25
5	HATRPPM	1/20	29
6	TFNFPPV	1/20	0
7	AETHINQ	1/20	29
8	TMHGYDT	1/20	29
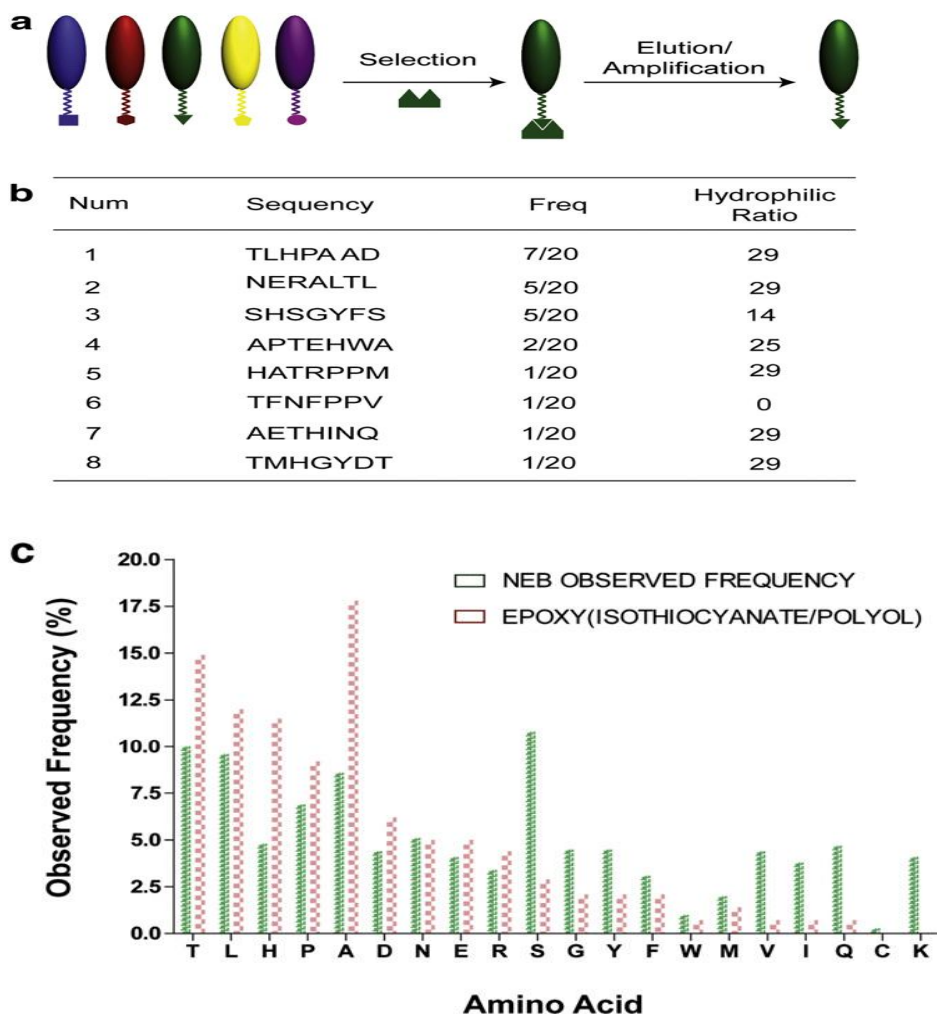
Fig. 14. (a) Schematic of the phage displayed analysis on epoxy surface. (b) Table showing the phage displayed peptides specific to epoxy surface, (c) plot analysis of the amino acids in the phage displayed peptide in comparison to the NEB library observed frequency [26].

In addition, the location of amino acids (charged, hydrophobic and polar) in the peptide sequence also plays an important role in the binding kinetics. The amino acids with hydrophobic groups (e.g. alanine and leucine) and amino acids with hydroxyl groups (e.g. serine, threonine and tyrosine) contribute to hydrophobic/hydrogen bonding interactions.

The presence of charged amino acids (e.g. aspartic acid, histidine, arginine and glutamic acid) contributes to the ionic interactions.

The dominant phage displayed peptide was also isolated as a single colony and selected for further investigation. First, the fluorescent characterization for the binding of TLHPAAD to a flat epoxy surface was investigated, as shown in Fig. 15a. Significantly, the surface with peptide-displaying phages shows much higher fluorescent intensity relative to the one incubated with M13 phages (without phage displayed peptides on the coat). The absence of phage displayed peptide on the coat of the M13 phage can be correlated to the absence of fluorescence on the surface of the epoxy. Thus, the phage displayed peptide is essential for binding to the epoxy surface.

The water contact angles of the epoxy resin before and after incubation with peptide-displaying phages were also investigated using a Goniometer. As shown in Fig. 15b, an epoxy surface has a contact angle of 75°, while an epoxy surface after incubation with the peptide-displaying phages shows a contact angle of 30°. The results suggest that the change of the surface behavior of the epoxy is due to the strong binding of phage displayed peptides to epoxy. Further, we investigated the localized binding of phage displayed peptide (TLHPAAD) to epoxy microstructures.

The epoxy microstructures on glass were generated by using stencil masks to cover epoxy, followed by plasma oxidation. The phage displayed peptides were then allowed to bind to these epoxy microstructures, and the bindings were characterized with fluorescent characterization, as shown in Fig. 16. Significantly, stronger fluorescent signals were observed localized on the epoxy patterns, relative to the glass substrate. This result clearly indicates that the microstructured epoxy in parts enhanced binding affinity toward phage displayed peptides over the host glass substrate.

Fig.15. (a) Fluorescent characterization of the phage displayed peptide TLHPAAD on the plain epoxy surface and control with no phage displayed peptide, (b) Goniometer analysis of the phage displayed peptide on epoxy surface. Scale bar: 20 μm [26].
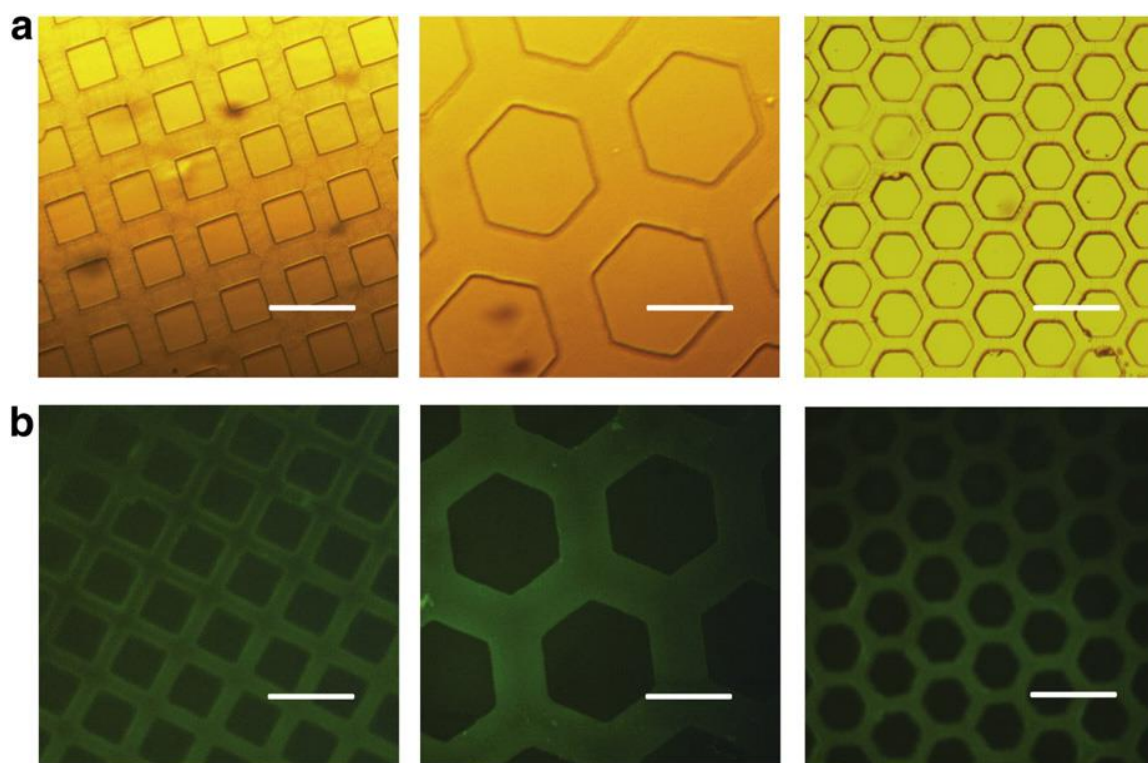
Fig. 16. Fluorescent characterization of TLHPAAD phage displayed peptide on epoxy microstructured surfaces (a) optical images and (b) fluorescent images. Scale bar: 50 µm [26].

2.5. Conclusion

In this work, we have demonstrated for the first time the recognition of epoxy with peptides identified from a biocombinatorial phage display screening. Further, we demonstrated the selective recognition of epoxy microstructures with the phage-displayed

peptides. The results may open new avenues in fundamental studies and practical applications, including biological analytical devices, self-assembly of epoxy based hybrid materials, surface and interface, cell biology, etc.

CHAPTER 3

RECOGNITION OF (POLY) ETHYLENETETRAPHTHALATE USING PHAGE -DISPLAYED PEPTIDES [48]

3.1. Abstract

A powerful yet benign approach for identification of binding motifs to (poly) ethylene tetraphthalate PET *via* comprehensively screened phage displayed peptides is demonstrated for the first time. These results show that PET can be selectively recognized with peptide-displaying phages and bifunctional peptides. Further, along with the development of PET-based micropatterns using photlithography, recognition of PET with phage displayed peptides can be specifically localized in these microstructures. In addition, bifunctional peptides were designed to induce the self-assembly of hybrid materials on the PET surface. These results are expected to open prospects in the fabrication of sensors, analytical devices and immunoassay studies.

3.2. Introduction

PET (Polyethylene Terephthalate) is a thermoplastic, polyester resin that is known for mechanical flexibility and sturdiness. It is being employed as a model substrate in sensors [49], flexible batteries [50, 51], thin film transistors [52], biological scaffolds [53], therapeutic protein release platforms, mechanical and optical applications [54]. Though PET is as such an inert polymer, surface functionalization [25, 55] or the assembling of composites [49] onto its surface has increased its reactivity and detection abilities. In the recent years, PET is being extensively used in the design of transparent conductive films by the immobilization of conducting fillers like carbon nanotubes onto surface modified PET films [49, 56]. The films are not only cost effective but also find use in the development of transparent electrodes [49], organic light-emitting diodes [57], liquid crystal displays [54, 58] and photovoltaic cells [59]. It is thus expected that recognising the phage displayed peptide specific to PET could create new avenues in the fabrication of novel devices and hybrid materials for various applications.

3.3. Experimental

Peptide recognition via Phage display: An aliquot of phage display library was

incubated with a 1cm/1cm PET film in Tris buffered saline containing 0.1-0.5% Tween-20 (TBST) for 1 h at room temperature. The PET film was then washed several times with TBST buffer. The phages were eluted from the film by addition of glycine-HCl (pH 2.2) for 15 min, neutralized with Tris-HCl, pH 9.1, amplified, and subjected to additional panning rounds. Eluted phages were then amplified in *E. coli*, and the panning was repeated for up to three rounds, under increasingly stringent conditions, to obtain phage clones expressing peptides having the highest binding affinities to the PET samples. After the final round of panning, DNA sequence analysis of the isolated phage clones yielded heptameric PET-binding peptides.

Fluorescent characterization of PET: A 1cm x1cm PET film was exposed to 10 μl of PET binding phage displayed peptides in TBS buffer for 0.5 h in a 35mm petri dish, followed by washing with TBS buffer, and incubated with 0.1 M $NaHCO_3$, 1% BSA, at pH 8.6 for 0.5 h in order to reduce the non-specific adsorptions of antibody and FITC on the substrate. Then, the surface was exposed to anti-M13 phage antibody (1 μg in 1.5 ml buffer) for 0.5 h with gently shaking, and then rinsed with TBS to remove the unconjugated antibody. Finally, avidin–FITC label (2.0 unit ml^{-1}) was applied to the biotin conjugated phage through a biotin–avidin interaction, and the surface was exposed to the FITC label for 0.5 h, and then rinsed several times with TBS to remove the unconjugated avidin–FITC label. The color intensity of the surface was observed by a fluorescence microscope (Microscopes, Inc., St. Louis, MO). A control experiment was also conducted with M13 phage without phage displayed peptides, following the above procedure.

Photolithography on (Poly) ethyleneterephthalate: A 3x5 cm PET film was fixed on glass to conduct photolithography using AZ 5214. The films were coated with HMDS at 4000 rpm and 45 s, followed by AZ 5214 at 2000 rpm and 30 s. The films were soft baked at 105 °C for 1 min and covered with a photomask. Exposure was done at 6 s using a UV source of 20 mJ/Wcm^{-2}. The films were finally developed for 1 min 30 s for further fluorescent characterization.

Fluorescent characterization on patterned (poly) ethylenetetraphthalate: A patterned PET film was exposed to 10 µl of PET binding phage displayed peptides in TBS buffer for 0.5 h in a 35mm petri dish, followed by washing with TBS buffer, and incubated with 0.1 M NaHCO$_3$, 1% BSA, at pH 8.6 for 0.5 h in order to reduce the non-specific adsorptions of antibody and FITC on the substrate. Then, the surface was exposed to anti-M13 phage antibody (1 µg in 1.5 ml buffer) for 0.5 h with gently shaking, and then rinsed with TBS to remove the unconjugated antibody. Finally, avidin–FITC label (2.0 unit ml^{-1}) was applied to the biotin conjugated phage through a biotin–avidin interaction, and the surface was exposed to the FITC label for 0.5 h, and then rinsed several times with TBS to remove the unconjugated avidin–FITC label. The color intensity of the surface was observed by a fluorescence microscope (Microscopes, Inc., St. Louis, MO).

Bi-functional peptide mediated silver nanoparticle synthesis on PET surface: A 1 cm x 1 cm PET film (both patterned and non-patterned) was incubated with 10 µl of 50

mM bifuctional peptide (PET binding motif) GGGGNPSSLFRYLPSD followed by 1.5 ml

of 30mM Silver nitrate solution in PBS buffer of pH 6 and 7 for 3 days in a 35 mm petri

dish. This was followed by washing with PBS pH 7.5 and distilled water and was blow

dried. This enabled the enabled the formation of uniformly-sized silver nanoparticles on

plain PET film. The silver nanoparticles were then characterized by an optical microscope

and Scanning electron microscope.

3.4. Results and Discussion

Analysis of the phage-displayed peptides that bind PET: A certain volume of phage

display library (New England BioLabs, Ph.D.7) of random 7-mer peptides was incubated

with the PET surface and then eluted from this substrate to collect the bound phage

molecules. These random 7-mer peptides have been appropriately designed by the

manufacturer to express in the specific pIII region of the filamentous phage molecule. An

aliquot of the diamond specific phage molecules were then amplified in *E. coli* (ER 2738)

followed by repeated centrifugation and PEG mediated (Polyethylene glycol) precipitation.

Finally, the refined libraries were prepared for DNA sequencing, which allowed for

identification of the diamond binding peptides. The phage displayed peptide is designed to

have an N-terminus being free and a C-terminus fused to the phage, which does not have a

free negatively charged carboxylate during biopanning. Fig. 17 shows the peptide sequences obtained from three rounds of biopanning.

S.No	Freq	Seq	Hyd ratio	pI	Charge pH 7	S.No	Freq	Seq	Hyd ratio	pI	Charge at pH 7
1	3/25	DEYCCNN	29	4	-2	12	1/25	HVTSVQT	14	7.9	1
2	1/25	IPYDNNQ	14	5.4	-1	13	1/25	ELLASPW	14	5.5	-1
3	1/25	AIVGTPF	0	7.8	0	14	1/25	YMGPASN	0	7.8	0
4	1/25	TIMEYRL	29	7.8	0	15	1/25	HAMRAQP	29	10.6	2
5	1/25	DEVKTIA	43	5.7	-1	16	1/25	TTNLDKA	29	7.8	0
6	1/25	ITLHMGM	14	7.9	1	17	2/25	LSNNNLR	14	10.6	1
7	1/25	HVPHPLL	29	7.93	2	19	1/25	SINAATS	0	7.8	0
8	2/25	NALVQIS	0	7.8	0	20	1/25	IDFTGAT	14	5.5	-1
9	1/25	MGTNS P	0	7.8	0	21	1/25	SYTTVVQ	0	7.8	0
10	1/25	YVATEIT	14	5.6	-1	22	1/25	FDTLKIL	29	7.8	0
11	1/25	YPGGYSR	14	9.2	1						

Fig. 17. Table of phage displayed peptides specific to (poly) ethylenetetraphthalate [48].

Two of the peptides DECYNN and NALVQIS were found to bind to the PET surface more frequently when compared to the other peptides which bind only once. As shown in Fig. 17, the natures of the peptides (with C-terminus amidated to avoid the free charge) were analyzed, including PI, net charge, average hydrophilicty, and ratio of hydrophilic residues to total number of residues. The PET-binding peptides obtained show a strong inclination towards hydrophobicity which is evident from the low average

hydrophilicity ratio of all the peptides. The isoelectric points and their corresponding net charge at pH 7.0 have also been analyzed in Fig. 17 .Majority of the peptide sequences carry no net charge / net negative and low net positive charge at neutral pH and also exhibit high values of pI.

Fluorescent characterization of PET- binding peptides: A 1cm x1cm PET film was exposed to 10 µl of PET binding phage displayed peptides (DEYCCNN / NALVQIS) were chosen for investigation. First, fluorescent characterization for the binding of these phage molecules to PET surfaces was investigated. This was accomplished by incubating the substrates sequentially to (1) amplified single-colony phage displayed peptide, (2) blocking buffer, (3) anti M13 phage coat protein- biotin conjugated monoclonal antibody, and (4) avidin-FITC, with buffer washing steps in between to remove non-specific binding. The intensity of FITC on the surface, which is a measure of the phage displayed peptides bound to PET, was observed by a fluorescence microscope as shown in Fig. 18. In addition to this, fluorescence characterization was also conducted using M13 phage alone without any phage displayed peptides, as a control, on PET surface as shown in Fig. 18.The absence of phage displayed peptide in the M13 phage can be correlated to the absence of fluorescence on the surface of both plain and plasma oxidized PET when compared to the ones obtained with phage displayed peptides on the PET surfaces. M13 phage without displayed peptides is incompetent to produce fluorescence as the displayed peptides are specific to PET. This concludes that the phage displayed peptides play an important role in determining the existence of fluorescence on PET.
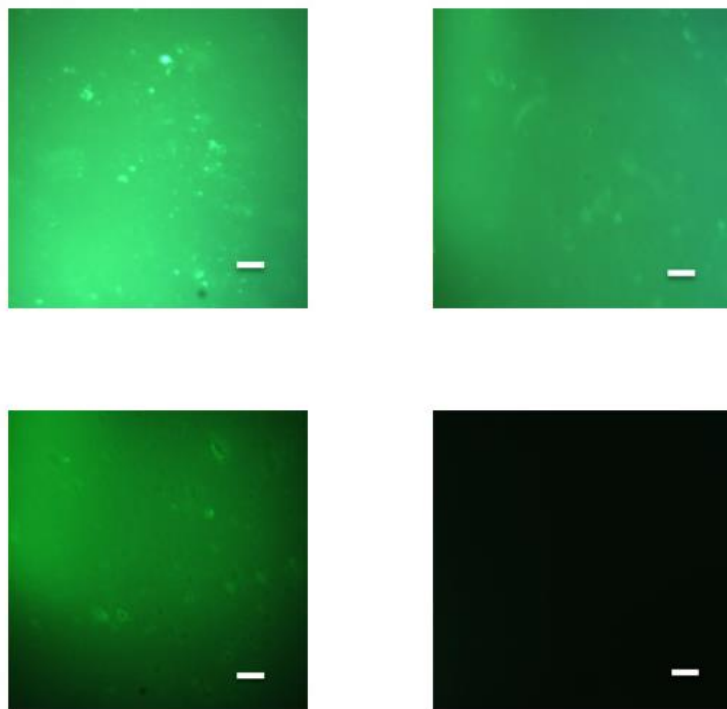
Fig. 18. Fluorescent characterization of PET binding phage displayed peptides (DEYCNN, NALVQIS, AIVGTPF and control from L to R). Scale bar: 10 μm [48].

Fluorescent characterization of PET binding peptides on patterned surface: A 3x5 cm PET film was exposed to 10 μl of PET binding phage displayed peptides (DEYCCNN) were chosen for investigation. First, fluorescent characterization for the binding of these phage molecules to PET surfaces was investigated. This was accomplished by incubating the substrates sequentially to (1) amplified single-colony phage displayed peptide, (2) blocking buffer, (3) anti M13 phage coat protein- biotin conjugated monoclonal antibody,

and (4) avidin-FITC, with buffer washing steps in between to remove non-specific binding. The intensity of FITC on the surface, which is a measure of the phage displayed peptides bound to PET, was observed by a fluorescence microscope as shown in Fig. 19.
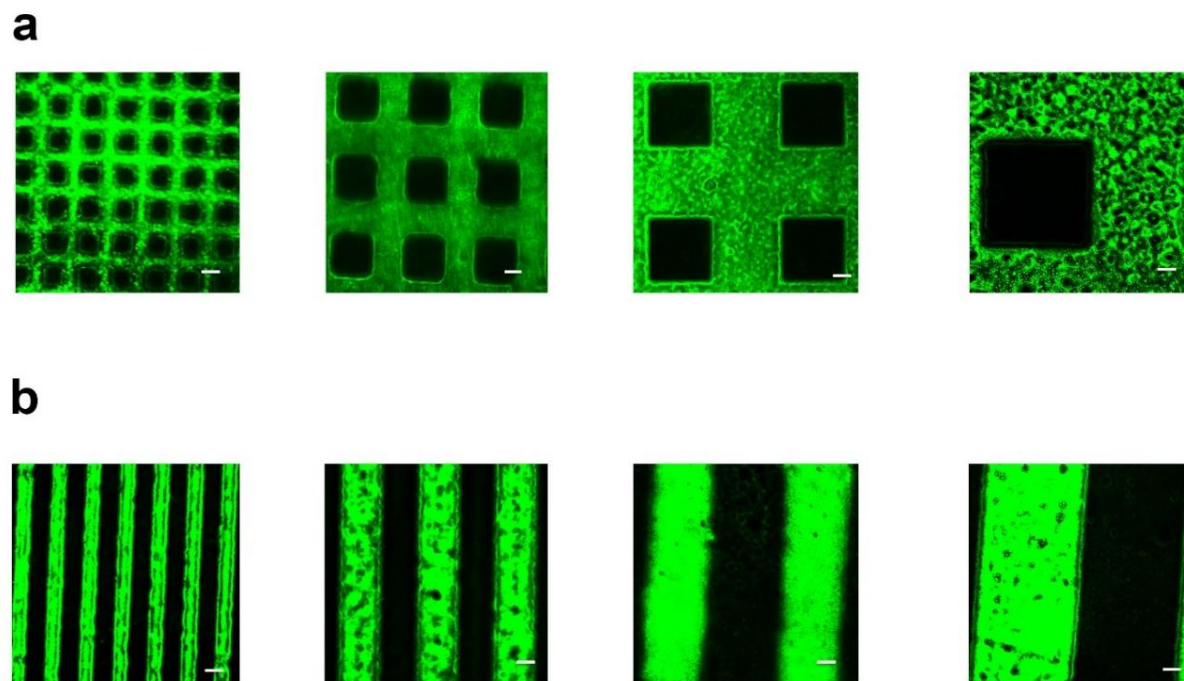
Fig. 19. Fluorescent characterization of PET specific phage-displayed peptide on patterned surface. Scale bar: 20 μm [48].

Bifunctional peptide enabled silver nanoparticle synthesis on PET surface: A 1cm x 1cm PET film (both patterned and non-patterned) was incubated with bifuctional peptide (PET binding motif) GGGGNPSSLFRYLPSD followed by silver nitrate solution in PBS buffer.
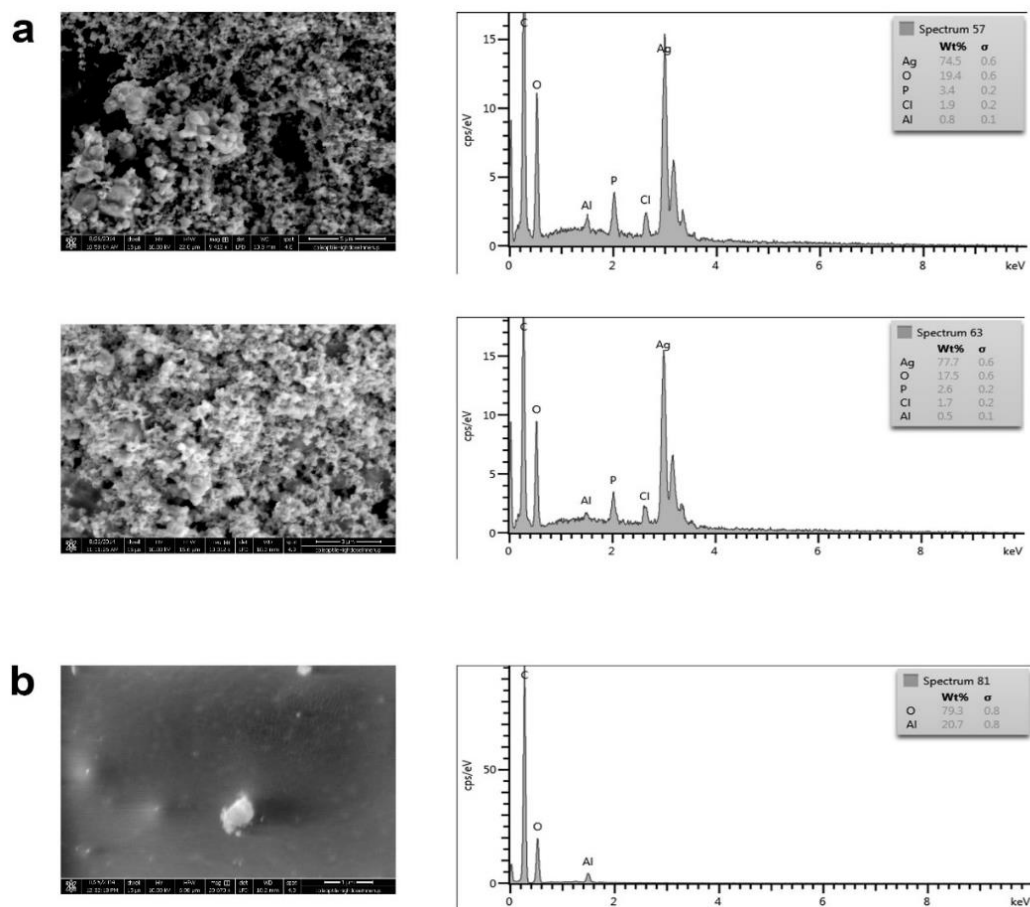
Fig. 20. SEM-EDX characterization of silver nanoparticles synthesized in-situ using bifunctional silver-PET peptide [48].

This enabled the enabled the formation of uniformly-sized silver nanoparticles on plain PET film. Fig. 20a shows the SEM characterization of growth of silver nanoparticles on the PET surface followed by the EDX measurement which shows an Ag percentage of over 70 while in the control (Fig. 20b) shows no Ag measurement at all. This proves that

the bifunctional peptide is specific to PET and enables the growth of silver particles on only those surfaces incubated with the peptide.

3.5. Conclusion

In summary, we have demonstrated for the first time the recognition of (poly) ethylenetetraphthalate with specific peptides identified from a combinatorial phage display library. The approach we describe here may open new avenues for a variety of PET-based fundamental studies and practical applications, including biological analytical devices, self-assembly of other PET-based hybrid materials, surface and interface, cell biology, etc. Although these results are promising, further studies are needed to help elucidate the mechanism of the peptides in recognizing PET, and the properties of the peptide functionalized PET.

CHAPTER 4

CHARACTERIZATION OF PEPTIDE NANOTUBES USING PHAGE DISPLAYED PEPTIDES [60]

4.1. Abstract

Bionanostructures built over precisely controlled molecular self-assembly on macrosurfaces have been finding wide applications in the area of bionanotechnology. Diphenylalanine aromatic peptide nanotubes are self-assembled nanostructures which have been gaining importance owing to their biocompatibility, mechanical rigidity, and inherent property of bio-recognition with unique physical and chemical stability. This study elucidates the characterization of peptide nanotubes using phage displayed peptides. Further, the most dominant peptide was chosen to build bifunctional peptides that can capture bacterial cells or synthesize silver nanoparticles on localized peptide nanotube surfaces. These chemically functionalized surfaces can be employed in the designing of electrodes, energy storage and several other applications.

4.2. Introduction:

Peptide nanotubes are desirable organic building blocks for various bionanotechnological applications owing to their chemical flexibility [61, 62], biocompatibility [63], biological recognition abilities [64], thermal [65], and mechanical stability [66] that enable them to hierarchically assemble themselves into useful devices [67]. Self -assembly at the molecular level is the central basis of bottom up fabrication of bulk devices with well-defined nanosturutures [67]. This structural organization of these cyclic peptides into nanotubes is mediated by the non-covalent interactions between the amino acid residues [68]. These devices can find use as biosensors [69, 70], energy storage devices [71], in tissue engineering [72], environmental monitoring [73], and various other applications [74].

Peptides are versatile, combinatorial amino acid sequences that are widely being used as recognition motifs. Being chemically diverse (hydropathy, acidity etc.), they can be modified accordingly to bind to specific target molecules on a defined substrate [75]. Peptides can be synthetically tailored to harbor certain molecules to form conjugate peptides that aid in binding to the specific target and also help in the formation of intricate hierarchal self- assemblies of different target molecules [76].

The fabrication of diphenylalanine based peptide nanotube composites using phage displayed peptides that act as nanoscaffolds for bottom-up hierarichal assembly is highlighted. The biocompatibility of the dipeptides combined with phage display peptides that mediate the self-assembly of silver nanoparticles or bacterial cells serve as effective analytical devices.

4.3. Experimental

Preparation of Peptide nanotubes and phage display: The peptide nanotubes H-Phe-Phe-OH was purchased from Bachem (Torrance, CA) and NH2 -Phe(D)- Phe (L)-COOH from Peptide 2.0 (Chantilly, VA) and 1,1,1,3,3,3 hexaflouro 2-proponol (Matrix Scientific, Columbia, SC). The peptide nanotubes were grown by dissolving the lyophilized powder in 1, 1, 1, 3, 3, 3 hexaflouro-2-proponol to a final concentration of 100mg/ml and left to grow for 1 hr. A volume of 10 µl of phage display library (New England BioLabs, Ph.D. 7, 10^{13} pfu ml^{-1}) in 1.5 ml Tris.HCl (50 mM, pH 7.5) and NaCl (150 mM) buffer solution (TBS) with 0.1%tween-20, was incubated on the surface of PDMS for 1 h in 35 mm petri dish, then eluted from the substrate with 1.5 ml glycine-HCl +1%BSA (0.2 M, pH 2.2) and neutralized with 1 M Tris-HCl buffer at pH 9.1. The eluted phages were incubated with a SiO$_2$/Si substrate for 1 h, to conduct negative screening of the phages which bind only to this substrate, followed by amplification in 20 ml of a 1:100

dilution of log phase *Escherichia coli* (ER 2738) grown in sterile LB media at 37 °C for 4.5 h Phage particles were precipitated from the supernatant through the addition of 1/5 of the volume 20% (w/v) PEG-8000, 2.5 M NaCl. The phage pellet after centrifugation was resuspended in 1 ml TBS. This purification and precipitation processes were repeated and finally the phage molecules were suspended in 0.2 ml TBS. The entire "biopanning" process was repeated a total of three times, using TBST buffer with tween-20 ranging from 0.1%, 0.3% to 0.5% in every rotation of selection. After the third round of panning, the refined libraries were prepared for DNA sequencing to identify the peptides specific to peptide nanotubes. Following the third round of panning, bacteria was mixed with dilutions of the eluted phage Sequencing of the DNA samples was performed in Eton Bioscience (San Francisco, CA).

Fluorescence characterization of the peptide nanotubes: A SiO_2 wafer containing the grown peptide nanotube solution was exposed to 10 µl of Peptide nanotube binding phage displayed peptides in TBS buffer for 0.5 h in a 35 mm petri dish, followed by washing with TBS buffer, and incubated with 0.1 M $NaHCO_3$, 1% BSA, at pH 8.6 for 0.5 h in order to reduce the non-specific adsorptions of antibody and FITC on the substrate. Then, the surface was exposed to anti-M13 phage antibody (1 µg in 1.5 ml buffer) for 0.5 h with gently shaking, and then rinsed with TBS to remove the unconjugated antibody. Finally, avidin–FITC label (2.0 unit ml^{-1}) was applied to the biotin conjugated phage through a biotin–avidin interaction, and the surface was exposed to the FITC label for 0.5 h, and then rinsed several times with TBS to remove the unconjugated avidin–FITC label.

The color intensity of the surface was observed by a fluorescence microscope (Microscopes, Inc., St. Louis, MO), followed by characterizations.

AFM characterization of the phage-displayed on the peptide nanotube surface: Peptide nanotubes were grown in HFP at 2 mg/ml for 30 min in shaking condition. A SiO_2 wafer containing the grown peptide nanotube solution was exposed to 20 µl of peptide nanotube binding phage displayed peptides in TBS buffer for 1 h in a 35mm petri dish followed by washing with TBS buffer and distilled water. This was then used to characterize the phage on peptide nanotube using Atomic force Spectroscopy.

Bi-functional peptide mediated bacterial adhesion and fluorescence on peptide nanotube surface: *Escherichia coli O157: H7* Kwik-sticks and Anti- *E.coli O157: H7* biotin antibody was purchased from Fisher Scientific (Pittsburg, PA). *E.coliO157: H7* overnight culture was centrifuged and diluted in 2 ml of 50 mM PBS buffer of pH 7.5. A SiO_2 wafer was bacteria characterized with 10 µl of the *E.coliO157: H7* overnight culture for 30 min in 1.5 ml of 50 mM of PBS pH 7.5, followed by 30 µl of the grown peptide nanotube solution was incubated with 10 µl of 50 mM bifuctional peptide (PNT binding motif) GGGGGIGKFLHSAGKFGKAFVGEIMKS, then 1.5 ml of 0.1% Blocking buffer, 1 µl of Anti- *E.coliO157: H7* antibody diluted in 1.5 ml of 50 mM PBS buffer pH 7.5 and finally incubated with 10 µl FITC-streptavidin diluted in 1.5 ml of 50 mM PBS buffer pH 7.5. The color intensity of the surface was observed by a fluorescence microscope.

Bi-functional peptide mediated silver nanoparticle synthesis on peptide nanotube surface: A SiO$_2$ wafer containing 30 µl of the grown peptide nanotube solution was incubated with 10 µl of 50 mM bifuctional peptide (PNT binding motif) GGGGNPSSLFRYLPSD followed by 1.5 ml of 30 mM Silver nitrate solution in PBS buffer of pH 6 and 7 for 3 days in a 35 mm petri dish. This was followed by washing with PBS pH 7.5 and distilled water and was blow dried. The silver nanoparticles were then characterized by an optical microscope and Scanning electron microscope [14].

4.4. Results and Discussion

Phage-displayed analysis of peptide nanotube surface: Peptide nanotubes were grown in the HFP solution at 2mg/ml for 1 h. The peptides specific to binding to peptide nanotubes were sequenced and analyzed. Fig. 21 shows the peptide sequences obtained from three rounds of biopanning. As shown in Fig. 21, the natures of the peptides (with C-terminus amidated to avoid the free charge) were analyzed, including PI, net charge and average hydrophilicty. The Peptide nanotube-binding peptides obtained show a strong inclination towards hydrophobicity which is evident from the average hydrophilicity ratio of the two peptides. The isoelectric points and their corresponding net charge at pH 7.0 have also been analyzed in Table 1. All the peptide sequences carry a net positive charge at neutral pH and also exhibit high values of pI. From the table, it is observed that Leucine

and Asparagine are the most commonly binding amino acids with RHLLLNQ being the
most dominant peptide.

Number	Frequency	Sequence	Avg. Hyd. ratio	Isoelectric point	Net charge at pH7
1	10/15	RHLLLNQ	29%	10.55	2
2	2/15	MTGNHNS	14%	7.87	1
3	1/15	SFSLKNW	14%	9.69	1
4	1/15	GERHYPQ	14%	7.87	1

Fig. 21. Table of phage displayed peptides specific to peptide nanotubes [60].

The dominant peptide (RHLLLNQ) was also isolated as a single colony and
selected for fluorescent investigation. This was accomplished by incubating the peptide
nanotube substrate sequentially to (1) amplified single-colony phage displayed peptide, (2)
blocking buffer, (3) anti M13 phage coat protein- biotin conjugated monoclonal antibody,
and (4) avidin-FITC, with buffer washing steps in between to remove non-specific binding.
The intensity of FITC on the surface, which is a measure of the phage displayed peptides
bound to peptide nanotubes, was observed by a fluorescence microscope as shown in Fig.

22. In addition to this, fluorescence characterization was also conducted using M13 phage library and without any phage displayed peptide as a control.

The absence of phage displayed peptide in the M13 phage can be correlated to the absence of fluorescence on the peptide nanotube surface when compared to the ones obtained with phage displayed peptides on the PNT surfaces. M13 phage is incompetent to produce fluorescence as the displayed peptides are specific to PNT surfaces. This concludes that the phage displayed peptides play an important role in determining the existence of fluorescence on PNT.
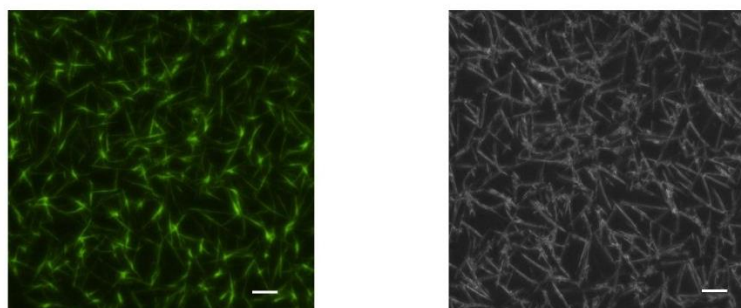
Fig. 22. Flourescent characterization of PNT surface (L) and control with no phage displayed peptide (R). Scale bar : 20 μm [60].

AFM characterization of the phage-displayed on the peptide nanotube surface: Peptide nanotubes were grown in the HFP solution at 2 mg/ml for 30 min. A SiO_2 wafer

containing the grown peptide nanotube solution was visualized using atomic force microscope. The surface of the overlapping peptide nanotubes of 2 micron width were visualized for the phage visualization. The phage was found to be 800 nm long and 10 nm high. The surface of the peptide nanotubes showed several phage particles on its surface. The nearby silicon dioxide did not show any phage particles which showed that the binding of the phage displayed peptide was specific to the peptide nanotube surface as shown in Fig. 23.
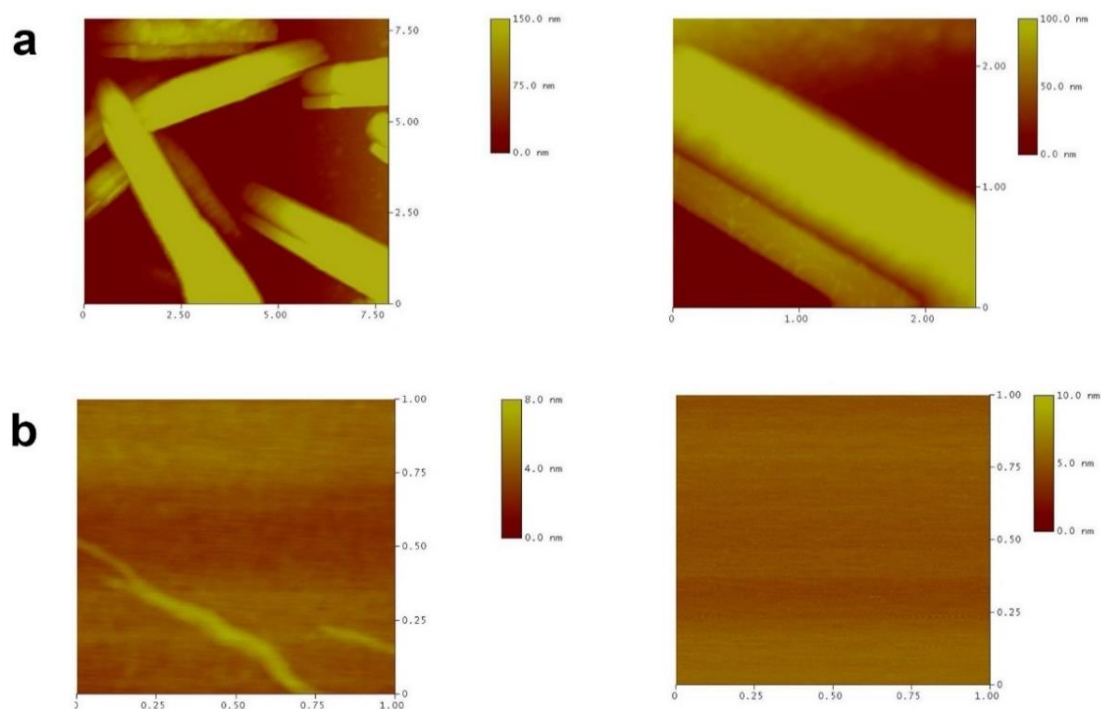
Fig. 23. AFM characterization of the phage displayed peptide on peptide nanotube surface . (a) peptide nanotubes on silicon dioxide, (b) phage on peptide nanotube surface, (c) silicon dioxide surface with no phage control [60].

Bi-functional peptide mediated bacterial adhesion and fluorescence on peptide nanotube surface: E.coliO157: H7 was incubated with the bifunctional peptide and peptide nanotubes on SiO_2 surface. This was then visualized using an optical microscope, it was found that the bacteria was around 500nm in width and 700nm in length. A fluorescence characterization was also conducted to confirm the absence of the bacteria on SiO_2 surface. It was seen that only the peptide nanotubes were fluorescent and not the surrounding SiO_2. Another fluorescent characterization was conducted without the bifunctional peptide which showed no fluorescence as there was no adherence of bacteria on the peptide nanotubes. A second control was conducted using another type of bacteria Lactobacteria lactis (purchased from Fisher Scientific Pittsburgh, PA) which also showed the absence of fluorescence, indicating no binding of the bifunctional peptide with the round shaped bacteria. The above results highlight the importance of the bifunctional peptide's role in obtaining the bacteria to bind on the peptide nanotube surface.

Bi-functional peptide mediated silver nanoparticle synthesis on Peptide Nanotube surface: An in situ silver nanoparticle synthesis was conducted in the presence of the bifunctional peptide (RNLLLHQ) and 30m M silver nitrate solution. Since the nanotubes get very easily washed off the surface after three days of incubation in the silver nitrate solution, the SiO2 surface was coated with a layer of Su8 and cured for 6 min. When the coated Su8 layer is still sticky, the peptide nanotubes solution was dropped onto the SiO2 surface and heated at $200°C$ for 10 min.
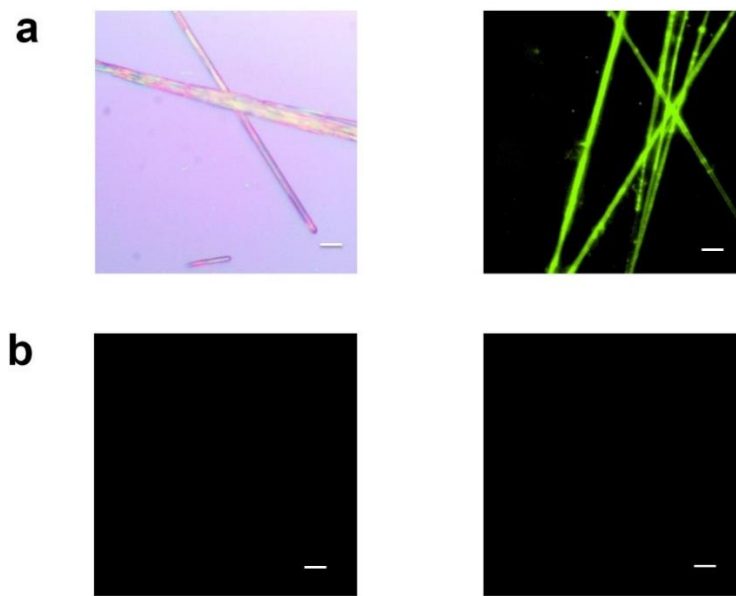
Fig. 24. Flourescent characterization of the bifunctional peptide mediated bacterial adhesion on peptide nanotube surface. (a) optical (L) and flourescent image (R) and (b) controls (L) no bifunctional peptide and L. lactis on peptide nanotube surface (R). Scale bar : 20 µm [60].
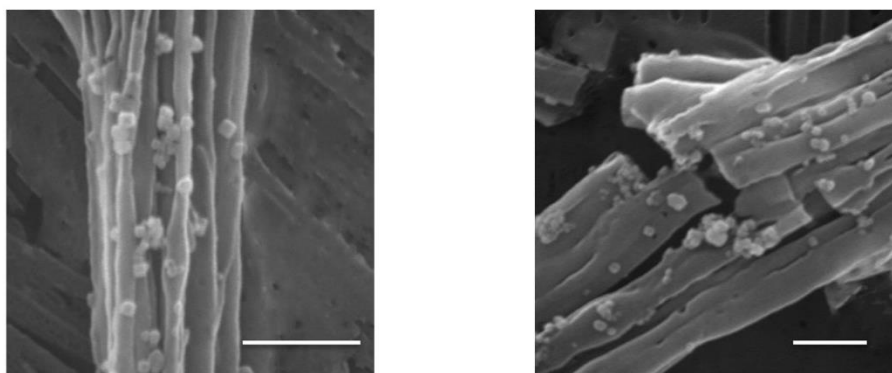
Fig. 25. Silver bifunctional peptide mediated growth of silver nanoparticles on peptide nanotube surface. Scale bar: 500nm [60].

The SiO$_2$ with the peptide nanotubes was then incubated with the bifunctional peptide for 30 min in a shaker at 70 rpm and then later transferred to a petri dish containing 2 ml silver nitrate solution and left in a dark room on a shaker for 3 days. These were then visualized under an optical microscope and scanning electron microscope as shown in Fig. 25. The silver nanoparticles synthesized had an average diameter of 150.0±16.8 nm, which was determined using Jimage.

4.5. Conclusion

In summary, we have demonstrated for the first time the recognition of peptide nanotubes with specific peptides identified from a combinatorial phage display library. The approach we describe here may open new avenues for a variety of PNT-based fundamental studies and practical applications, including biological analytical devices, self-assembly of other PNT-based hybrid materials, surface and interface, cell biology, etc. Although these results are promising, further studies are needed to help elucidate the mechanism of the peptides in recognizing PNT, and the properties of the peptide functionalized PNT.

PART II

MICROFABRICATION

CHAPTER 5

1-D, 2-D AND 3-D NANOSTRUCTURES IN SILK FIBROIN VIA TRANSLATION OF INDUCED ELASTOMERIC INSTABILITY [77]

5.1. Abstract

The development of a facile approach for fabricating a library of precisely positioned nanostructures offers exciting opportunities in fundamental research and practical applications. The current top-down nanofabrication methods have been restricted in accessibility in standard labs due to their due to the high cost and complexity. Likewise, bottom-up synthesis of nanowires has been limited in methods for positioning these structures at precisely defined locations. Nanostructured silk fibroin is a promising candidate for a variety of applications that merge the fields of biomedical optics and biomaterials due to silk fibroin being one of the strongest, transparent and biocompatible materials. A novel fabrication method which requires only a simple etching tool to generate a library of 1-D, 2-D, and 3-D silk fibroin nanostructures in a large area via inducing elastomeric instability, pattern transfer and controlled etching is reported in this study. The patterning method could also be used for fabricating a wide range of

nanostructures in other materials such as semiconductors, metals, and biomaterials. It is anticipated that the large scale nanopatterning with hierarchical assembly of functional materials could open exciting opportunities in fundamental biochemical recognition studies, as well as applications ranging from sensors to energy storage devices.

5.2. Introduction

Nanostructures exhibit unique and extraordinary surface [78-80], electronic [81, 82], photonic [83], mechanical [82], and thermal [84, 85] properties compared to bulk surface properties. Many of these applications require nanostructures to be patterned over large areas at precisely defined locations. Thus, to generate nanostructures for practical applications, it is highly desirable to develop a fabrication method that is high-throughput, low-cost, easy-to-perform, and capable of generating highly ordered nanostructures on a large-scale area. Recently, a variety of conventional and unconventional nanofabrication methods have been developed for generating nanostructures at precisely defined locations, including e-beam lithography [86], superlattice nanowire pattern transfer [87], lithographically patterned nanowire electrodeposition [88], photolithography and etching for nanoscale lithography, nanoskiving, and nanoindentation lithography, and the nanostructures generated by these methods can also function as molds/masters for further

transferring the nanostructures into other materials or substrates. However, these methods require state-of-the-art facilities, high-cost, time-consuming experiments.

Recently, spontaneous formations of surface pattern [32, 89-91] have attracted great attention and have been investigated under a variety of methodologies. Typically, poly(dimethyl siloxane) (PDMS) is thermally [92] or mechanically stretched, followed by exposure to oxygen plasma [92, 93], argon plasma [89], flame, or UV ozone [94], to form a thin, hard layer on the surface. The typical resulting wrinkle patterns resulting after a release in strain are easy to fabricate and range from ~50 nm up to several micrometers.

Silks are natural protein polymers that represent a unique family of biopolymers due to their novel structural and biological properties. They offer unlimited opportunities for functionalization, processing and biological integration [95, 96]. Silk fibroin from *Bombyx mori* silkworm cocoons, is one of the strongest fibers in nature, and has attracted significant recent interest due to its remarkable biocompatible and surface properties [95, 96]. Silk can find a wide range of applications in biophotonics [97, 98], holograms [99-101], diffraction patterns [102], microlens arrays [103], medical implants [104, 105], and drug delivery [106-108]. Dried silk film can be dissolved in water reversibly. With treatment by methanol, heat, etc., silk crystalline structures can also be made insoluble in water [109-117].

Nanoimprint lithography and soft lithography have recently been developed for the generation of silk nanostructures [97, 116]. However, a mold of nanostructures in silicon (Si) is always required, since fabrication of Si mold uses high end techniques. However, these methods suffer the disadvantages of requiring capital equipment, small-scale fabrication, and time-consuming processes. Thus, a simple and rapid method for large-scale, low-cost fabrication of silk nanostructures is highly desirable.

5.3. Experimental [77]

Generation of PDMS wrinkle: PDMS prepolymer and curing agent (Sylgard 184) were thoroughly mixed at a weight ratio of 10:1, followed by degassing for 20 min and curing at 80° C for 2 h. A PDMS film is stretched by 25% with a uniaxial stretching strain, followed by exposure to oxygen plasma for 1.5 min at 80W to generate 400-500 nm sized wrinkles.

Transfer of PDMS wrinkle to PMMA surface: SiO_2 wafer was coated with 4 %PMMA in chlorobenzene at 2000 rpm for 30 s to generate a 200-300 nm thin film. Similar results were obtained using a glass slide; however a SiO_2 wafer shows distinct color changes when coated and provides visual cues for etching efficiency in later steps. This

film was dried at 60^0 C for 10 min. A capillary lithography was conducted by placing the PMMA coated wafer samples facing upward on a glass slide with the PDMS master facing the wrinkles. Drops of ethanol were added on top of the glass slides to enable solvent-assisted transfer of patterns. This was left in the oven for 15 min at 60^0 C. The wrinkles were exactly repeated onto the PMMA surface which was observed in the optical microscope as shown in Fig. 26. The wrinkles were then subjected to plasma oxidation at different times to generate different sized wrinkles. After capillary lithography, the wrinkles are completely transferred onto the PMMA wrinkles creating a replica of the PDMS master. This was then subjected to plasma oxidation at different times, to observe the generation of the ribbons.
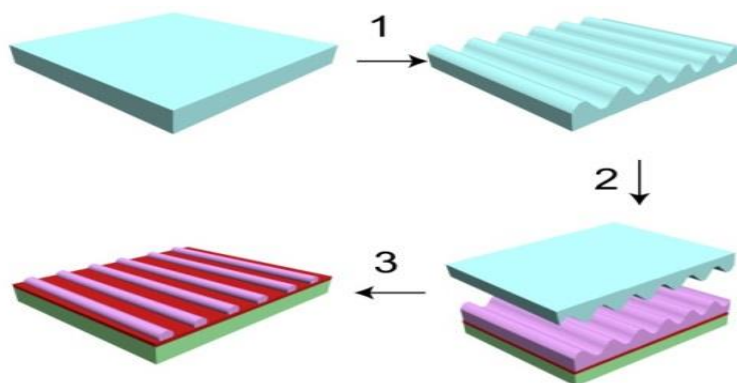
Fig. 26. Schematic of the capillary lithography transfer of the wrinkles onto the PMMA surface [77].

Generation of silk nanoribbons: A SiO_2 wafer was first coated with 1:10 diluted silk produced from *B. mori* cocoons, at 3000 rpm and 45 s to produce a thin silk film of nearly 50 nm thick and dried at 60 °C for 5 min. This was followed by coating with 4% PMMA in chlorobenzene and later dried 60 °C for 5 min. Capillary lithography was conducted by placing the PMMA or silk-coated wafer samples facing toward the PDMS master containing wrinkles and drops of acetone were added on top of the glass slides to enable solvent-assisted transfer of patterns. This was left in the oven for 15 min at 60 °C. The PMMA film with the wrinkles was then subjected to plasma oxidation at 80 W for 2.5 min to generate the wrinkle hills. The remaining PMMA was washed away using acetone to reveal the silk nanoribbons. For the methanol treated silk nanoribbons, the wrinkle hills were first generated, then treated with methanol to treat the silk in the areas beside the hills and finally washed with acetone and water to remove the PMMA and non-methanol treated silk as shown in Fig. 27.
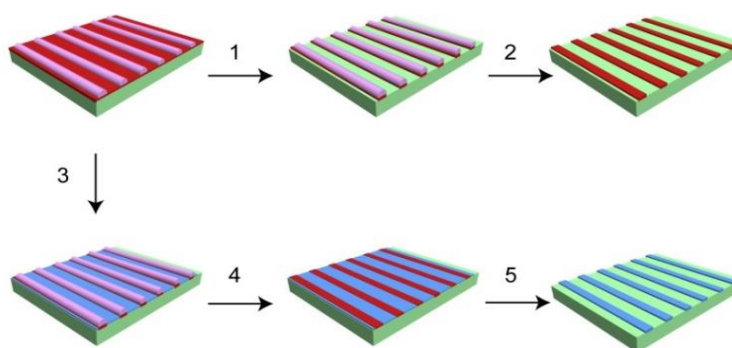
Fig. 27. Schematic of the generation of 1D silk ribbons (treated/ untreated with methanol) [77].

Generation of silk 2-D nanoribbons: Silk 1D ribbons were first created and treated with methanol before re-coating the silicon dioxide surface with silk. A capillary lithography was conducted at 90° to the original direction of ribbons for 15 min at 60°C as shown in Fig. 28. The spin coating rate of silk for both the layers is 3000 rpm and 45 s to generate a thickness of 50 nm.
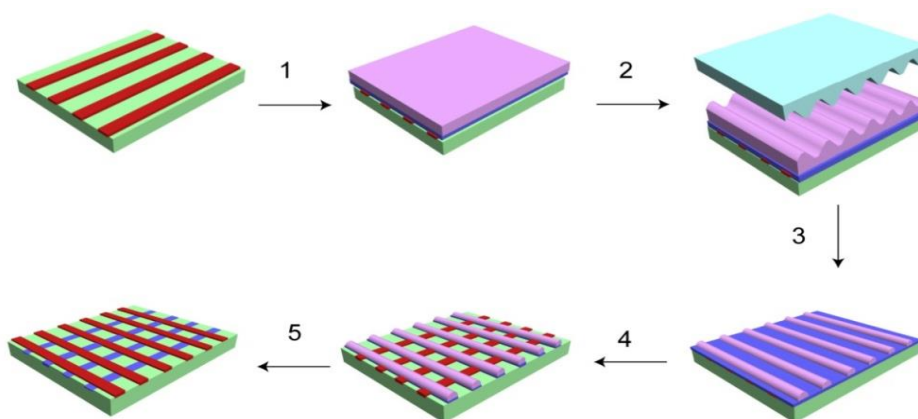
Fig. 28. Schematic of the generation of 2D silk nanoribbons [77].

Generation of silk-3D ribbons: A SiO$_2$ wafer was first coated with 1:20 diluted silk at 3000 rpm and 60 s to produce a thin silk film of nearly 50 nm thick and dried at 60^0 C for 5 min. The patterns were transferred directly onto the silk membrane by a process similar to the capillary lithography with acetone as the solvent but this was conducted at 160 ^{0}C for 15 min. Another method was also adopted to cause pattern transfer onto the silk

substrate by placing it in vacuum for 15 min and drops of water was used here instead of the acetone.
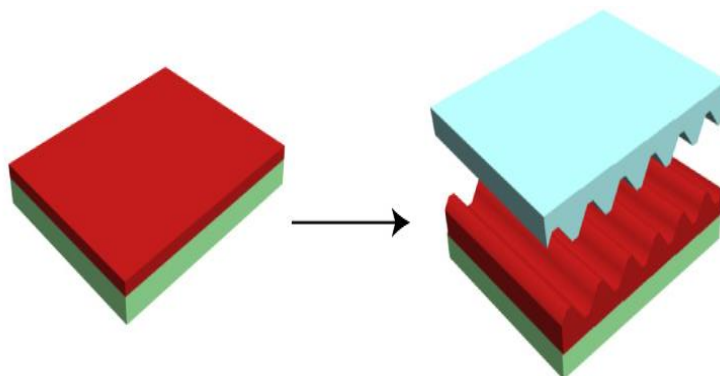
Fig. 29. Schematic of the generation of 3D silk nanoribbons [77].

Generation of wrinkles on silk fibroin Film: A PDMS template was subjected to 25% uniaxial stretching strain for 1 min 30 s and 80 W, silk (0.2 mg/ml) was poured onto the PDMS template and left to dry for 1-2 days. The silk was then peeled off the template mechanically by dipping in methanol for 20 min and using a razor blade. The peeled silk film contains the required wrinkles.

5.4. Results and Discussion

The transfer of PDMS into a thin film of resist is a key step for the generation of silk nanoribbons, since it will function as a mask for the silk layer. We will first investigate the generation of PMMA nanoribbons. Fig. 26 outlines the process for generating a template in PMMA from wrinkled PDMS. A PDMS wrinkled elastomeric substrate is generated via stretching a PDMS film, followed by plasma oxidation and releasing the stretching strain (step 1). A wafer is spin-coated with a thin film of poly (methyl methacrylate) (PMMA). The PDMS with wrinkle patterns serves as a master to transfer the patterns onto the PMMA via capillary force (step 2). Thus, the PMMA film will show a sinusoidal wave structure on silk, which is followed by reactive ion etching (RIE) to narrow the width of the PMMA ribbon and open a window for the underlying layer (silk). The initial thickness of the PMMA layer is controlled by the spin or dip coating process and provides the basis for desired etching exposure times for the material. Thicker material layers require additional etching to remove the trough areas of the sinusoidal wave leaving the crest areas to produce nanoribbons. To preserve the pattern transferred into the material, a balance of etching time and material thickness should be observed. Fig. 30 shows the AFM images of PDMS wrinkles and the wrinkles transferred on PMMA, and it shows that the width of the wrinkle pattern is 1.0 μm nm, and the height of the wrinkle patterns are 200 nm. The wrinkle patterns in PMMA are negative patterns of those in PDMS. With further plasma etching of PMMA, the height and width of PMMA ribbons were narrowed. With an etching time of 30 s, the pattern begins to define large ribbon structures with a

width of nearly 500 nm and a height of 200 nm, similar to the dimensions of the initial PMMA wrinklesobtained after capillary lithography. Larger intrastitial holes were created when the PMMA wrinkles were subjected to etching at 60 s and 90 s to produce 300 nm and 200 nm width ribbons but the PMMA still remained unetched in most parts of the wafer. On further etching the wrinkles separated from one another to produce very clear ribbons at 150 s and 210 s of 100 nm and nearly 60 nm widths respectively as shown in Fig. 1c. With an etching time longer than 2 min 10 s, it was seen that the wrinkles were entirely etched away leaving no trace of PMMA on the wafer surface. This is a clear indication of the effect of oxidation on the wrinkles width, which shows that with the increase in the time of oxidation a reduction in the width of wrinkles is observed. Therefore, at very long periods the wrinkle width becomes narrower and eventually disappears from the SiO_2 surface. A nearly proportional decrease in PMMA wrinkle width, nearly 50 %, is observed as oxidation time increases every minute until the 2min 10s mark after which additional etching completely removes the pattern from the surface. The resulting nanoribbons are thus tunable by altering the etching times and can achieve a variety of widths dependent on etching time and the thickness of the PMMA layer.

Finally, biaxial patterns were created by transferring the patterns created on PDMS that has been simultaneously stretched on both directions. The biaxial PMMA wrinkles were characterized by AFM before and after oxidation as shown in Fig. 31.
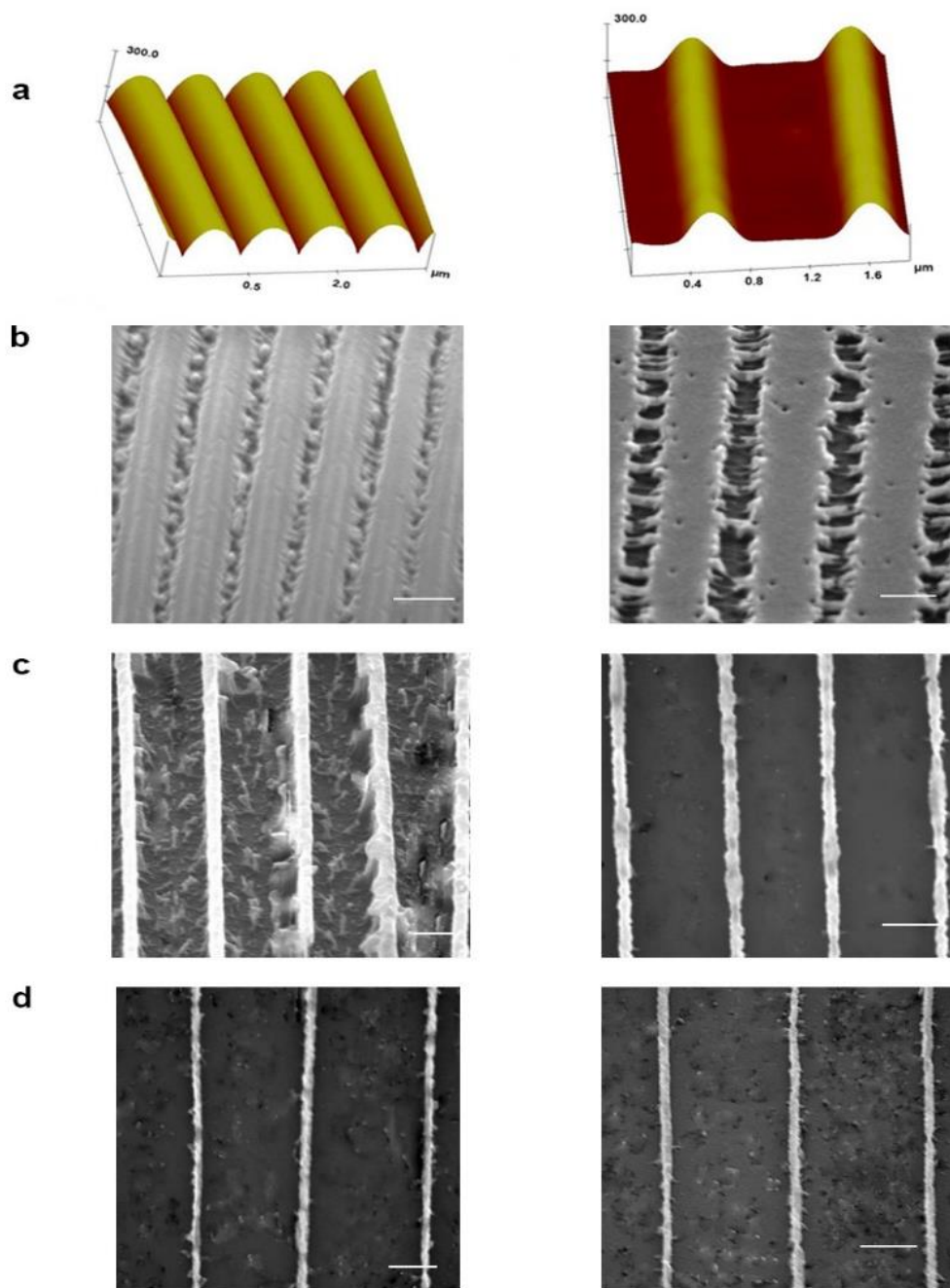
Fig. 30. PMMA based nanoribbons generated at different times of etching conditions. (a) capillary lithography (b)30 s and 1 min of etching (c) 2 min and 2min 30 s, (d) 3 min 30 s of etching times. Scale bar: 500 nm [77].

The use of pre-generated wrinkle patterns transferred through capillary lithography allowed for controlled etching, thereby removing the areas between the wrinkles leaving easily controlled nanoribbons with widths dependent on etching time.
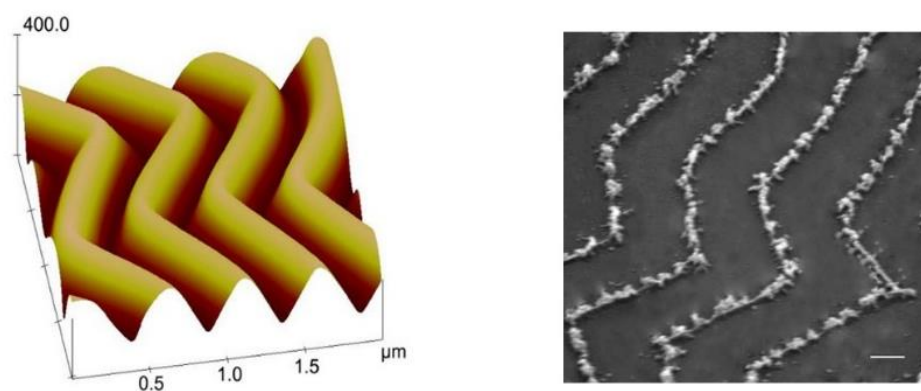
Fig. 31. Biaxial PMMA patterns on SiO$_2$. Capillary (L) and after etching for 3 min 30 s (R). Scale bar: 500nm [77].

Next, we will investigate the translation of PMMA nanoribbons into the underlaying silk layer. Through the use of solvents and the selectively-soluble polymers, PMMA and silk fibronin, surface geometries were successfully modified to generate a nanoribbon with controllable 1-D dimensions. Fig. 27 outlines the process for producing silk nanoribbons with tunable 1-D surfaces. Step 1 is the creation of PMMA wrinkles where the wrinkle pattern from the PDMS was transferred onto the PMMA surface by capillary lithography, holes were created by etching the PMMA surface for 45 s. Step 2 is the creation of the silk nanoribbons by using the PMMA wrinkles as a mask and etching at

120 s to result in nearly 100 nm structures. Utilizing a solvent that would selectively dissolve only the PMMA, in Step 3 the surface was further washed with acetone to remove the PMMA layer while preserving the silk layer on the wafer. Step 3 is washing the surface with acetone, a solvent that selectively dissolves PMMA but does not affect the underlying silk layer, to remove the PMMA mask and result in silk Fibroin nanoribbon structures. Step 3 starts with the pattern transfer onto PMMA via capillary lithography, followed by etching to create holes in the PMMA layer exposing the underlying silk layer. In Step 4, the exposed silk regions were treated with methanol to strengthen the β sheet structure of the silk protein, thereby making it insoluble in water whereas the untreated silk fibroin solution is capable of being dissolved in water. Upon additional etching, the methanol treated silk areas are etched to appropriate widths for nanoribbons. In step 5, the entire sample is washed with acetone followed by water to remove all the PMMA and untreated silk leaving only the methanol treated silk nano-ribbons.

The PMMA film acts as a mask containing the wrinkle patterns and the silk retains the pattern after the PMMA mask is removed to produce the ribbons. The silk nanoribbons thus generated are equidistantly oriented on the silicon dioxide surface of width ranging 60-80 nm and a height of 50 nm. AFM characterization being shown in Fig. 32a and the SEM characterized image in Fig. 32a. Biaxial patterned silk ribbons were also created by transferring the PDMS patterns obtained by stretching on both directions following the same Experimental as silk one-dimensional nanoribbons. The AFM and SEM characterization images are shown in Fig. 32b.

The next aim was to decrease the lability of the silk nanoribbons by inducing a chemical change in the underlying silk film. A methanol treatment was employed to decrease the water soluble properties of the silk film and the resulting nanoribbons. The areas of Silk coated with the PMMA are untreated with methanol due to the PMMA mask and remain water soluble and are removed during the washing process. These methanol treated ribbons are 60-80 nm wide and 150 nm high, where both AFM and SEM characterizations are shown in Fig. 32c.

It can be understood that durable nanoscale ribbons can be generated using silk which, after treatment with methanol, can remain stable without dissolving in various solvents including water for a long period. We hypothesize that the use of additional chemical treatments could further increase or decrease solubility resistance, opening new possibilities of timed dissolution of nanoribbons and other nanostructures. This can be further applied in designing systems where water based buffers and solutions are used for various applications like bio sensing; surface and interface studies; and so on.
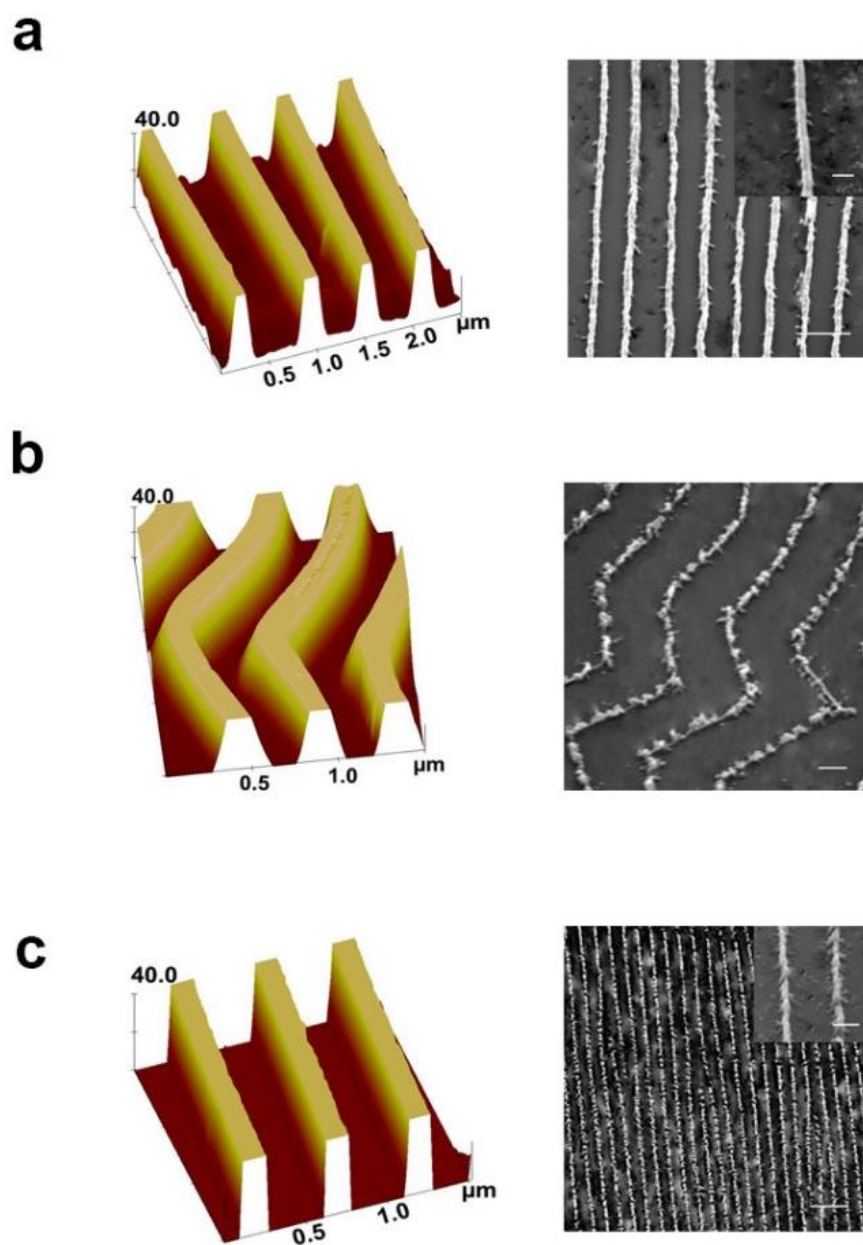
Fig. 32. 1D nanoribbons generated on silk. (a) uniaxial ribbons, Scale bar: 500 nm (Inset: 120 nm) (b) biaxial ribbons, Scale bar: 500 nm, (c) methanol treated ribbons, Scale bar: 1μm (Inset : 200 nm) [77].

The efficient generation of more complex nano-scale geometries continues to be a sought after goal, including tunable 2-D nanoribbon patterns. After the generation of silk one-dimensional structures, the generation of silk two-dimensional nanoribbons was investigated. Fig. 28 outlines the schematic for the fabrication of two-dimensional structures. Silk 1D nanoribbons were first generated on a SiO_2 wafer as described in the above Experimental and then treated with methanol for 5 min to decrease water solubility. This methanol treatment is done to avoid the ribbons dissolving in the second silk layer, which is applied in an aqueous solution over the existing structures. The second layer of silk and PMMA were coated on the created silk 1D nanoribbons and the PDMS master was placed at 90° to the original nanoribbon orientation during capillary lithography for pattern transfer. This was then subjected to careful etching for 150 s ensuring only the PMMA holes are created and the underlying layers are protected. The PMMA is removed by washing the surface with acetone to reveal the second layer of silk nanoribbons. The second layer of silk nanoribbons, thus produced, is perpendicular to the original layer of silk nanoribbons and are about 100 nm in width as shown in Fig. 33 (left).

A series of box patterns were also created in the above mentioned directions by etching away the nicks between the ribbon overlaps. The silk layer layering the methanol treated silk ribbons become more susceptible to etching, as the water from the silk layer seeps into the methanol silk making it more susceptive to be removed much easier than the surrounding ribbon areas as shown in Fig. 33b.

a　　　　　　　　　　　　　**b**
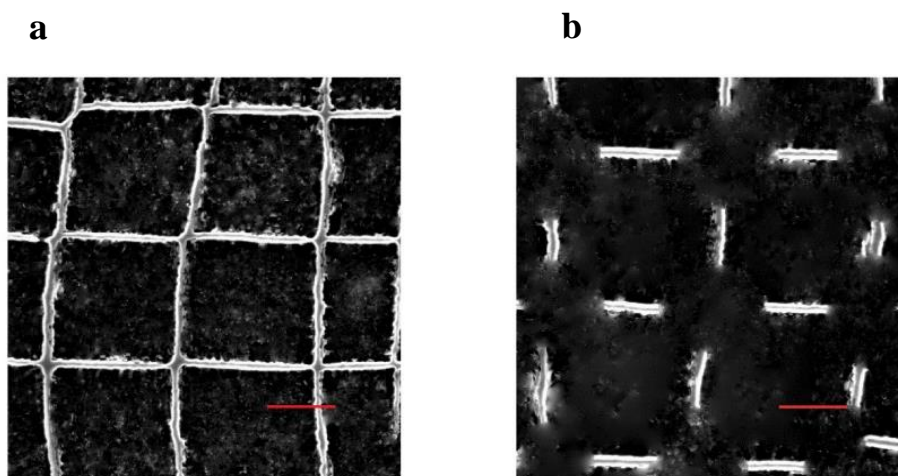
Fig. 33. 2D silk nanostructures (a) and box patterns (b). Scale bar: 500 nm [77].

On further etching, the surface silk ribbons get etched faster leaving just short lines or boxes of the methanol treated silk as seen Fig. 33b. The generation of 2-D structures introduces several new techniques to be explored with different pattern masks and selectively-soluble polymers to produce other nanoribbon geometries and patterns. This type of tunable, controlled patterning that result in precise, well-organised structures has been finding wide applications in various fields.

Further, we will explore the generation of 3D silk nanoribbons. Fig. 29 depicts the schematic of the production of three dimensional silk nanoribbons. First the pattern transfer is transferred from PDMS to silk coated on SiO_2 either in oven or under vacuum, followed by plasma oxidation for 120 s similar to the PMMA wrinkles. Fig. 34a shows the silk 3-D

wrinkle transferred from the PDMS template before plasma oxidation. Fig. 34b shows the silk 3D nanoribbons created after etching at 100 s, both the AFM and SEM characterizations. The results indicate the creation of well organized, wave-like wrinkle patterns on the surface of the silk layer using controlled etching conditions. The silk 3D nanoribbons generated after plasma oxidation were found to be 50 nm high and nearly 100 nm in width. The 3-D nanoribbons also show a width of nanoscale, but in the spatial, it shows a hill-like structure, instead of a flat ribbon.
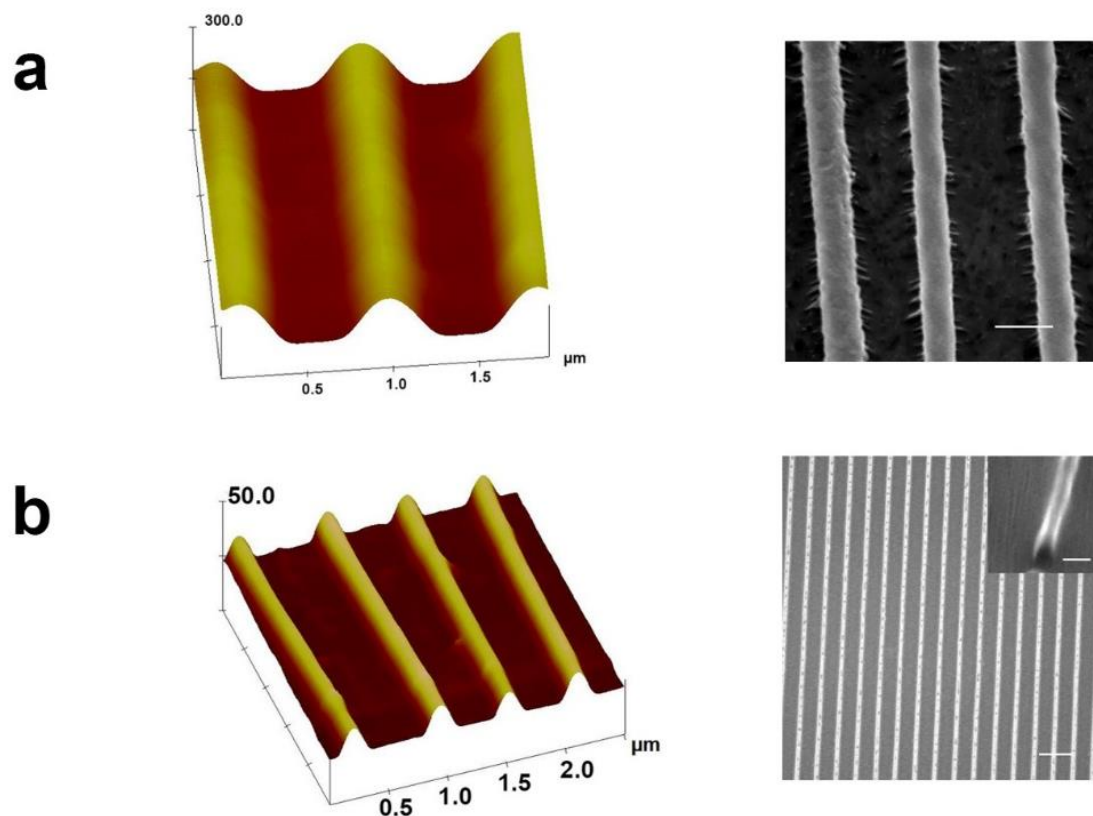
Fig. 34. 3D silk nanostructures (a) capillary lithography Scale bar: 1 μm and (b) after etching for 2 min, Scale bar: 2 μm (Inset : 150 nm) [77].
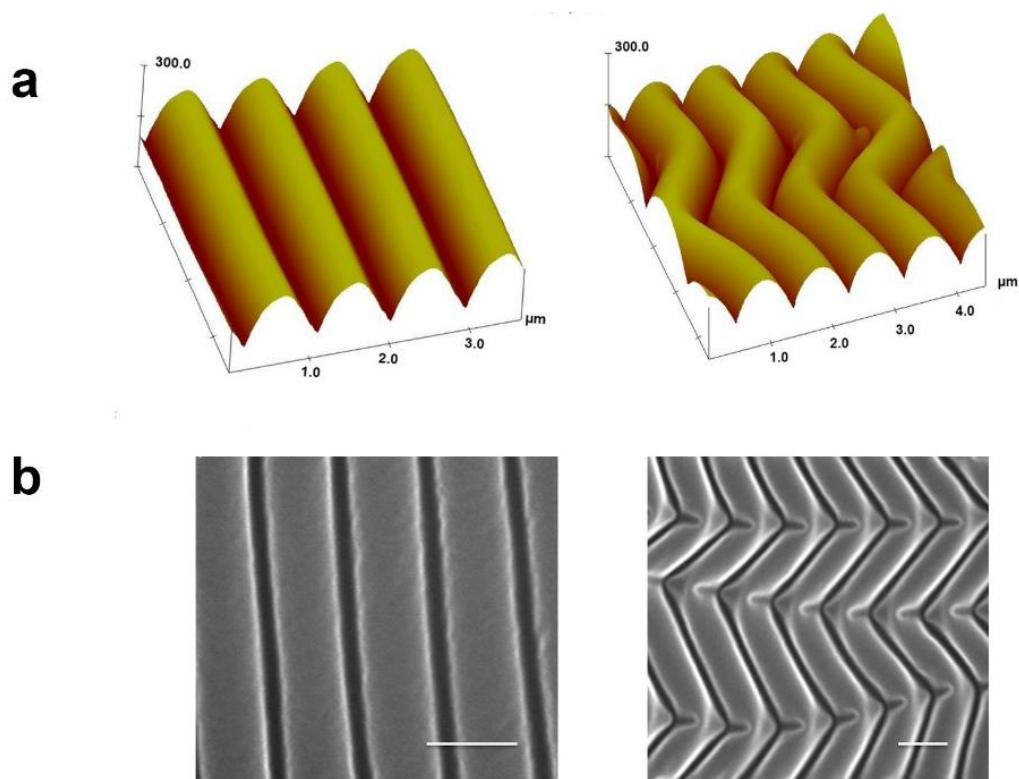
Fig. 35. Uniaxial and biaxial silk film containing the wrinkles (a) AFM characterization and (b) SEM characterization. Scale bar: 1μm [77].

Another method was employed to produce the wrinkles, both uniaxial, were produced directly on silk film. This was achieved by producing a PDMS template stretched uniaxially and subjected to plasma oxidation at 80 W and 2 min to produce 1μm wrinkles of 200 nm height. Raw silk was then poured onto this PDMS template and left to dry for 1-2 days. This silk film was then mechanically peeled off the template to reveal both uniaxial and biaxial wrinkles as shown in Fig. 35. The same was repeated by bending the

PDMS in convex and concave directions to produce the silk film containing the wrinkles with the bent directions as shown in Fig. 36.
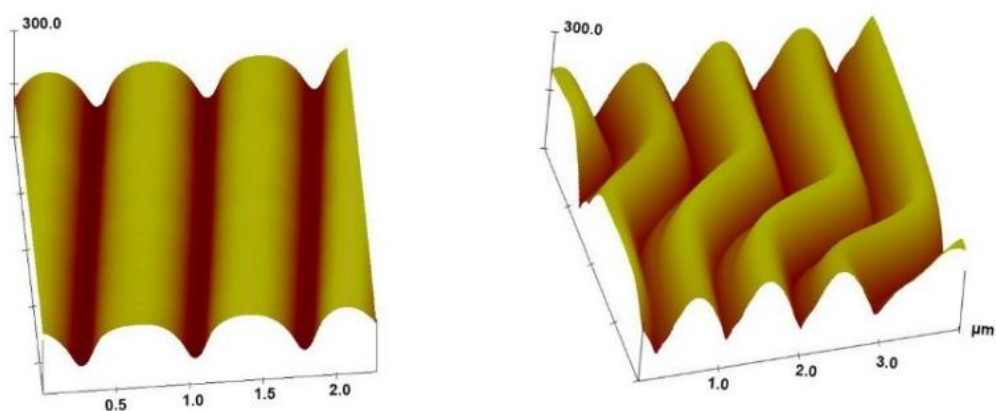
Fig. 36. Convex bending of wrinkles silk film (L) and concave bending of wrinkles replicated into a silk film (R) [77].

One recurring problem of ribbons being lost in between was noticed, when subjected to higher etching conditions making the pinch greater between the nanowrinkles. The results indicate that by transferring directly from PDMS with controlled etching, a nanoscale structures in silk can be generated with similar dimension ratios. Using a variety of different master patterns additional 3-D nanostructures can be generated allowing for a more complete spatial differentiation of dimensions on a nanoscale. Additional

investigation is needed on the limits of feasible patterning with the lithographic methods outlined above. However, promising results of efficient nanopattern control and tunability contribute to several exciting and potential applications.

5.5. Conclusion

In summary, we have successfully created a library of nanostructures in silk fibroin via translation of induced elastomeric instability. Our approach is transformative in that it will create a new process for fabricating a variety of micro/nanostructures in diverse materials at precisely-defined locations without using lithographic techniques. The method will also use this process for fabricating silk nanostructures which can process unique properties for applications in optical sensors, optical waveguides, tissue engineering scaffolds, and neural electrode arrays. This is a radical paradigm shift away from standard lithographic fabrication. The approach is a facile method involving controlled etching and pattern transfer, and the fabrication process is simple, easy to perform, low cost, and rapid. The interaction among materials instability, materials transfer and materials etching invents a new fabrication technology process. The method will also fill critical gaps in understanding the interactions between materials instability, pattern transfer and controlled

etching for creating this new fabrication technology process, and will advance our fundamental knowledge of non-lithographic nano-manufacturing.

CHAPTER 6

FABRICATION OF MAMMALIAN HAIR BASED MICROFLUIDICS[118]

6.1. Abstract

The development of a simple approach for the generation of microstructures could expand opportunities in both fundamental studies and practical applications. Mammalian hair is a filamentous biomaterial which is mechanically strong, flexible, abundant, and easily harvested. It is demonstrated for the first time a simple generation of microfluidic channels from mammalian hairs. Our results show that hairs with different widths result in the generation of microfluidic channels with different widths. Furthermore, with different textures of hairs, the shape of microfluidic channels can be varied. Finally, the utility of this microfluidic channel for bioassays and micro wire synthesis is analyzed. It is anticipated that these results could open exciting opportunities for investigating a variety of biological materials to fabricate micro/nano-structures and devices for fundamental studies, as well as applications ranging from biological analysis to materials synthesis.

6.2. Introduction

Microfluidics is of interest for a wide spectrum of applications due to their high-throughput and low-cost mass fabrication and has been finding use in electronic devices [119, 120], optical devices [121, 122], bioanalysis [123, 124], cell biology [125, 126], and materials synthesis [127, 128]. It is based on the capillary system owing to the reduced consumption of reagent quantities in analysis, making it prominent in the field of bioanalysis. The fabrication of microfluidic devices were first conducted in into silicon [129, 130] and glass [131] which involves expensive processing procedures. Polydimethylsiloxane (PDMS) is a biocompatible silicon elastomer that has been widely used for the fabrication of microfluidic devices through soft lithography due to its low cost, less time consuming and facile prototyping and manufacturing. The PDMS based microfluidic channels are widely generated by replicating a master via soft lithography that is created by photolithography or other high end techniques involving expensive facilities [132, 133]. Therefore, it is highly desired to find masters that are easily available, inexpensive and less time consuming. Recently, several low cost options have been studied for the fabrication of microfluidic channels, including ink-jet printing on shrinky- dinks [134, 135], paper and thread based microfluidics [136, 137]. However, these methods do not offer micrometer sized channel resolution which inhibits additional applications like microwire synthesis and bio-analysis [118].

Hair is proteinaceous biological composite material which is formed heirarchicaly via intermediary fibrils, from α- keratin chains. Hair is usually found in mammals, with a resolution ranging from 10 to 100 μm, with different geometries, varying morphological components and diameters [138, 139]. The hydrophobic nature of hair along with its internal hydrophilic amino acid residues attributes to its mechanical strength and in addition makes it malleable into different shapes for different applications. Hair is naturally available in abundance and hence eliminates the need for any expensive manufacturing techniques [140].

6.3. Experimental [118]

Fabrication of microchannels from hairs: PDMS prepolymer and its curing agent (sylgard184) were thoroughly mixed at a weight ratio of 10:1, followed by degassing in vacuum for 1 h. Hair was selected and then cut to a desired length and fixed on to a flat surface with an adhesive tape between the hair and the surface to prevent curling. Then the degassed PDMS was poured over the hair. After curing at 80^0C for2 h, the PDMS slab can be peeled from the hair easily, as hair is hydrophobic in nature, resulting in a microchannel. After drilling holes at both ends of the channels and sealing the PDMS elastomer on to glass, microfluidic channels were generated.

Immunoassay: The channels fabricated from hairs were incubated with 100 mg ml^{-1} of rabbit Ig G for 15 min. Next, the channels were incubated with bovine serum albumin blocking solution for 30 min. Finally, they were incubated with 25 mg ml^{-1} of anti-rabbit IgG conjugated with fluorescein isothiocyanate dissolved in the buffer solution. Washing steps were performed in between each step. The fluorescent signals were characterized with a fluorescent microscope.

Live yeast cell analysis: The microfluidic channels were fabricated from hairs as described above in a line pattern and sealed onto glass. Upon completion of fabrication these channels were flushed with deionized water for 5 min to clean the channels of any contaminants. Following this, the yeast cells Saccharomyces cerviseae and Saccharomyces pombe were allowed to flow through the channel for 20 s. These were then visualized and imaged with an inverted microscope.

Synthesis of epoxy microwire: The PDMS microfluidic channels were fabricated and sealed to glass slides. Degassed epoxy without curing agent was poured into a syringe. Using the syringe epoxy was injected into the channels. The epoxy in the channels was then cured in an oven for 2 h at 70 ^{0}C. After curing the samples were removed and allowed to cool. The PDMS slabs were then removed from the glass slides by scraping with a sharp blade, exposing the channels. Using forceps, the cured epoxy was delicately removed from the microchannel, and the wire structure was characterized by SEM.

Synthesis of silk microwire: Raw silk was obtained from Bombyx mori cocoons using a reported procedure [141].The PDMS microchannels were designed as mentioned and were not allowed to seal firmly with glass. A syringe filled with raw silk was injected into the channels and allowed to cure rapidly at 60°C for 15 min. The PDMS slab was then easily peeled off glass and the channel contained the cured silk microwires. These wires were then carefully removed from the channels using forceps for further characterization using SEM [118].

6.4. Results and Discussion

Mammalian hairs from different sources have been investigated. Hairs can be manually cut to different lengths, and the hairs can have widths varying from a few micrometers to hundreds of micrometers. The SEM images show that the hair surfaces are very rough, and the surface roughness properties for a human hair and a cat hair are different. shows microchannels fabricated from hairs. The length of the channel depends on the length of the hair, and the width of the channel is equal to the diameter of the hair.

Most significantly, a microfluidic channel fabricated from fine hair can reproducibly achieve a sub-20 mm width with high accuracy. Using thicker hair, a microchannel with a width of 80 mm can be achieved. When the hairs were obtained from the same source, the reproducibility of the fabricated channel in terms of height and morphology is very high. The hairs were firmly fixed on petri dishes with adhesive tapes, which avoided the curling of the hairs and prevented the hairs from being engulfed in PDMS entirely, resulting in the widths of the channels to be the same as the diameters of the hairs. Hairs from different sources exhibit a variety of surface morphologies, and after translating the hairs into microchannels, negative patterns of these surface morphologies can be formed in PDMS channels, and sub-features and wrinkles in the channels can be seen.

By varying the positions of hairs manually, microfluidic channels can be fabricated in different geometries. All of these properties can then be further altered by changing the initial width or length of the hair. Other channels were formed by bending and twisting the hair into desired shapes such as curves or semicircles. The flexibility and durability of hair allow it to be worked into a specific form for a specific function. Furthermore, multiple hairs were used to create elaborate designs and shapes of microfluidic channels, such as Y-shaped or X-shaped channels by manipulating two hairs.

This hair-based bio-inspired microfluidics fabrication method has several

advantages: (i) the entire fabrication Experimental can be carried out in ambient temperatures, and does not require harsh chemicals or cleanroom facilities. (ii) Hair lengths can be varied from a small scale to a large scale (millimeter to meter), therefore the length of the resulting channel can exceed the standard photolithography fabrication range, which is limited to the size of a wafer. (iii) The width of the microfluidic channel can be as low as a few micrometers. (iv) Due to the resilient and flexible nature of hair, the shape of the channel can be manually changed by manipulating the hair.

Microfluidic channels have been widely used in combinatorial protein screening, immunoassay and studies in cell sorting, counting and manipulations [14], and in this work, hair-based fabricated microfluidic channels were also investigated for application in biological analysis. As shown in Fig. 37a, the microfluidic channels were incubated with rabbit IgG, BSA, and anti-rabbit IgG conjugated with FITC. Washing steps were performed for each step in between. This fluorescent signals clearly indicate that strong binding of anti-rabbit IgG to rabbit IgG was performed in the channel. We also used yeast cells for analyzing various strains of cells in microfluidic channels. Two different kinds of yeast strains, S. cervisieae (oval shaped) and S. pombe (rod shaped) were allowed to flow through the hair based channels, and were visualized using an inverted microscope as shown in Fig. 37b [118].
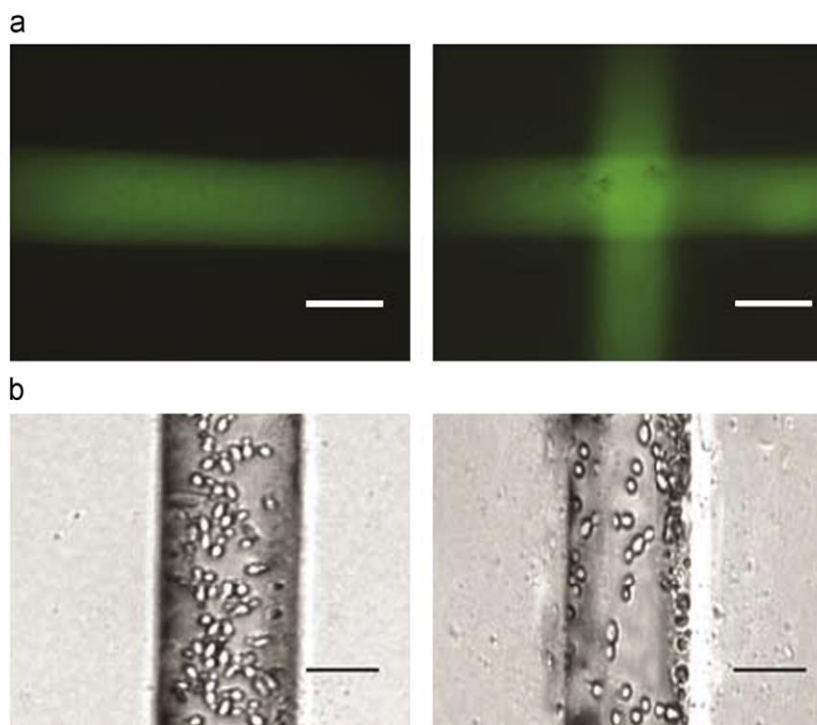
Fig. 37. Immunoassay (a) and live yeast cell analysis using the hair based microfluidic channels. Scale bar : 50 μm [118].

In addition, a microfluidic channel fabricated from a mammalian hair was investigated for fabricating a microwire, as shown in Fig. 38. By using preexisting microchannels as templates it was possible to synthesize wires with the same contours as the channels. When these microwires were removed from the channels they imitate the original hair that was used to form the channel. As shown in Fig. 38a, the resulting epoxy microwire, which replicated the PDMS channel effectively, has a semicircular cross section, and shows the same sub-features as the original hair. Silk microwire was also

synthesized, as shown in Fig. 38b.
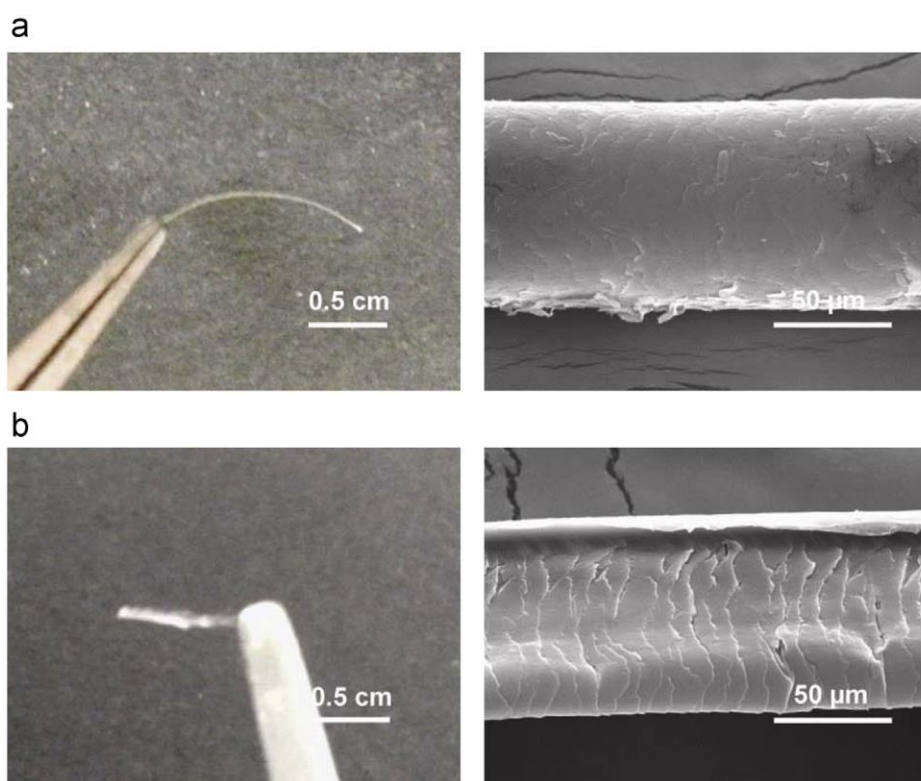
Fig. 38. Microwire synthesis using hair based microfluidic channels (a) epoxy and (b) silk [118] .

During the curing process the silk solution evaporated, decreasing in volume and settling on one side of the channel. The silk-based wire appears ribbon-like and does not

replicate the structure of the channel entirely. Moreover, bio-inspired hairfabricated microfluidic channels could be used for fabricating microwires in a variety of other materials, such as metal, protein fibers, etc. By using hair with a smaller diameter or varying the hair shapes and lengths, templates could be created to fabricate a variety of microwire structure.

6.5. Conclusion

In this work, we have demonstrated a bio-inspired mammalian hair-based fabrication of microfluidic channels, and their application for bioanalysis and microwire synthesis. The method provides a simple, low cost, and easy-to-handle approach for the fabrication of microfluidic channels due to the flexible, abundant, and easily harvested nature of hairs. The approach we describe here may open new avenues for applications in various fields, including immunoassay, cell analysis, or microwire synthesis.

CHAPTER 7

SUPER HYDROPHOBIC, TRANSPARENT, AND BIODEGRADABLE MATERIALS [142]

7.1. Abstract

A super hydrophobic surface has been created by aligning of nanostructures of peptide nanotubes on the surface of biodegradable silk macrosurface. Depending on the type of biomaterial, super hydrophobic surfaces have proven to be anti-adhesive, anti-contaminating and electrically conductive surfaces. Silk surfaces being biodegradable, optically transparent and the ease of being molded have found use in several applications. Peptide nanotubes, on the other hand, are chemically diverse and biological recognition units that are hydrophobic in nature. The alignment of the hydrophobic peptide nanotubes on the surface of hydrophilic silk will result in the design of super hydrophobic, transparent and biodegradable surface. A UV-Vis spectrometer analysis was also conducted to the super hydrophobic surface. These chemically modified surfaces can open exciting ventures finding use as biosensors and storage devices.

7.2. Introduction

Many applications of substances are majorly dependent on the bulk and surface properties of substances. The bulk properties include stiffness, toughness, optical clarity and the ability to biodegrade while surface properties include adhesion, biocompatibity and wettability. The controlled wettability of surfaces is a very important property for the production of functionally significant devices. Super-hydrophobic surfaces with a contact angle greater than 120 degrees have been gaining momentum in avoiding adhesion, contamination and electric conductivity on surfaces. This is usually determined by the surface microstructure and the chemical composition of the surface and these can be created wither by altering the roughness of the surface or by the assembly of nanostructures to create a low surface energy on the surface [143-145]. This water repelling nature can control the hydration of silk surfaces, thereby preventing its biodegradation.

Optically transparent and biodegradable substrates are important for fabricating flexible and green electronic devices by incorporating light emitting diodes [146-148] or by incorporating gold nanoparticles. Thus it is highly desired to design a highly hydrophobic and transparent surface that can find use as functional biomaterials.

Silk Fibroin obtained from Bombyx mori is an important biomaterial owing to its biocompatibility, easier degradation in vivo, chemical flexibility, mechanical stability, ease of molding into different structures and optical transparency [141]. It has been finding wide applications in bone and tissue engineering as scaffolds [149, 150], drug delivery [151, 152], and biosensors [153, 154]. While peptide nanotubes are desirable organic building blocks for various bio-nanotechnological applications owing to their chemical flexibility [61], biocompatibility [62], biological recognition abilities [63], thermal [64], and mechanical stability [66] that enable them to hierarchically assemble themselves into useful devices [96]. Self-assembly at the molecular level is the central basis of bottom up fabrication of bulk devices with well-defined nanostructures [67]. The alignment of the hydrophobic peptide nanotubes on the surface of hydrophilic silk will result in the design of super-hydrophobic, transparent, and biodegradable surface. These devices can find use as biosensors, energy storage devices, in tissue engineering, environmental monitoring, and various other applications.

7.3. Experimental

Vertical Alignment of the peptide nanotubes on silk surface: Silk fibroin film is produced using a published protocol. ADNTs were deposited on the silk surface using a biomolecular vapour deposition method. In a typical deposition method, 10 mg of the

diphenylalanine lyophilized peptide powder NH_2- Phe-Phe-OH and was dissolved in 1 ml of the 1,1,1,3,3,3-hexafluoro-2-proponol was put on silk fibroin film and the substrate was placed 2 cm from the peptide nanotube solution. This setup was kept at 220°C from 5- 60 min to deposit the peptide nanotubes vertically on the downward side of the substrate. The substrate was then reheated at 220°C for 30 min to stabilize the vertical peptide nanotubes.

Horizontal alignment of peptide nanotubes on the silk surface by solution mediated peptide growth: A 10 mg/ ml of the peptide solution dissolved in HFP was left to grow in an eppendorf from 5 – 60 min on a shaker. This was then aliquoted on a silk film surface and allowed to dry in room temperature for 1 h. These randomly arranged horizontal peptide nanotubes were visualized using an optical microscope.

UV- Vis adsorbance spectroscopy of peptide nanotubes assembled on silk surface: A UV-Vis study was conducted on the silk fims containing the peptide nanotubes grown at different times, both vertically and horizontally, using the BioTek Synergy Multimode plate reader. The adsorbance system makes use of a Xenon Flash monochromator measuring the adsorbance over the wavelength range of 200-990 nm in the increments of 1 nm. Silk films with peptide nanotubes grown vertically and horizontally at 0, 10 min, 20 min, 30 min, 45 min, and 1 h were prepared for the UV-Vis analyses. A spectrum curve of the different samples was conducted between 200-800nm at an increment of 10 nm to study the characteristics of the silk film containing peptide nanotubes grown at various densities.

7.4. Results and Discussion

*Surface studies on vertically aligned peptide nanotubes on silk surface using a goniometer:*The surface properties of the peptide nanotubes assembled on the silk surface can be studied using a goniometer. Water contact angle studies were taken on vertically aligned peptide nanotubes on silk surfaces.
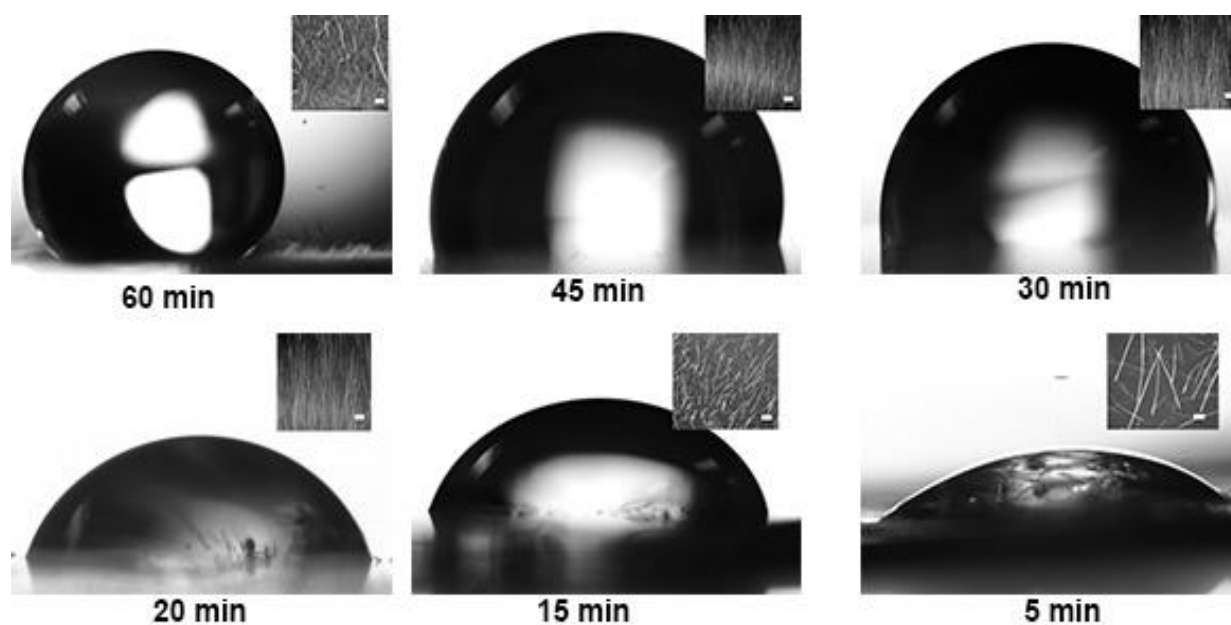
Fig. 39. Goniometer characterization of vertically grown peptide nanotubes on silk surface at different times . Scale bar : 50 μm [142].

Different times were employed to get different densities on the silk surface. At 1 h the peptide nanotubes were found to be dense with a water contact angle of 135 degrees. With decresing times the peptide nanotube density decreased proportionally, so at 45 min, 30 min, 15 min, and 5 min of growth the water contact angle reduced to 105 degrees, 80 degrees, 55 degrees, and 35 degrees, respectively.

Surface studies on horizontally aligned peptide nanotubes on silk surface using a goniometer: Water contact angle studies were taken on horizontally aligned peptide nanotubes on silk surfaces to examine the surface properties of horizontally aligned peptide nanotubes on the silk surface. Different times were employed in this condition as well to get different densities on the silk surface. At 1 h the peptide nanotubes were found to be dense with a water contact angle of 120 degrees. With decreasing times the peptide nanotube density decreased proportionally, so at 45 min, 30 min, 15 min, and 5 min of growth the water contact angle reduced to 105 degrees, 75 degrees, 50 degrees and 25 degrees, respectively. This shows that the peptide nanotube density, irrespective of the alignment, plays a direct role in increasing the hydrophobicity of the substrate and decreases the solubility time of the underlying silk.

Surface characterization of the hydrophobic surfaces using UV-VIS spectroscopy: To demonstrate the transparency of the silk surface with assembled peptide nanotube, a UV-Vis study was conducted with respect to blank silk film. A spectrum curve was obtained

in the wavelength range of 200 nm -800 nm for both the blank silk film and the silk film assembled with vertically and horizontally aligned peptide nanotubes.
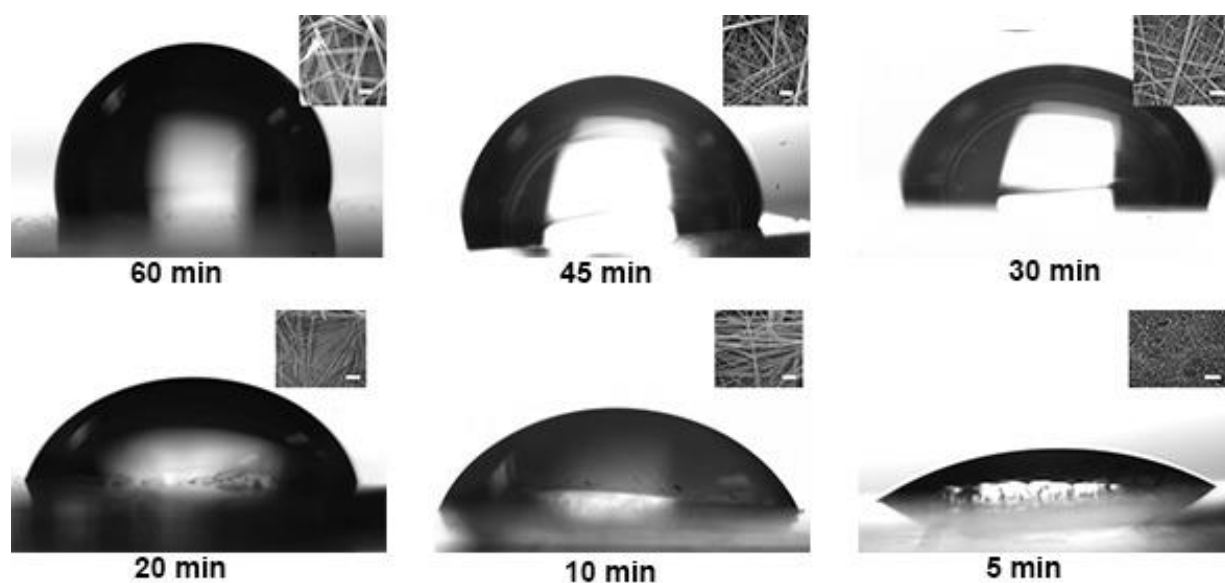
Fig. 40. Goniometer characterization of horizontally grown peptide nanotubes on silk surface at different times . Scale bar : 50 µm [142].

The spectrum curves obtained for all the silk surfaces with/ without peptide nanotubes all have similar OD values, which indicate that the surface still remains transparent irrespective of the peptide nanotubes. This establishes that the hydrophobicity of the biomaterial is determined by the density of the peptide nanotubes on the surface while the transparency of the surface is still maintained.
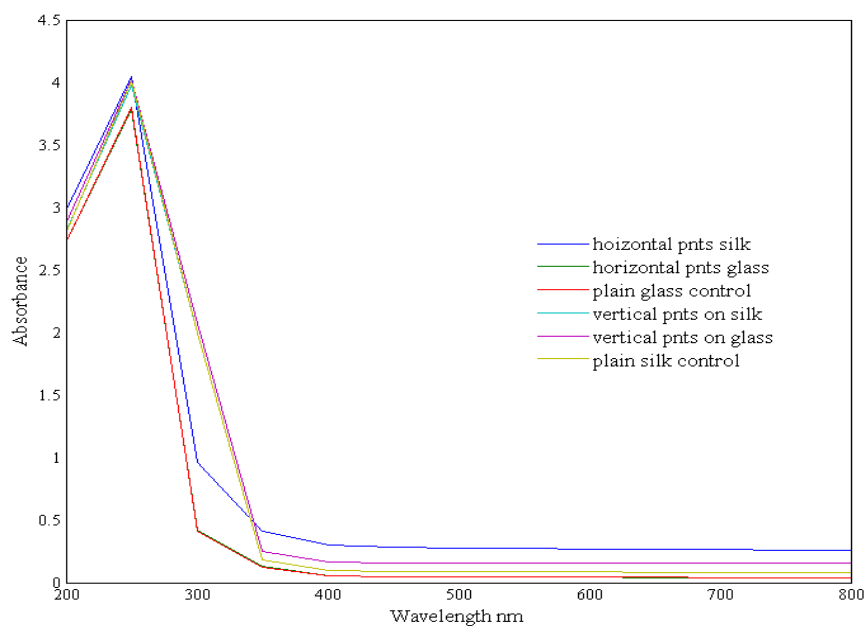
Fig. 41. UV-VIS spectroscopy of the peptide nanotubes based silk hydrophobic surfaces [142].

7.5. Conclusion

In this report, we have demonstrated for the assembly of peptide nanotubes on silk surface for the purpose of turning the highly hydrophilic silk substrate into a hydrophobic one. The approach we describe here may open new avenues for a variety of silk and peptide nanotube-based fundamental studies and practical applications, including biological analytical devices, self-assembly of silk-based hybrid materials, surface and interface, cell

biology, etc. Although these results are promising, further studies are needed to help elucidate the application of the peptide nanotube-silk for the construction of a variety of biological, chemical, optical, mechanical, and electrical devices.

CHAPTER 8

GRAPHENE BASED BIOSENSOR TO DETECT CARDIAC MARKER

8.1. Abstract

Coronary heart disease is the primary cause of death in the United States. Though lifestyle changes and medicines are available to control CHD, early diagnosis is required for the elimination of its incidence. Currently, hospitals depend on the detection of cardiac troponin to predict the onset of CHD in patients. A sensitive graphene based nanosensor has been reported in this study to conduct the detection of this cardiac troponin I along with miRNAs responsible for CHD. It is believed that these results can help elucidate the elimination of heart disease, thereby improving the contemporary medical cure techniques.

8.2. Introduction

Coronary heart disease or heart attack mainly occurs due to the poor oxygenation of the coronary arteries, inadvertently stopping the blood supply to the heart. This is caused by the blockage in arteries due to the accumulation of lymphocytes, fat and cholesterol, resulting in the death of over 25% mortality rate. It is hence required to identify or eliminate the presence of cardiac markers required for the maintenance of proper heart functioning, thereby improving medical care and cure. The present technology is laborious and presents only 50% sensitivity to the cardiac markers [155]. Troponin I present in the myofilaments and is considered to be highly specific in the detection of cardiac muscle injury and coronary heart diseases [156]. Graphene has attracted strong attention in the scientific and technological domain owing to its large surface area [157], unique physiochemical properties [158, 159], excellent conductivity [160-162], and mechanical [20] properties. Microfluidic devices based on capillary action require low sample volume for the simultaneous analysis of a large number of biologically important molecules, thereby making it indispensable for bioanalysis [123, 163-165]. It is thus desired to develop a new sensor involving a microfluidic device assembled on the graphene electrode surface, combined with AC measurement of the impedance change to conduct the detection of the biomarkers of interest.

8.3. Experimental

Single-Bilayer Graphene grown on Cu film is first transferred onto SiO_2 using a sacrificial layer of heavy polymer like PMMA (polymethylmethacralate), that will help it stay afloat when subjected to etching in ferric nitrate solution, to eliminate the copper layer off graphene. It is further dipped in 30% (HCl +hydrogen peroxide) and 30% (Ammonium hydroxide +hydrogen peroxide) for 15 mins each, followed by rinsing in distilled water.

a   **b**   **c**
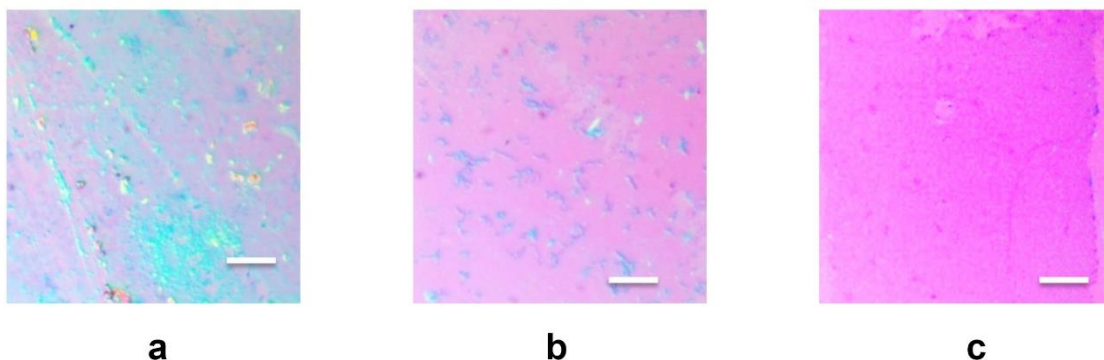
Fig. 42. Generation of PMMA free graphene film on SiO_2. Scale bar: 20 μm.

The graphene, thus produced, on SiO_2 is then dipped in acetone to wash off that sacrificial PMMA layer. The nanosensing device is based on antibody immobilized graphene nanosheet on SiO_2 with an AC signal measurement. By using signal rate

(impedance vs time), analysis of different concentrations of samples can be performed continuously. The detection is performed with the nanosensor in a microfluidic channel as shown in Fig. 43. The sample is delivered to the electrode by the microfluidic device. The graphene electrode is immobilized with anti-troponinI via the linker, 1-pyrenebutanoic acid succinimidyl ester, followed by the anti-TroponinI antibody and finally, BSA to prevent non-specific interactions.
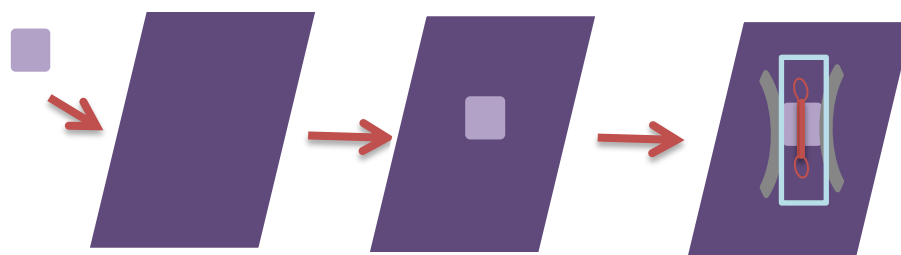
Fig. 43. Schematic of the biosensor device.

The device is now characterized for the sensing of TroponinI. The binding of the TroponinI with anti-troponinI immobilized on the electrode surface is hypothesized to change the impedance signal. This will assist in the investigation the detection limit of the cardiac marker.

8.4. Results and discussion

Fluorescent characterization of the miRNA and their respective PNA molecule: 1µM of PNA 208b was incubated on the graphene film surface overnight enabled by the linked molecule and 2 h BSA 1%. The fluorescence was done by using the RNA208b FITC molecule. The control samples were incubated using 1 µm PNA 1 and PNA 133a and the fluorescence was tested using RNA 208b-FITC. The absence of fluorescence shows the specificity of binding of the RNA208b to PNA 208b as shown in Fig. 44.
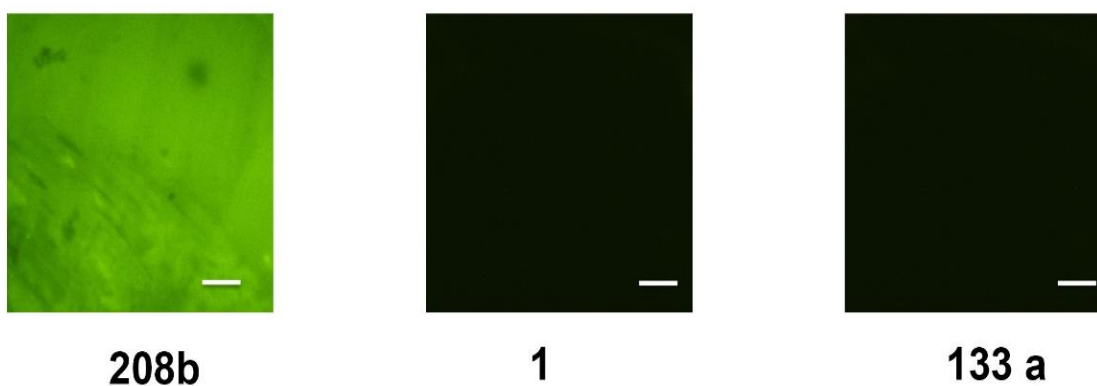
Fig. 44. miRNA 208b- PNA 208b binding characterization using fluorescence characterization. Scale bar: 20 µm.

8.4. Conclusion

This research is still underway in conducting sensing experiments. Though the fluorescence study has given primary results, it is still to be tested on the sensing platform using impedance measurement on graphene based microfluidic sensor.

REFERENCES

[1] Swaminathan S, Cui Y. Recognition of poly(dimethylsiloxane) with phage displayed peptides. Rsc Adv 2012;2:12724-7.

[2] Stryer L. Biochemistry. 4th edition ed. New York: W.H. Freeman & Company; 1995.

[3] Pender MJ, Sowards LA, Hartgerink JD, Stone MO, Naik RR. Peptide-mediated formation of single-wall carbon nanotube composites. Nano Lett 2006;6:40-4.

[4] Zuo RJ, Ornek D, Wood TK. Aluminum- and mild steel-binding peptides from phage display. Appl Microbiol Biot 2005;68:505-9.

[5] Naik RR, Stringer SJ, Agarwal G, Jones SE, Stone MO. Biomimetic synthesis and patterning of silver nanoparticles. Nat Mater 2002;1:169-72.

[6] Mao CB, Solis DJ, Reiss BD, Kottmann ST, Sweeney RY, Hayhurst A, et al. Virus-based toolkit for the directed synthesis of magnetic and semiconducting nanowires. Science 2004;303:213-7.

[7] Estephan E, Saab MB, Larroque C, Martin M, Olsson F, Lourdudoss S, et al. Peptides for functionalization of InP semiconductors. J Colloid Interf Sci 2009;337:358-63.

[8] Estephan E, Saab MB, Martin M, Larroque C, Cuisinier FJG, Briot O, et al. Phages recognizing the indium nitride semiconductor surface via their peptides. J Pept Sci 2011;17:143-7.

[9] Sanghvi AB, Miller KPH, Belcher AM, Schmidt CE. Biomaterials functionalization using a novel peptide that selectively binds to a conducting polymer. Nat Mater 2005;4:496-502.

[10] Vodnik M, Strukelj B, Lunder M. HWGMWSY, an unanticipated polystyrene binding peptide from random phage display libraries. Anal Biochem 2012;424:83-6.

[11] Sugawara F. Small molecule binding peptides and the related genes determined by phage display cloning. J Pestic Sci 2004;29:279-83.

[12] Cui Y, Kim SN, Jones SE, Wissler LL, Naik RR, McAlpine MC. Chemical functionalization of graphene enabled by phage displayed peptides. Nano Lett 2010;10:4559-65.

[13] Cui Y, Pattabiraman A, Lisko B, Collins SC, McAlpine MC. Recognition of patterned molecular ink with phage displayed peptides. J Am Chem Soc 2010;132:1204-5.

[14] Swaminathan S, Bullough M, Li QF, Zhou AH, Cui Y. Non-lithographic patterning of phage-displayed peptides with wrinkled elastomers. J R Soc Interface 2014;11.

[15] Zheng WF, Wang Z, Zhang W, Jiang XY. A simple PDMS-based microfluidic channel design that removes bubbles for long-term on-chip culture of mammalian cells. Lab Chip 2010;10:2906-10.

[16] Xue CY, Zhang W, Choo WHS, Yang KL. Simplest method for creating micropatterned nanostructures on PDMS with UV Light. Langmuir 2011;27:13410-4.

[17] Wu MH. Simple poly(dimethylsiloxane) surface modification to control cell adhesion. Surf Interface Anal 2009;41:11-6.

[18] Misra A, Raney JR, De Nardo L, Craig AE, Daraio C. Synthesis and characterization of carbon nanotube-polymer multilayer structures. Acs Nano 2011;5:7713-21.

[19] Hsieh CH, Huang CJC, Huang YY. Patterned PDMS based cell array system: a novel method for fast cell array fabrication. Biomed Microdevices 2010;12:897-905.

[20] Liu M, Sun JR, Sun Y, Bock C, Chen QF. Thickness-dependent mechanical properties of polydimethylsiloxane membranes. J Micromech Microeng 2009;19.

[21] Lee J, Kim J. Fabrication of strongly anchored, high aspect ratio elastomeric microwires for mechanical and optical applications. J Micromech Microeng 2011;21.

[22] Wang R, Yang YL, Qin M, Wang LK, Yu L, Shao B, et al. Biocompatible hydrophilic modifications of poly(dimethylsiloxane) using self-assembled hydrophobins. Chem Mater 2007;19:3227-31.

[23] Mills KL, Zhu XY, Takayama SC, Thouless MD. The mechanical properties of a surface-modified layer on polydimethylsiloxane. J Mater Res 2008;23:37-48.

[24] Niu XZ, Peng SL, Liu LY, Wen WJ, Sheng P. Characterizing and patterning of PDMS-based conducting composites. Adv Mater 2007;19:2682-6.

[25] Sharma V, Dhayal M, Govind, Shivaprasad SM, Jain SC. Surface characterization of plasma-treated and PEG-grafted PDMS for micro fluidic applications. Vacuum 2007;81:1094-100.

[26] Swaminathan S, Cui Y. Recognition of epoxy with phage displayed peptides. Mat Sci Eng C-Mater 2013;33:3082-4.

[27] Wong I, Ho CM. Surface molecular property modifications for poly(dimethylsiloxane) (PDMS) based microfluidic devices. Microfluid Nanofluid 2009;7:291-306.

[28] Horiuchi S, Fujita T, Hayakawa T, Nakao Y. Micropatterning of metal nanoparticles via UV photolithography. Adv Mater 2003;15:1449-52.

[29] Donthu S, Pan ZX, Myers B, Shekhawat G, Wu NG, Dravid V. Facile scheme for fabricating solid-state nanostructures using e-beam lithography and solution precursors. Nano Lett 2005;5:1710-5.

[30] Cui Y, Pattabiraman A, Lisko B, Collins SC, McAlpine MC. Recognition of patterned molecular ink with phage displayed peptides. J Am Chem Soc 2010;132:1204-5.

[31] Evensen HT, Jiang H, Gotrik KW, Denes F, Carpick RW. Transformations in wrinkle patterns: cooperation between nanoscale cross-linked surface layers and the submicrometer bulk in wafer-spun, plasma-treated polydimethylsiloxane. Nano Lett 2009;9:2884-90.

[32] Chan EP, Crosby AJ. Spontaneous formation of stable aligned wrinkling patterns. Soft Matter 2006;2:324-8.

[33] Kim P, Abkarian M, Stone HA. Hierarchical folding of elastic membranes under biaxial compressive stress. Nat Mater 2011;10:952-7.

[34] Bullough M, Cui Y. A library of large-scale surface patterns induced by flame on elastomers. Soft Matter 2012;8:3304-7.

[35] Grimes A, Breslauer DN, Long M, Pegan J, Lee LP, Khine M. Shrinky-dink microfluidics: rapid generation of deep and rounded patterns. Lab Chip 2008;8:170-2.

[36] Yu LT, Banerjee IA, Matsui H. Direct growth of shape-controlled nanocrystals on nanotubes via biological recognition. J Am Chem Soc 2003;125:14837-40.

[37] Ferreira A, Cardoso P, Klosterman D, Covas JA, van Hattum FWJ, Vaz F, et al. Effect of filler dispersion on the electromechanical response of epoxy/vapor-grown carbon nanofiber composites. Smart Mater Struct 2012;21:075008.

[38] Liu ZQ, Tian YH, Kang SM, Zhang XJ. Synthesis and characterization of novel epoxy-modified waterborne polyurethanes and their use in carbon fiber sizing. J Appl Polym Sci 2012;125:3490-9.

[39] Mochalin VN, Neitzel I, Etzold BJM, Peterson A, Palmese G, Gogotsi Y. Covalent incorporation of aminated nanodiamond into an epoxy polymer network. Acs Nano 2011;5:7494-502.

[40] Gansen P, Dittgen M. Polyurethanes as self adhesive matrix for the transdermal drug delivery of testosterone. Drug Dev Ind Pharm 2012;38:597-602.

[41] Noh SM, Lee JW, Nam JH, Park JM, Jung HW. Analysis of scratch characteristics of automotive clearcoats containing silane modified blocked isocyanates via carwash and nano-scratch tests. Prog Org Coat 2012;74:192-203.

[42] Ho TH, Wang JH, Wang CS. Modification of epoxy resins with polysiloxane TPU for electronic encapsulation J Appl Polym Sci 1996;60:1097-107.

[43] Pauliukaite R, Ghica ME, Fatibello O, Brett CMA. Graphite-epoxy electrodes modified with functionalised carbon nanotubes and chitosan for the rapid electrochemical determination of dipyrone. Comb Chem High T Scr 2010;13:590-8.

[44] Pavli P, Petrou PS, Niakoula D, Douvas AM, Chatzichristidi M, Kakabakos SE, et al. Chemical binding of biomolecules to micropatterned epoxy modified surfaces for biosensing applications. Microelectron Eng 2009;86:1473-6.

[45] Castellanos G, Arzt E, Kamperman M. Effect of viscoelasticity on adhesion of bioinspired micropatterned epoxy surfaces. Langmuir 2011;27:7752-9.

[46] Nam Y, Branch DW, Wheeler BC. Epoxy-silane linking of biomolecules is simple and effective for patterning neuronal cultures. Biosens Bioelectron 2006;22:589-97.

[47] Ingrosso C, Sardella E, Keller S, Dohn S, Striccoli M, Agostiano A, et al. Surface functionalization of epoxy-resist- based microcantilevers with iron oxide nanocrystals. Adv Mater 2010;22:3288-92.

[48] Swaminathan S, Cui Y. Recognition of (poly)ethylenetetraphthalate using phage displayed peptides. In preparation.

[49] Lee SH, Teng CC, Ma CCM, Wang I. Highly transparent and conductive thin films fabricated with nano-silver/double-walled carbon nanotube composites. J Colloid Interf Sci 2011;364:1-9.

[50] Liu ZH, Pan CT, Chen YC, Liang PH. Interfacial characteristics of polyethylene terephthalate-based piezoelectric multi-layer films. Thin Solid Films 2013;531:284-93.

[51] Socol G, Socol M, Stefan N, Axente E, Popescu-Pelin G, Craciun D, et al. Pulsed laser deposition of transparent conductive oxide thin films on flexible substrates. Appl Surf Sci 2012;260:42-6.

[52] Cao Y, Zhou CG. Magnetic anisotropy properties of CoZrNb thin films deposited on PET substrate by magnetron sputtering. J Magn Magn Mater 2012;324:1832-6.

[53] Mirzadeh H, Moghadam EV, Mivehchi H. Laser-modified nanostructures of PET films and cell behavior. J Biomed Mater Res A 2011;98A:63-71.

[54] Oh CS, Lee SM, Kim EH, Lee EW, Park LS. Electro-optical properties of index matched ITO-PET film for touch panel application. Mol Cryst Liq Cryst 2012;568:32-7.

[55] Gotoh K, Kobayashi Y, Yasukawa A, Ishigami Y. Surface modification of PET films by atmospheric pressure plasma exposure with three reactive gas sources. Colloid Polym Sci 2012;290:1005-14.

[56] Gong Y, Li CH, Huang XM, Luo YH, Li DM, Meng QB, et al. Simple method for manufacturing Pt counter electrodes on conductive plastic substrates for dye-sensitized solar cells. Acs Appl Mater Inter 2013;5:795-800.

[57] Lee SM, Choi BH, Park JS, Kim TH, Bae HK, Park LS. Effect of ITO/Ag/ITO multilayer electrode deposited onto glass and PET substrate on the performance of organic light-emitting diodes. Mol Cryst Liq Cryst 2010;530:266-71.

[58] Park C, Kim SW, Lee YS, Lee SH, Song KH, Park LS. Spray coating of carbon nanotube on polyethylene terephthalate film for touch panel application. J Nanosci Nanotechno 2012;12:5351-5.

[59] Sibinski M, Znajdek K, Sawczak M, Gorski M. AZO layers deposited by PLD method as flexible transparent emitter electrodes for solar cells. Microelectron Eng 2014;127:57-60.

[60] Swaminathan S, Cui Y. Characterization of peptide nanotubes using phage displayed peptides. In preparation.

[61] Adler-Abramovich L, Reches M, Sedman VL, Allen S, Tendler SJ, Gazit E. Thermal and chemical stability of diphenylalanine peptide nanotubes: implications for nanotechnological applications. Langmuir 2006;22:1313-20.

[62] Andersen KB, Castillo-Leon J, Hedstrom M, Svendsen WE. Stability of diphenylalanine peptide nanotubes in solution. Nanoscale 2011;3:994-8.

[63] Kol N, Adler-Abramovich L, Barlam D, Shneck RZ, Gazit E, Rousso I. Self-assembled peptide nanotubes are uniquely rigid bioinspired supramolecular structures. Nano Lett 2005;5:1343-6.

[64] Kim JH, Lim SY, Nam DH, Ryu J, Ku SH, Park CB. Self-assembled, photoluminescent peptide hydrogel as a versatile platform for enzyme-based optical biosensors. Biosens Bioelectron 2011;26:1860-5.

[65] Gan Z, Wu X, Zhang J, Zhu X, Chu PK. In situ thermal imaging and absolute temperature monitoring by luminescent diphenylalanine nanotubes. Biomacromolecules 2013;14:2112-6.

[66] Amdursky N, Beker P, Koren I, Bank-Srour B, Mishina E, Semin S, et al. Structural transition in peptide nanotubes. Biomacromolecules 2011;12:1349-54.

[67] Mammadov R, Tekinay AB, Dana A, Guler MO. Microscopic characterization of peptide nanostructures. Micron 2012;43:69-84.

[68] Adler-Abramovich L, Aronov D, Beker P, Yevnin M, Stempler S, Buzhansky L, et al. Self-assembled arrays of peptide nanotubes by vapour deposition. Nature Nano 2009;4:849-54.

[69] Matos Ide O, Alves WA. Electrochemical determination of dopamine based on self-assembled peptide nanostructure. ACS Appl Mater Interfaces 2011;3:4437-43.

[70] Yemini M, Reches M, Gazit E, Rishpon J. Peptide nanotube-modified electrodes for enzyme-biosensor applications. Anal Chem 2005;77:5155-9.

[71] Rosenman G, Beker P, Koren I, Yevnin M, Bank-Srour B, Mishina E, et al. Bioinspired peptide nanotubes: deposition technology, basic physics and nanotechnology applications. Journal Of Peptide Science : An Official Publication Of The European Peptide Soc 2011;17:75-87.

[72] Yan X, Zhu P, Li J. Self-assembly and application of diphenylalanine-based nanostructures. Chem Soc Rev 2010;39:1877-90.

[73] Adler-Abramovich L, Badihi-Mossberg M, Gazit E, Rishpon J. Characterization of peptide-nanostructure-modified electrodes and their application for ultrasensitive environmental monitoring. Small 2010;6:825-31.

[74] Ulijn RV, Smith AM. Designing peptide based nanomaterials. Chem Soc Rev 2008;37:664-75.

[75] Cui Y, Kim SN, Jones SE, Wissler LL, Naik RR, McAlpine MC. Chemical Functionalization of Graphene Enabled by Phage Displayed Peptides. Nano Lett 2010;10:4559-65.

[76] Pender MJ, Sowards LA, Hartgerink JD, Stone MO, Naik RR. Peptide-mediated formation of single-wall carbon nanotube composites. Nano Lett 2006;6:40-4.

[77] Swaminathan S, Cui Y. 1D, 2D ,3D silk nanostructures via translation of elastomeric instability. In preparation.

[78] Xia DY, Brueck SRJ. Strongly anisotropic wetting on one-dimensional nanopatterned surfaces. Nano Lett 2008;8:2819-24.

[79] Lee SG, Lee DY, Lim HS, Lee DH, Lee S, Cho K. Switchable transparency and wetting of elastomeric smart windows. Adv Mater 2010;22:5013-7.

[80] Varenberg M, Gorb SN. Hexagonal surface micropattern for dry and wet friction. Adv Mater 2009;21:483-6.

[81] Cui Y, Kim SN, Jones SE, Wissler LL, Naik RR, McAlpine MC. Chemical functionalization of graphene enabled by phage displayed peptides. Nano Lett 2010;10:4559-65.

[82] Nguyen TD, Nagarah JM, Qi Y, Nonnenmann SS, Morozov AV, Li S, et al. Wafer-scale nanopatterning and translation into high-performance piezoelectric nanowires. Nano Lett 2010;10:4595-9.

[83] Xu T, Zhu N, Xu MYC, Wosinski L, Aitchison JS, Ruda HE. A pillar-array based two-dimensional photonic crystal microcavity. Appl Phys Lett 2009;94.

[84] Biswas KG, Sands TD, Cola BA, Xu XF. Thermal conductivity of bismuth telluride nanowire array-epoxy composite. Appl Phys Lett 2009;94.

[85] Persson AI, Koh YK, Cahill DG, Samuelson L, Linke H. Thermal conductance of in ss nanowire composites. Nano Lett 2009;9:4484-8.

[86] Donthu S, Pan ZX, Myers B, Shekhawat G, Wu NG, Dravid V. Facile scheme for fabricating solid-state nanostructures using e-beam lithography and solution precursors. Nano Lett 2005;5:1710-5.

[87] Melosh NA, Boukai A, Diana F, Gerardot B, Badolato A, Petroff PM, et al. Ultrahigh-density nanowire lattices and circuits. Science 2003;300:112-5.

[88] Menke EJ, Thompson MA, Xiang C, Yang LC, Penner RM. Lithographically patterned nanowire electrodeposition. Nature Mater 2006;5:914-9.

[89] Evensen HT, Jiang H, Gotrik KW, Denes F, Carpick RW. Transformations in Wrinkle Patterns: Cooperation between Nanoscale Cross-Linked Surface Layers and the Submicrometer Bulk in Wafer-Spun, Plasma-Treated Polydimethylsiloxane. Nano Lett 2009;9:2884-90.

[90] Chan EP, Crosby AJ. Fabricating microlens arrays by surface wrinkling. Adv Mater 2006;18:3238-42.

[91] Kim P, Abkarian M, Stone HA. Hierarchical folding of elastic membranes under biaxial compressive stress. Nat Mater 2011;10:952-7.

[92] Bowden N, Huck WTS, Paul KE, Whitesides GM. The controlled formation of ordered, sinusoidal structures by plasma oxidation of an elastomeric polymer. Appl Phys Lett 1999;75:2557-9.

[93] Chua DBH, Ng HT, Li SFY. Spontaneous formation of complex and ordered structures on oxygen-plasma-treated elastomeric polydimethylsiloxane. Appl Phys Lett 2000;76:721-3.

[94] Yu CJ, Jiang HQ. Forming wrinkled stiff films on polymeric substrates at room temperature for stretchable interconnects applications. Thin Solid Films 2010;519:818-22.

[95] Altman GH, Diaz F, Jakuba C, Calabro T, Horan RL, Chen J, et al. Silk-based biomaterials. Biomaterials 2003;24:401-16.

[96] Tao H, Kaplan DL, Omenetto FG. Silk materials - A road to sustainable high technology. Adv Mater 2012;24:2824-37.

[97] Amsden JJ, Domachuk P, Gopinath A, White RD, Dal Negro L, Kaplan DL, et al. Rapid nanoimprinting of silk fibroin films for biophotonic applications. Adv Mater 2010;22:1746-9.

[98] Omenetto FG, KapLan DL. A new route for silk. Nat Photonics 2008;2:641-3.

[99] Bourzac K. Spinning silk into sensors. Technol Rev 2009;112:80-2.

[100] Cronin-Golomb M, Murphy AR, Mondia JP, Kaplan DL, Omenetto FG. Optically induced birefringence and holography in silk. J Polym Sci Pol Phys 2012;50:257-62.

[101] Parker ST, Domachuk P, Amsden J, Bressner J, Lewis JA, Kaplan DL, et al. Biocompatible silk printed optical waveguides. Adv Mater 2009;21:2411-5.

[102] Sangappa, Mahesh SS, Somashekar R, Subramanya G. Analysis of diffraction line profile from silk fibers using various distribution functions. J Polym Res 2005;12:465-72.

[103] Galeotti F, Andicsova A, Yunus S, Botta C. Precise surface patterning of silk fibroin films by breath figures. Soft Matter 2012;8:4815-21.

[104] Cassinelli C, Cascardo G, Morra M, Draghi L, Motta A, Catapano G. Physical-chemical and biological characterization of silk fibroin-coated porous membranes for medical applications. Int J Artif Organs 2006;29:881-92.

[105] Miroiu FM, Socol G, Visan A, Stefan N, Craciun D, Craciun V, et al. Composite biocompatible hydroxyapatite-silk fibroin coatings for medical implants obtained by matrix assisted pulsed laser evaporation. Mater Sci Eng B-Adv 2010;169:151-8.

[106] Pritchard EM, Kaplan DL. Silk fibroin biomaterials for controlled release drug delivery. Expert Opin Drug Del 2011;8:797-811.

[107] Tsioris K, Raja WK, Pritchard EM, Panilaitis B, Kaplan DL, Omenetto FG. Fabrication of silk microneedles for controlled-release drug delivery. Adv Funct Mater 2012;22:330-5.

[108] Zhao Z, Chen AZ, Li Y, Hu JY, Liu X, Li JS, et al. Fabrication of silk fibroin nanoparticles for controlled drug delivery. J Nanopart Res 2012;14.

[109] Altman GH, Diaz F, Jakuba C, Calabro T, Horan RL, Chen JS, et al. Silk-based biomaterials. Biomaterials 2003;24:401-16.

[110] Amsden JJ, Domachuk P, Gopinath A, White RD, Dal Negro L, Kaplan DL, et al. Rapid nanoimprinting of silk fibroin films for biophotonic applications. Adv Mater 2010;22:1746-+.

[111] Arai T, Freddi G, Innocenti R, Tsukada M. Biodegradation of Bombyx mori silk fibroin fibers and films. J Appl Polym Sci 2004;91:2383-90.

[112] Kim UJ, Park J, Kim HJ, Wada M, Kaplan DL. Three-dimensional aqueous-derived biomaterial scaffolds from silk fibroin. Biomaterials 2005;26:2775-85.

[113] Lawrence BD, Omenetto F, Chui K, Kaplan DL. Processing methods to control silk fibroin film biomaterial features. J Mater Sci 2008;43:6967-85.

[114] Mondia JP, Amsden JJ, Lin D, Dal Negro L, Kaplan DL, Omenetto FG. Rapid nanoimprinting of doped silk films for enhanced fluorescent emission. Adv Mater 2010;22:4596-9.

[115] Omenetto FG, KapLan DL. A new route for silk. Nat Photonics 2008;2:641-3.

[116] Perry H, Gopinath A, Kaplan DL, Dal Negro L, Omenetto FG. Nano- and micropatterning of optically transparent, mechanically robust, biocompatible silk fibroin films. Adv Mater 2008;20:3070-2.

[117] White RD, Gray C, Mandelup E, Amsden JJ, Kaplan DL, Omenetto FG. Rapid nano impact printing of silk biopolymer thin films. J Micromech Microeng 2011;21.

[118] Swaminathan S, Harris T, McClellan D, Cui Y. Bio-inspired mammalian hair-fabricated microfluidics. Mater Lett 2013;106:208-12.

[119] Drzaic P. Microfluidic electronic paper. Nat Photonics 2009;3:248-9.

[120] Kim DR, Lee CH, Zheng XL. Probing flow velocity with silicon nanowire sensors. Nano Lett 2009;9:1984-8.

[121] MacDonald MP, Spalding GC, Dholakia K. Microfluidic sorting in an optical lattice. Nature 2003;426:421-4.

[122] Sershen SR, Mensing GA, Ng M, Halas NJ, Beebe DJ, West JL. Independent optical control of microfluidic valves formed from optomechanically responsive nanocomposite hydrogels. Adv Mater 2005;17:1366-8.

[123] Lettieri GL, Dodge A, Boer G, de Rooij NF, Verpoorte E. A novel microfluidic concept for bioanalysis using freely moving beads trapped in recirculating flows. Lab on a Chip 2003;3:34-9.

[124] Yager P, Edwards T, Fu E, Helton K, Nelson K, Tam MR, et al. Microfluidic diagnostic technologies for global public health. Nature 2006;442:412-8.

[125] Stricker J, Cookson S, Bennett MR, Mather WH, Tsimring LS, Hasty J. A fast, robust and tunable synthetic gene oscillator. Nature 2008;456:516-U39.

[126] Nagrath S, Sequist LV, Maheswaran S, Bell DW, Irimia D, Ulkus L, et al. Isolation of rare circulating tumour cells in cancer patients by microchip technology. Nature 2007;450:1235-U10.

[127] Abate AR, Kutsovsky M, Seiffert S, Windbergs M, Pinto LFV, Rotem A, et al. Synthesis of monodisperse microparticles from non-newtonian polymer solutions with microfluidic devices. Adv Mater 2011;23:1757-60.

[128] Kim J, Li ZY, Park I. Direct synthesis and integration of functional nanostructures in microfluidic devices. Lab on a Chip 2011;11:1946-51.

[129] Baragwanath AJ, Swift GP, Dai D, Gallant AJ, Chamberlain JM. Silicon based microfluidic cell for terahertz frequencies. J Appl Phys 2010;108.

[130] Chen X, Cui DF, Chen J. Design, fabrication and characterization of nano-filters in silicon microfluidic channels based on MEMS technology. Electrophoresis 2009;30:3168-73.

[131] Zhu L, Hou LY, Zhang WY. A new fabrication method for glass microfluidic devices used in micro chemical system. Sens Actuator B-Chem 2010;148:135-46.

[132] Yuan B, Li Y, Wang D, Xie YY, Liu YY, Cui L, et al. A general approach for patterning multiple types of cells Using holey PDMS membranes and microfluidic Channels. Adv Funct Mater 2010;20:3715-20.

[133] Ashley JF, Cramer NB, Davis RH, Bowman CN. Soft-lithography fabrication of microfluidic features using thiol-ene formulations. Lab Chip 2011;11:2772-8.

[134] Grimes A, Breslauer DN, Long M, Pegan J, Lee LP, Khine M. Shrinky-Dink microfluidics: rapid generation of deep and rounded patterns. Lab Chip 2008;8:170-2.

[135] Chen CS, Breslauer DN, Luna JI, Grimes A, Chin WC, Leeb LP, et al. Shrinky-dink microfluidics: 3D polystyrene chips. Lab Chip 2008;8:622-4.

[136] Li X, Tian JF, Shen W. Thread as a versatile material for low-cost microfluidic diagnostics. Acs Appl Mater Inter 2010;2:1-6.

[137] Reches M, Mirica KA, Dasgupta R, Dickey MD, Butte MJ, Whitesides GM. Thread as a matrix for biomedical assays. Acs Appl Mater Inter 2010;2:1722-8.

[138] Sessions BD, Hess WM, Skidmore W. Can hair width and scale pattern and direction of dorsal scapular mammalian hair be a relatively simple means to identify species? J Nat Hist 2009;43:489-507.

[139] LaTorre C, Bhushan B. Investigation of scale effects and directionality dependence on friction and adhesion of human hair using AFM and macroscale friction test apparatus. Ultramicroscopy 2006;106:720-34.

[140] Popescu C, Hocker H. Hair - the most sophisticated biological composite material. Chem Soc Rev 2007;36:1282-91.

[141] Rockwood DN, Preda RC, Yucel T, Wang XQ, Lovett ML, Kaplan DL. Materials fabrication from Bombyx mori silk fibroin. Nat Protoc 2011;6:1612-31.

[142] Swaminathan S, Cui Y. Super hydrophobic, transparent and biodegradable materials. In preparation.

[143] Huovinen E, Takkunen L, Korpela T, Suvanto M, Pakkanen TT, Pakkanen TA. Mechanically robust superhydrophobic polymer surfaces based on protective micropillars. Langmuir 2014;30:1435-43.

[144] Aytug T, Simpson JT, Lupini AR, Trejo RM, Jellison GE, Ivanov IN, et al. Optically transparent, mechanically durable, nanostructured superhydrophobic surfaces enabled by spinodally phase-separated glass thin films. Nanotechnology 2013;24.

[145] Verho T, Bower C, Andrew P, Franssila S, Ikkala O, Ras RHA. Mechanically durable superhydrophobic surfaces. Adv Mater 2011;23:673-8.

[146] Zhu HL, Xiao ZG, Liu DT, Li YY, Weadock NJ, Fang ZQ, et al. Biodegradable transparent substrates for flexible organic-light-emitting diodes. Energ Environ Sci 2013;6:2105-11.

[147] Irimia-Vladu M. "Green" electronics: biodegradable and biocompatible materials and devices for sustainable future. Chem Soc Rev 2014;43:588-610.

[148] dos Santos DS, Goulet PJG, Pieczonka NPW, Oliveira ON, Aroca RF. Gold nanoparticle embedded, self-sustained chitosan films as substrates for surface-enhanced raman scattering. Langmuir 2004;20:10273-7.

[149] Altman GH, Horan RL, Lu HH, Moreau J, I M, Richmond JC, et al. Silk matrix for tissue engineered anterior cruciate ligaments. Biomaterials 2002;23:4131-41.

[150] Jiang XQ, Zhao J, Wang SY, Sun XJ, Zhang XL, Chen J, et al. Mandibular repair in rats with premineralized silk scaffolds and BMP-2-modified bMSCs. Biomaterials 2009;30:4522-32.

[151] Wang XQ, Yucel T, Lu Q, Hu X, Kaplan DL. Silk nanospheres and microspheres from silk/pva blend films for drug delivery. Biomaterials 2010;31:1025-35.

[152] Wilz A, Pritchard EM, Li T, Lan JQ, Kaplan DL, Boison D. Silk polymer-based adenosine release: Therapeutic potential for epilepsy. Biomaterials 2008;29:3609-16.

[153] Diao YY, Liu XY, Toh GW, Shi L, Zi J. Multiple structural coloring of silk-fibroin photonic crystals and humidity-responsive color sensing. Adv Funct Mater 2013;23:5373-80.

[154] Zhang YQ, Zhu J, Gu RA. Improved biosensor for glucose based on glucose oxidase-immobilized silk fibroin membrane. Appl Biochem Biotech 1998;75:215-33.

[155] Yang Z, Zhou DM. Cardiac markers and their point-of-care testing for diagnosis of acute myocardial infarction. Clin Biochem 2006;39:771-80.

[156] Lewandrowski K, Chen A, Januzzi J. Cardiac markers for myocardial infarction. A brief review. Am J of Clin Path 2002;118 Suppl:S93-9.

[157] Novoselov KS, Geim AK, Morozov SV, Jiang D, Zhang Y, Dubonos SV, et al. Electric field effect in atomically thin carbon films. Science 2004;306:666-9.

[158] Bai JW, Duan XF, Huang Y. Rational fabrication of graphene nanoribbons using a nanowire etch mask. Nano Lett 2009;9:2083-7.

[159] Mueller T, Xia F, Avouris P. Graphene photodetectors for high-speed optical communications. Nat Photonics 2010;4:297-301.

[160] Ratinac KR, Yang WR, Ringer SP, Braet F. Toward Ubiquitous Environmental Gas Sensors-Capitalizing on the Promise of Graphene. Environ Sci Technol 2010;44:1167-76.

[161] Dan YP, Lu Y, Kybert NJ, Luo ZT, Johnson ATC. Intrinsic response of Graphene vapor sensors. Nano Lett 2009;9:1472-5.

[162] Schedin F, Geim AK, Morozov SV, Hill EW, Blake P, Katsnelson MI, et al. Detection of individual gas molecules adsorbed on graphene. Nature Mater 2007;6:652-5.

[163] Liu B, Deng Y, Qin BB, Li ZY. Application of microfluidics technology in bioanalysis. Adv Sci Lett 2011;4:150-5.

[164] Peoples MC, Karnes HT. Microfluidic immunoaffinity separations for bioanalysis. J Chromatogr B 2008;866:14-25.

[165] Coupland P. Microfluidics for the upstream pipeline of DNA sequencing - a worthy application? Lab Chip 2010;10:544-7.

APPENDICES

APPENDIX A

PERMISSIONS FROM AUTHORS TO REPRINT PUBLISHED MATERIALS

Feb 09, 2015

To whom it may concern,

My name is Thomas Harris. Swathi Swaminathan and I wrote the manuscript titled: "Bio-inspired mammalian hair fabricated microfluidics." This paper was published in Materials Letters Journal in 2013. Swathi was first author and contributed equally to the manuscript. I give her permission to reprint the manuscript in its entirety in her PhD dissertation.

Sincerely,

Thomas Harris

APPENDIX B

COPYRIGHTS AND PERMISSIONS

CHAPTER 1 RECOGNITION AND NON-LITHOGRAPHIC PATTERNING OF (POLY) DIMETHYLSILOXANE USING PHAGE DISPLAYED PEPTIDES

(i)   Acknowledgements to be used by RSC authors

Authors of RSC books and journal articles can reproduce material (for example a figure) from the RSC publication in a non-RSC publication, including theses, without formally requesting permission providing that the correct acknowledgement is given to the RSC publication. This permission extends to reproduction of large portions of text or the whole article or book chapter when being reproduced in a thesis. The acknowledgement to be used depends on the RSC publication in which the material was published and the form of the acknowledgements is as follows:

• For material being reproduced from an article in New Journal of Chemistry the acknowledgement should be in the form: o [Original citation] - Reproduced by permission of The Royal Society of Chemistry (RSC) on behalf of the Centre National de la Recherche Scientifique (CNRS) and the RSC

• For material being reproduced from an article Photochemical & Photobiological Sciences the acknowledgement should be in the form: o [Original citation] - Reproduced by permission of The Royal Society of Chemistry (RSC) on behalf of the European Society for Photobiology, the European Photochemistry Association, and RSC

• For material being reproduced from an article in Physical Chemistry Chemical Physics the acknowledgement should be in the form: o [Original citation] - Reproduced by permission of the PCCP Owner Societies

• For material reproduced from books and any other journal the acknowledgement should be in the form: o [Original citation] - Reproduced by permission of The Royal Society of Chemistry

The acknowledgement should also include a hyperlink to the article on the RSC website. The form of the acknowledgement is also specified in the RSC agreement/licence signed by the corresponding author.

Except in cases of republication in a thesis, this express permission does not cover the reproduction of large portions of text from the RSC publication or reproduction of the whole article or book chapter.

A publisher of a non-RSC publication can use this document as proof that permission is granted to use the material in the non-RSC publication.

Rightslink Printable License

https://s100.copyright.com/App/PrintableLicenseFrame.jsp?publisherID=315&publisher

Name=theroysoc&publication=14712946&publicationID=70371&rightID… 1/3

THE ROYAL SOCIETY LICENSE

TERMS AND CONDITIONS

Feb 10, 2015

This Agreement between Swathi Swaminathan ("You") and The Royal Society ("The

Royal

Society") consists of your license details and the terms and conditions provided by The

Royal Society and Copyright Clearance Center.

All payments must be made in full to CCC. For payment instructions, please see

information listed at the bottom of this form.

License Number 3565571078928

License date Feb 10, 2015

Licensed Content Publisher The Royal Society

Licensed Content Publication Proceedings A

Licensed Content Title Nonlithographic

patterning of phagedisplayed

peptides with wrinkled

elastomers

Licensed Content Author Swathi Swaminathan,Mitchell Bullough,Qifei Li,Anhong

Zhou,Yue Cui

Licensed Content Date 20150210

Licensed Content Volume

Number 11

Licensed Content Issue Number 91

Volume number 11

Issue number 91

Type of Use Thesis/Dissertation

Requestor type academic/educational

Format print and electronic

Portion figures/tables/images

Quantity 4

Will you be translating? no

Circulation 10000

Order reference number None

Title of your thesis /

dissertation

Bio Inspired materials and micro/nanostructures enabled by peptides and proteins

Expected completion date May 2015

Estimated size (number of

pages)

150

Requestor Location Swathi Swaminathan

649 E 800N Apt20 LOGAN, UT 84321 United States

Attn: Swathi Swaminathan

Billing Type Credit Card

Credit card info Visa ending in 9085

Credit card expiration 08/2017

Total 4.20 USD

3. The following credit line appears wherever the material is used: author, title, journal, year, volume, issue number, pagination, by permission of the Royal Society.

4. For the reproduction of a full article from a Royal Society journal for whatever purpose, the corresponding author of the material concerned should be informed of the proposed use. Contact details for the corresponding authors of all Royal Society journals can be found alongside either the abstract or full text of the article concerned, accessible from royalsocietypublishing.org.

5. If the credit line in our publication indicates that any of the figures, images or photos was reproduced from an earlier source it will be necessary for you to clear this permission with the original publisher as well. If this permission has not been obtained, please note that this material cannot be included in your publication/photocopies.

6. Licenses may be exercised anywhere in the world.

7. While you may exercise the rights licensed immediately upon issuance of the license at the end of the licensing process for the transaction, provided that you have disclosed complete and accurate details of your proposed use, no license is finally effective unless and until full payment is received from you (either by publisher or by CCC) as provided in CCC's Billing and Payment terms and conditions. If full payment is not received on a timely basis, then any license preliminarily granted shall be deemed automatically revoked and shall be void as if never granted. Further, in the event that you breach any of these terms and conditions or any of CCC's Billing and Payment terms and conditions, the license is automatically revoked and shall be void as if never granted. Use of materials as described in a revoked license, as well as any use of the materials beyond the scope of an unrevoked

license, may constitute copyright infringement and publisher reserves the right to take any and all action to protect its copyright in the materials.

8. Publisher reserves all rights not specifically granted in the combination of (i) the license details provided by you and accepted in the course of this licensing transaction, (ii) these terms and conditions and (iii) CCC's Billing and Payment terms and conditions.

9. Publisher makes no representations or warranties with respect to the licensed material.

10. You hereby indemnify and agree to hold harmless publisher and CCC, and their respective officers, directors, employees and agents, from and against any and all claims arising out of your use of the licensed material other than as specifically authorized pursuant to this license.

11. This license may not be amended except in a writing signed by both parties (or, in the case of publisher, by CCC on publisher's behalf).

CHAPTER 2

RECOGNITION OF EPOXY USING PHAGE DISPLAYED PEPTIDES

2/10/2015   **Rightslink Printable License**

https://s100.copyright.com/App/PrintableLicenseFrame.jsp?publisherID=70&publisherName=ELS&publication=09284931& publicationID=13363&rightID=1&ty… 1/6

ELSEVIER LICENSE

TERMS AND CONDITIONS

Feb 10, 2015

This is a License Agreement between Swathi Swaminathan ("You") and Elsevier ("Elsevier") provided by Copyright Clearance Center ("CCC"). The license consists of your order details, the terms and conditions provided by Elsevier, and the payment terms and conditions. All payments must be made in full to CCC. For payment instructions, please see information listed at the bottom of this form.

Customer name Swathi Swaminathan

Customer address 649 E 800N Apt20 LOGAN, UT 84321

License number 3565560004233

License date Feb 10, 2015

Licensed content publisher Elsevier

Licensed content publication Materials Science and Engineering: C

Licensed content title Recognition of epoxy with phage displayed peptides

Licensed content author none

Licensed content date 1 July 2013

Licensed content volume Number 33

Licensed content issue number 5

Number of pages 3

Start Page 3082

End Page 3084

Type of Use reuse in a thesis/dissertation

Portion full article

Format both print and electronic

Are you the author of this Elsevier article? Yes

Will you be translating? No

Title of your thesis/dissertation

Bio Inspired materials and micro/nanostructures enabled by peptides and proteins

Expected completion date May 2015

Estimated size (number of pages) 150

Elsevier VAT number GB 494 6272 12

Permissions price 0.00 USD

VAT/Local Sales Tax 0.00 USD / 0.00 GBP

Total 0.00 USD

Terms and Conditions

INTRODUCTION

1. The publisher for this copyrighted material is Elsevier. By clicking "accept" in connection with completing this licensing transaction, you agree that the following terms and conditions apply to this transaction (along with the Billing and Payment terms and conditions established by Copyright Clearance Center, Inc. ("CCC"), at the time that you opened your Rightslink account and that are available at any time at http://myaccount.copyright.com).

GENERAL TERMS

2. Elsevier hereby grants you permission to reproduce the aforementioned material subject to the terms and conditions indicated.

3. Acknowledgement: If any part of the material to be used (for example, figures) has appeared in our publication with credit or acknowledgement to another source, permission must also be sought from that source. If such permission is not obtained then that material may not be included in your publication/copies. Suitable acknowledgement to the source must be made, either as a footnote or in a reference list at the end of your publication, as follows:

"Reprinted from Publication title, Vol /edition number, Author(s), Title of article / title of chapter, Pages No., Copyright (Year), with permission from Elsevier [OR APPLICABLE SOCIETY COPYRIGHT OWNER]." Also Lancet special credit "Reprinted from The Lancet, Vol. number, Author(s), Title of article, Pages No., Copyright (Year), with permission from Elsevier."

4. Reproduction of this material is confined to the purpose and/or media for which permission is hereby given.

5. Altering/Modifying Material: Not Permitted. However figures and illustrations may be altered/adapted minimally to serve your work. Any other abbreviations, additions, deletions and/or any other alterations shall be made only with prior written authorization of Elsevier Ltd. (Please contact Elsevier at permissions@elsevier.com)

6. If the permission fee for the requested use of our material is waived in this instance, please be advised that your future requests for Elsevier materials may attract a fee.

7. Reservation of Rights: Publisher reserves all rights not specifically granted in the combination of (i) the license details provided by you and accepted in the course of this licensing transaction, (ii) these terms and conditions and (iii) CCC's Billing and Payment

8. License Contingent upon Payment: While you may exercise the rights licensed immediately upon issuance of the license at the end of the licensing process for the transaction, provided that you have disclosed complete and accurate details of your proposed use, no license is finally effective unless and until full payment is received from you (either by publisher or by CCC) as provided in CCC's Billing and Payment terms and conditions. If full payment is not received on a timely basis, then any license preliminarily granted shall be deemed automatically revoked and shall be void as if never granted. Further, in the event that you breach any of these terms and conditions or any of CCC's Billing and Payment terms and conditions, the license is automatically revoked and shall be void as if never granted. Use of materials as described in a revoked license, as well as any use of the materials beyond the scope of an unrevoked license, may constitute copyright infringement and publisher reserves the right to take any and all action to protect its copyright in the materials.

9. Warranties: Publisher makes no representations or warranties with respect to the licensed material.

10. Indemnity: You hereby indemnify and agree to hold harmless publisher and CCC, and their respective officers, directors, employees and agents, from and against any and all claims arising out of your use of the licensed material other than as specifically authorized pursuant to this license.

11. No Transfer of License: This license is personal to you and may not be sublicensed, assigned, or transferred by you to any other person without publisher's written permission.

12. No Amendment Except in Writing: This license may not be amended except in a writing signed by both parties (or, in the case of publisher, by CCC on publisher's behalf).

13. Objection to Contrary Terms: Publisher hereby objects to any terms contained in any purchase order, acknowledgment, check endorsement or other writing prepared by you, which terms are inconsistent with these terms and conditions or CCC's Billing and Payment terms and conditions. These terms and conditions, together with CCC's Billing and Payment terms and conditions (which are incorporated herein), comprise the entire agreement between you and publisher (and CCC) concerning this licensing transaction. In the event of any conflict between your obligations established by these terms and conditions and those established by CCC's Billing and Payment terms and conditions, these terms and conditions shall control.

14. Revocation: Elsevier or Copyright Clearance Center may deny the permissions described in this License at their sole discretion, for any reason or no reason, with a full refund payable to you. Notice of such denial will be made using the contact information provided by you. Failure to receive such notice will not alter or invalidate the denial. In no event will Elsevier or Copyright Clearance Center be responsible or liable for any costs, expenses or damage incurred by you as a result of a denial of your permission request, other than a refund of the amount(s) paid by you to Elsevier and/or Copyright Clearance Center for denied permissions.

LIMITED LICENSE

The following terms and conditions apply only to specific license types:

15. Translation: This permission is granted for nonexclusive world English rights only unless your license was granted for translation rights. If you licensed translation rights you may only translate this content into the languages you requested. A professional translator must perform all translations and reproduce the content word for word preserving the integrity of the article. If this license is to reuse 1 or 2 figures then permission is granted for nonexclusive world rights in all languages.

16. Posting licensed content on any Website: The following terms and conditions apply as follows: Licensing material from an Elsevier journal: All content posted to the web site must maintain the copyright information line on the bottom of each image; A hypertext must be included to the Homepage of the journal from which you are licensing at http://www.sciencedirect.com/science/journal/xxxxx or the Elsevier homepage for books at http://www.elsevier.com; Central Storage: This license does not include permission for a scanned version of the material to be stored in a central repository such as that provided by Heron/XanEdu. Licensing material from an Elsevier book: A hypertext link must be included to the Elsevier homepage at http://www.elsevier.com. All content posted to the web site must maintain the copyright information line on the bottom of each image.

Posting licensed content on Electronic reserve: In addition to the above the following clauses are applicable: The web site must be password protected and made available only to bona fide students registered on a relevant course. This permission is granted for 1 year only. You may obtain a new license for future website posting.

17. for journal authors: the following clauses are applicable in addition to the above:

  Permission granted is limited to the author accepted manuscript version* of your paper.

*Accepted Author Manuscript (AAM) Definition: An accepted author manuscript (AAM) is the author's version of the manuscript of an article that has been accepted for publication and which may include any author incorporated changes suggested through the processes of submission processing, peer review, and editor author communications. AAMs do not include other publisher value added contributions such as copyediting, formatting, technical enhancements and (if relevant) pagination.

You are not allowed to download and post the published journal article (whether PDF or HTML, proof or final version), nor may you scan the printed edition to create an electronic version. A hypertext must be included to the Homepage of the journal from which you are licensing at http://www.sciencedirect.com/science/journal/xxxxx. As part of our normal production process, you will receive an email notice when your article appears on Elsevier's online service ScienceDirect (www.sciencedirect.com). That email will include the article's Digital Object Identifier (DOI). This number provides the electronic link to the published article and should be included in the posting of your personal version. We ask that you wait until you receive this email and have the DOI to do any posting.

18. Posting to a repository: Authors may post their AAM immediately to their employer'sinstitutional repository for internal use only and may make their manuscript publically available after the journal specific embargo period has ended. Please also refer to Elsevier's Article Posting Policy for further information.

19. For book authors the following clauses are applicable in addition to the above:

Authors are permitted to place a brief summary of their work online only. You are not allowed to download and post the published electronic version of your chapter, nor may you scan the printed edition to create an electronic version. Posting to a repository: Authors are permitted to post a summary of their chapter only in their institution's repository.

20. Thesis/Dissertation: If your license is for use in a thesis/dissertation your thesis may be submitted to your institution in either print or electronic form. Should your thesis be published commercially, please reapply for permission. These requirements include permission for the Library and Archives of Canada to supply single copies, on demand, of the complete thesis and include permission for Proquest/UMI to supply single copies, on demand, of the complete thesis. Should your thesis be published commercially, please reapply for permission.

Elsevier Open Access Terms and Conditions

Elsevier publishes Open Access articles in both its Open Access journals and via its Open Access articles option in subscription journals. Authors publishing in an Open Access journal or who choose to make their article Open Access in an Elsevier subscription journal select one of the following Creative Commons user licenses, which define how a reader may reuse their work:

Creative Commons Attribution License (CC BY), Creative Commons Attribution – Non Commercial Share Alike (CC BY NC SA) and

Creative Commons Attribution – Non Commercial – No Derivatives (CC BY NC ND)

Terms & Conditions applicable to all Elsevier Open Access articles:

CHAPTER 6

FABRICATION OF MAMMALIAN HAIR BASED MICROFLUIDICS

ELSEVIER LICENSE

TERMS AND CONDITIONS

Feb 10, 2015

This is a License Agreement between Swathi Swaminathan ("You") and Elsevier ("Elsevier") provided by Copyright Clearance Center ("CCC"). The license consists of your order details, the terms and conditions provided by Elsevier, and the payment terms and conditions.

All payments must be made in full to CCC. For payment instructions, please see information listed at the bottom of this form.

Supplier Elsevier Limited

The Boulevard,Langford Lane

Kidlington,Oxford,OX5 1GB,UK

Registered Company Number 1982084

Customer name Swathi Swaminathan

Customer address 649 E 800N Apt20 LOGAN, UT 84321

License number 3565560177539

License date Feb 10, 2015

Licensed content publisher Elsevier

Licensed content publication Materials Letters

Licensed content title Bio-inspired mammalian hair fabricated microfluidics

Licensed content author none

Licensed content date 1 September 2013

Licensed content volume Number 106

Licensed content issue Number N/A

Number of pages 5

Start Page 208

End Page 212

Type of Use reuse in a thesis/dissertation

Intended publisher of new work other Portion full article

Format both print and electronic

Are you the author of this Elsevier article? Yes

Will you be translating? No

Title of your thesis/dissertation

Bio Inspired materials and micro/nanostructures enabled by peptides and proteins

Expected completion date May 2015

Estimated size (number of pages) 150

Elsevier VAT number GB 494 6272 12

Permissions price 0.00 USD

VAT/Local Sales Tax 0.00 USD / 0.00 GBP

Total 0.00 USD

TERMS AND CONDITIONS

INTRODUCTION

1. The publisher for this copyrighted material is Elsevier. By clicking "accept" in connection with completing this licensing transaction, you agree that the following terms and conditions apply to this transaction (along with the Billing and Payment terms and conditions established by Copyright Clearance Center, Inc. ("CCC"), at the time that you opened your Rightslink account and that are available at any time at http://myaccount.copyright.com).

GENERAL TERMS

2. Elsevier hereby grants you permission to reproduce the aforementioned material subject to the terms and conditions indicated.

3. Acknowledgement: If any part of the material to be used (for example, figures) has appeared in our publication with credit or acknowledgement to another source, permission must also be sought from that source. If such permission is not obtained then that material may not be included in your publication/copies. Suitable acknowledgement to the source must be made, either as a footnote or in a reference list at the end of your publication, as follows: "Reprinted from Publication title, Vol /edition number, Author(s), Title of article / title of chapter, Pages No., Copyright (Year), with permission from Elsevier [OR APPLICABLE

SOCIETY COPYRIGHT OWNER]." Also Lancet special credit "Reprinted from The Lancet, Vol. number, Author(s), Title of article, Pages No., Copyright (Year), with permission from Elsevier."

4. Reproduction of this material is confined to the purpose and/or media for which permission is hereby given.

5. Altering/Modifying Material: Not Permitted. However figures and illustrations may be altered/adapted minimally to serve your work. Any other abbreviations, additions, deletions and/or any other alterations shall be made only with prior written authorization of Elsevier Ltd. (Please contact Elsevier at permissions@elsevier.com)

6. If the permission fee for the requested use of our material is waived in this instance, please be advised that your future requests for Elsevier materials may attract a fee.

7. Reservation of Rights: Publisher reserves all rights not specifically granted in the combination of (i) the license details provided by you and accepted in the course of this licensing transaction, (ii) these terms and conditions and (iii) CCC's Billing and Payment terms and conditions.

8. License Contingent Upon Payment: While you may exercise the rights licensed immediately upon issuance of the license at the end of the licensing process for the transaction, provided that you have disclosed complete and accurate details of your proposed use, no license is finally effective unless and until full payment is received from you (either by publisher or by CCC) as provided in CCC's Billing and Payment terms and conditions. If full payment is not received on a timely basis, then any license preliminarily granted shall be deemed automatically revoked and shall be void as if never granted. Further, in the event that you breach any of these terms and conditions or any of CCC's Billing and Payment

terms and conditions, the license is automatically revoked and shall be void as if never granted. Use of materials as described in a revoked license, as well as any use of the materials beyond the scope of an unrevoked license, may constitute copyright infringement and publisher reserves the right to take any and all action to protect its copyright in the materials.

9. Warranties: Publisher makes no representations or warranties with respect to the licensed material.

10. Indemnity: You hereby indemnify and agree to hold harmless publisher and CCC, and their respective officers, directors, employees and agents, from and against any and all

claims arising out of your use of the licensed material other than as specifically authorized pursuant to this license.

11. No Transfer of License: This license is personal to you and may not be sublicensed, assigned, or transferred by you to any other person without publisher's written permission.

12. No Amendment Except in Writing: This license may not be amended except in a writing signed by both parties (or, in the case of publisher, by CCC on publisher's behalf).

13. Objection to Contrary Terms: Publisher hereby objects to any terms contained in any purchase order, acknowledgment, check endorsement or other writing prepared by you, which terms are inconsistent with these terms and conditions or CCC's Billing and Payment terms and conditions. These terms and conditions, together with CCC's Billing and Payment terms and conditions (which are incorporated herein), comprise the entire agreement between you and publisher (and CCC) concerning this licensing transaction. In the event of any conflict between your obligations established by these terms and conditions and those

established by CCC's Billing and Payment terms and conditions, these terms and conditions shall control.

14. Revocation: Elsevier or Copyright Clearance Center may deny the permissions described in this License at their sole discretion, for any reason or no reason, with a full refund payable to you. Notice of such denial will be made using the contact information provided by you. Failure to receive such notice will not alter or invalidate the denial. In no event will Elsevier or Copyright Clearance Center be responsible or liable for any costs, expenses or damage incurred by you as a result of a denial of your permission request,

other than a refund of the amount(s) paid by you to Elsevier and/or Copyright Clearance Center for denied permissions.

LIMITED LICENSE

The following terms and conditions apply only to specific license types:

15. Translation: This permission is granted for nonexclusive world English rights only unless your license was granted for translation rights. If you licensed translation rights you may only translate this content into the languages you requested. A professional translator must perform all translations and reproduce the content word for word preserving the integrity of the article. If this license is to reuse 1 or 2 figures then permission is granted for Nonexclusive world rights in all languages.

16. Posting licensed content on any Website: The following terms and conditions apply as follows: Licensing material from an Elsevier journal: All content posted to the web site must maintain the copyright information line on the bottom of each image; A hypertext must be included to the Homepage of the journal from which you are licensing at http://www.sciencedirect.com/science/journal/xxxxx or the Elsevier homepage for books at http://www.elsevier.com; Central Storage: This license does not include permission for a scanned version of the material to be stored in a central repository such as that provided by Heron/XanEdu. Licensing material from an Elsevier book: A hypertext link must be included to the Elsevier homepage at http://www.elsevier.com . All content posted to the

web site must maintain the copyright information line on the bottom of each image. Posting licensed content on Electronic reserve: In addition to the above the following clauses are applicable: The web site must be password protected and made available only to bona fide students registered on a relevant course. This permission is granted for 1 year only. You may obtain a new license for future website posting.

17. for journal authors: the following clauses are applicable in addition to the above: Permission granted is limited to the author accepted manuscript version* of your paper. *Accepted Author Manuscript (AAM) Definition: An accepted author manuscript (AAM) is the author's version of the manuscript of an article that has been accepted for publication and which may include any author incorporated changes suggested through the processes of submission processing, peer review, and editor author communications. AAMs do not include other publisher value added contributions such as copyediting, formatting, technical enhancements and (if relevant) pagination. You are not allowed to download and post the published journal article (whether PDF or HTML, proof or final version), nor may you scan the printed edition to create an electronic version. A hypertext must be included to the Homepage of the journal from which you are licensing at http://www.sciencedirect.com/science/journal/xxxxx. As part of our normal production process, you will receive an email notice when your article appears on Elsevier's online service ScienceDirect (www.sciencedirect.com). That email will include the article's Digital Object Identifier (DOI). This number provides the electronic link to the published article and should be included in the posting of your personal version. We ask that you wait until you receive this email and have the DOI to do any posting.

18. Posting to a repository: Authors may post their AAM immediately to their employer's institutional repository for internal use only and may make their manuscript publically available after the journal specific embargo period has ended. Please also refer to Elsevier's Article Posting Policy for further information.

19. For book authors the following clauses are applicable in addition to the above: Authors are permitted to place a brief summary of their work online only. You are not allowed to download and post the published electronic version of your chapter, nor may you scan the printed edition to create an electronic version. Posting to a repository: Authors are permitted to post a summary of their chapter only in their institution's repository. 20. Thesis/Dissertation: If your license is for use in a thesis/dissertation your thesis may be submitted to your institution in either print or electronic form. Should your thesis be published commercially, please reapply for permission. These requirements include permission for the Library and Archives of Canada to supply single copies, on demand, of the complete thesis and include permission for Proquest/UMI to supply single copies, on demand, of the complete thesis. Should your thesis be published commercially, please reapply for permission.

Elsevier Open Access Terms and Conditions

Elsevier publishes Open Access articles in both its Open Access journals and via its Open Access articles option in subscription journals. Authors publishing in an Open Access journal or who choose to make their article Open Access in an Elsevier subscription journal

select one of the following Creative Commons user licenses, which define how a reader may reuse their work: Creative Commons Attribution License (CC BY), Creative Commons Attribution – Non Commercial Share Alike (CC BY NC SA) and Creative Commons Attribution – Non Commercial – No Derivatives (CC BY NC ND)

Terms & Conditions applicable to all Elsevier Open Access articles:

Any reuse of the article must not represent the author as endorsing the adaptation of the article nor should the article be modified in such a way as to damage the author's honour or reputation.

The author(s) must be appropriately credited. If any part of the material to be used (for example, figures) has appeared in our publication with credit or acknowledgement to another source it is the responsibility of the user to ensure their reuse complies with the terms and conditions determined by the rights holder.

Additional Terms & Conditions applicable to each Creative Commons user license

CC BY: You may distribute and copy the article, create extracts, abstracts, and other revised versions, adaptations or derivative works of or from an article (such as a translation), to include in a collective work (such as an anthology), to text or data mine the article, including for commercial purposes without permission from Elsevier.

CC BY NC SA: For noncommercial purposes you may distribute and copy the article, create extracts, abstracts and other revised versions, adaptations or derivative works of or from an article (such as a translation), to include in a collective work (such as an

anthology), to text and data mine the article and license new adaptations or creations under identical terms without permission from Elsevier.

CC BY NC ND: For noncommercial purposes you may distribute and copy the article and include it in a collective work (such as an anthology), provided you do not alter or modify the article, without permission from Elsevier. Any commercial reuse of Open Access articles published with a CC BY NC SA or CC BY NC ND license requires permission from Elsevier and will be subject to a fee.

Commercial reuse includes:

☐ Promotional purposes (advertising or marketing)

☐ Commercial exploitation (e.g. a product for sale or loan)

☐ Systematic distribution (for a fee or free of charge)

Please refer to Elsevier's Open Access Policy for further information.

CURRICLUM VITAE

SWATHI SWAMINATHAN
Department of Biological Engineering
Utah State University, Logan UT 84322
Cell phone: (435)5121373
E-mail: swathi.1287@gmail.com
Web: www.linkedin.com/pub/swathi-swaminathan/29/196/938/

EDUCATION:

- PhD Biological Engineering, Dec'14

  Utah State University, Logan, Utah, USA

  Thesis: Bio-inspired micro/ nanostructures enabled by peptides and proteins

  Advisor: Dr. Yue Cui

- Summer School, Nanomedicine , Jul'11

  University of Oxford, Oxfordshire, UK

- Master of Science, Molecular Genetics , Aug'10

  University of Leicester, Leicester, UK

  Thesis: Protein Engineering of Vascular Growth Factors

  Advisor: Dr. Nicholas Brindle

- Bachelor of Technology, Biotechnology, May'09

  SASTRA University, Thanjavur, India

  Thesis: Industrial Production and Optimization of Recombinant Proteins

  Advisor: Dr. Anita Balachander.

RESEARCH EXPERIENCE:

PhD Aug'11-present

Department of Biological Engineering, Utah State University, Logan, UT

- Developed Bio-MEMS for miniaturized sensors and diagnostics using microfluidics (single and double layered), oligonucleotide chips, photonic crystals and mammalian cell culture to detect biomarkers for cardiac myofarction along with ELISA and qPCR to validate our sensor, used MATLAB to conduct analysis.

- Successfully identified the recognition peptide moieties on biomaterials like diamond, (poly) dimethyl siloxane, (poly) ethylenetetraphthalate, Epoxy and aromatic Diphenylalanine peptide nanotubes using Phage displayed technique.

- Conducted surface characterization and imaging using Raman spectroscopy, Atomic force microscopy, scanning electron microscopy, Fluorescence microscopy and Fourier transform Infra-red spectroscopy.

- Carried out self-assembly of different materials on biofilms and also induced the in-situ synthesis of conductive nanoparticles mediated by peptides.

- Harvested neuronal stem cells for a study in polymer-cell interactions and imaged it with two photon confocal microscope.

- Coursework included advanced biomaterials with focus on tissue engineering and Design of experiments indulging in quantitative data analysis using SAS and R.

Nanomedicine summer student, **July 2011**

University of Oxford, Oxfordshire, UK

- Attended nanopore sensing workshop where nanopores were attached to DNA probes or ligands to find the DNA and proteins of interest.

Research Assistant Oct'10-Apr'11

Pondicherry Biotech Private Limited, Pondicherry, India

- Successfully studied the characterization of two different genes in a plant species, which could increase the quality and/or quantity of Biofuel production. This was accomplished using Molecular cloning, PCRs, total RNA isolation, plant expression systems (Agrobacterium) and Zinc finger nuclease technology.
- Constructed a library of 60 mutated clones for a study in HIV disease using TALENs and CRISPRs.

Research Assistant (Master's Thesis) Jan'10- Aug'10

Department of Cardiovascular surgery, Leicester Royal Infirmary, Leicester, UK

- Conducted a binding analysis study between two different growth factors (PLGF/ VEGF-A) with respect to one particular receptor molecule (VEGFR1), where binding of one ligand-receptor pair leads to pathogenesis while the other is beneficial to the normal functioning of the system. The binding studies on these biomarkers were done using Flow

cytometry (FACS) after site directed mutagenesis (PyMOL/ MOLSCRIPT) mammalian cell culture and transfection of the cell lines .Using the wild and mutant types at different concentrations of the biomarker PLGF , a competitive ELISA was conducted to study its binding with the receptor molecule to control its pathogenic angiogenesis. Also used techniques like PAGE, SDS/PAGE, confocal microscopy and RT-PCR.

▪ Successfully constructed a detrimental mutant ligand that can bind to the receptor molecule with a view to generate therapeutics. This was accomplished by molecular cloning, Real time PCR and Western Blotting.

▪ Coursework lab phase included northern/ southern blotting, DNA/ tissue microarrays, live mice studies, molecular cloning and SAGE.

Senior Project (Undergraduate thesis) Dec'08- Feb'09

SHASUN Drugs & Chemicals, Pvt. Ltd., Chennai, India

▪ Studied the downstream processing and purification of a protein concerning cancer treatment at an industrial scale by optimizing the physical and chemical condition to ensure efficient refolding of the protein.

▪ Utilized Homogenizers, density gradient and differential centrifugation and Ultra/ cross-flow filtration units, solubilization using guanidium isothiocyanate and urea at different pH and concentrations, Purification using HPLC/ IMAC and finally lyophilization.

Internship 1 (Analytical Techniques) Jun'08

Biochemistry, Central Leather Research Institute, Chennai, India

▪ Studied expression of proteins using PAGE/ SDS-PAGE, protein quantification using Liquid chromatography- Mass Spectrometry and Gas chromatography- Mass Spectrometry.

▪ Conducted basic protein Purification using HPLC, Ion exchange chromatography and Affinity chromatography.

Internship 2 (Cell-Cell communication short course) May'07

CSIR- Centre for Cellular & Molecular Biology, Hyderabad, India

▪ Investigated proteomics (MALDI/LC- MS/ electrophoresis).

▪ Reviewed basic cell culture techniques, live mice models, differential scanning calorimetry.

Internship 3 (Immunology short course) Dec'06

Sangene Biotech Private, Ltd. Bangalore, India

▪ Studied basic microbiology and immunology techniques including immunoelectrophoresis and ELISA.

LIST OF PUBLICATIONS:

•Recognition of poly (dimethylsiloxane) with phage displayed peptides. Swaminathan, S., and Cui, Y. *RSC Advances* (2012) 2: 12724–12727.

•Recognition of epoxy with phage displayed peptides. Swaminathan, S., Cui, Y. Materials Science and Engineering C (2013) 33: 3082–3084.

•Bio-inspired mammalian hair-fabricated microfluidics Swaminathan, S., Harris, T., McClellan, D., Cui, Y. Materials Letters (2013) 106: 208–212.

•Non-lithographic patterning of phage-displayed peptides with wrinkled elastomers. Swaminathan, S., Bullough, M., Li, Q., Zhou, A., Cui, Y. Journal of Royal Society Interface (2014) 11: 1742-5662.

•Recognition of (poly) ethylenetetraphthalate using Phage displayed peptides. Swaminathan, S., and Cui, Y (forthcoming)

•Characterization of peptide nanotubes using Phage displayed peptides. Swaminathan, S., and Cui, Y (forthcoming)

•Super hydrophobic, biodegradable and transparent materials. Swaminathan, S., and Cui, Y (forthcoming)

•1D, 2D, 3D nanostructures via translation of elastomeric instability. Swaminathan, S., Bullough, M., Britt, D. and Cui, Y (forthcoming)

PROFESSIONAL AFFLIATIONS:

Institute of Biological Engineering

Nucleo (Sub-editor)

TECHNICAL SKILLS:

• Computer skills : Programming in C, C++ , MATLAB, FORTRAN and Microsoft Office tools (Word, Excel, Powerpoint).

•Bio-computational tools: PYMOL, MOLSCRIPT, BLAST, FASTA, clustalw, ExPASy.

•Statistical and Data management tools: SAS and R.

•Languages: English- proficient; French - intermediate.

PRESENTATIONS AND PROFESSIONAL MEETINGS:

•Won the first place in Poster presentation on *Recognition of Phage displayed peptides on (poly) dimethylsiloxane* in the Institue of Biological Engineering conference, Utah State University, Logan UT. Oct'12

•Presented *Recognition of Phage displayed peptides on (poly) dimethylsiloxane* in Institute of Biological Engineering Conference at Raleigh, NC. Mar'13

•Presented a poster in *Recognition of epoxy using Phage Displayed Peptides* in NanoUTAH, COMS 2014, Salt Lake City, UT. Oct'14

•Presented a poster in *Bio-inspired mammalian hair-based microfluidics* in NanoUTAH-COMS 2014, Salt Lake city, UT. Oct'14

•Presented a poster in *Non-lithographic patterning of phage displayed peptides on wrinkled elastomers* in NanoUTAH- COMS 2014, Salt Lake City, UT. Oct'14